2010

Mechanism of IL-12 mediated enhancement of passive experimental autoimmunne myasthenia gravis

Paul Michael Brown
The University of Toledo

A Dissertation

entitled

Mechanism of IL-12 Mediated Enhancement of Passive Experimental Autoimmune Myasthenia Gravis

by

Paul Michael Brown

Submitted to the Graduate Faculty as partial fulfillment of the

requirements for the Doctor of Philosophy Degree in Medicinal Chemistry

_____

Dr. Katherine A. Wall, Committee Chair

_____

Dr. Marcia McInerney, Committee Member

_____

Dr. Surya Nauli, Committee Member

_____

Dr. Francis Pizza, Committee Member

_____

Dr. Patricia R. Komuniecki, Dean
College of Graduate Studies

The University of Toledo

December 2010

An Abstract of

Mechanism of IL-12 Mediated Enhancement of Passive Experimental Autoimmune Myasthenia Gravis

by

Paul Michael Brown

Submitted to the Graduate Faculty as partial fulfillment of the requirements for the Doctor of Philosophy Degree in Medicinal Chemistry

University of Toledo
December 2010

Myasthenia gravis (MG) is characterized by autoantibody-mediated reduction of nicotinic acetylcholine receptors (AChR). In myasthenia gravis, anti-acetylcholine receptor (AChR) antibody is thought to cause damage through the activation of complement, via the classical complement pathway, in addition to causing internalization of AChRs. Interleukin-12 (IL-12), a major inducer of interferon-gamma (IFN-γ) production, has been shown to enhance active and clinical passive experimental autoimmune myasthenia gravis (EAMG). IFN-γ is known to be produced by various cell types, including $CD4^+$ and $CD8^+$ T cells, natural killer (NK) cells, and $NK1.1^+$ T (NKT) cells.

Our current research was designed to investigate the effects of IL-12 on skeletal muscle tissue. We performed passive transfer experiments with mAb D6, a mouse anti-AChR monoclonal antibody recognizing the immunodominant mouse AChR epitope, using both B6 and IFN-$\gamma^{-/-}$ mice. The role of complement in disease induction in these mice was examined using fluorescent microscopy. When pre-treated with IL-12, B6 and IFN-$\gamma^{-/-}$ mice had similar amounts of antibody and complement bound at the

neuromuscular junction, although IFN-$\gamma^{-/-}$ mice were resistant to EAMG development. This suggests that IL-12, through IFN-γ, may increase susceptibility to disease through mechanisms downstream of antibody and complement binding.

In order to do investigate the roles of known IFN-γ producing cell types in passive disease enhancement, NK and NKT cells were depleted using the anti-$NK1.1^{+}$ monoclonal antibody PK136 prior to administration of IL-12 and passive transfer of mAb D6 in C57BL/6 (B6) mice. Comparatively, IL-12 treatment and passive transfer of mAb D6 was performed using TCRβ/TCRδ dual knock-out mice ($TCR\beta\delta^{-/-}$ mice), which possess B cells and NK cells but completely lack functional T cells and NKT cells. Interleukin-12 treatment failed to enhance passive disease in mAb PK136-treated B6 mice while definitively worsening passive disease in $TCR\beta\delta^{-/-}$ mice. Accordingly, after IL-12 treatment, serum IFN-γ levels were dramatically lowered in disease-resistant mAb PK136-treated B6 mice compared to susceptible $TCR\beta\delta^{-/-}$ mice. Interleukin-12 treated B6 mice exhibited moderate disease enhancement and moderate serum IFN-γ levels. These findings suggest innate NK cells play a primary role as the main cellular source of disease-enhancing IFN-γ upon administration of IL-12.

To determine what effects IL-12 and mAb D6 have on the levels of neuromuscular junction-localized complement in these mice, we performed immunohistochemical analysis of mouse diaphragm muscle tissue harvested from all mice groups assayed. The results of the immunohistochemical analyses again demonstrate that increased complement binding does not explain enhancement of passive disease. Separately, gene chip analysis of RNA isolated and purified from differentially treated B6 mouse diaphragm muscle tissue was performed. The gene chip analysis

demonstrated that IL-12 treatment alone dramatically influences specific gene expression levels in these mice. In all, these results demonstrate that IL-12 treatment enhances passive disease independently of localized complement deposition through innate NK cell-derived IFN-γ, which dramatically affects gene expression levels in the muscle microenvironment.

Acknowledgments

I would like to sincerely thank my advisor, Dr. Katherine Ann Wall, for all of her help and guidance throughout the course of my Ph.D. project. When I entered her lab in August of 2005 I had a great deal of ambition but very little knowledge of immunology or autoimmune disease. In addition to fostering my now expert knowledge of these subjects, Dr. Wall also allowed me the freedom to think independently and pursue my own ideas in regards to our research. Being the most important qualities necessary to becoming a successful scientist, I will always be indebted to Dr. Wall for these gifts.

I would like to extend special thanks to my committee members: Dr. Marcia McInerney, Dr. Surya Nauli, and Dr. Francis Pizza. Their extraordinary knowledge of experimental techniques and the unlimited access they provided me in using their specialized equipment was essential to the successful completion of my project. I would also like to thank them all for their input and advice as members of my thesis committee. I would like to especially thank Brandon Slotterbeck for his advice and assistance on countless assays throughout the years, as well as the entire Department of Medicinal and Biological Chemistry and my peers for all the relationships I have developed while studying here. Finally, I would like to thank my family, and most importantly my wife Lidiya. Without her steadfast patience and support through all of the difficult times, my successful completion of this degree would have been impossible. It's taken a very long time, but we've finally reached the light at the end of the tunnel! We made it, and I'm glad I get to share this moment with you!

Table of Contents

List of Figures

List of Tables

Chapter 1

Introduction

1.1 Objectives:

Myasthenia gravis (MG) is an autoimmune disease caused by the production of antibodies to the nicotinic acetylcholine receptor (AChR). The binding of anti-AChR antibodies to their targets at the post-synaptic membrane results in muscular weakness due to decreased neuromuscular transmission (2). The overall goal of this project was to understand the mechanisms whereby interleukin-12 (IL-12) and interferon-gamma (IFN-γ) enhance myasthenia gravis, in order to develop strategies that will counteract their effects. While B cells are clearly the source of the pathogenic anti-AChR antibodies produced during human MG, the role that T cells play in the development of autoimmune responses (3, 4) has generated interest in studying the specific impact that individual T cell subsets may have on MG severity. When studying the effect of IL-12 in Experimental Autoimmune Myasthenia Gravis (EAMG), the standard animal model in which C57BL/6J (B6) mice are immunized with *Torpedo* AChR, researchers have focused on IFN-γ- producing Th1 cells. These Th1 cells could affect anti-AChR antibody

quantity, isotype, or specificity while simultaneously altering the environment of the muscle or the muscle tissue itself (5, 6).

Similar to past experiments, our focus here was centered on the effector phase of the disease rather than on the induction phase in order to eliminate the variability of B cell responses by keeping the antibody response constant. This involved inducing EAMG in a B6 mouse by passively transferring a pathogenic monoclonal anti-AChR antibody and studying the mechanism of disease enhancement by interleukin-12. IL-12 and the resulting IFN-γ produced can alter the function of cells of the innate immune system, cells of the adaptive immune system, and the muscle tissue microenvironment. Simplifying the system by keeping the antibody response constant allowed us to determine which cells are involved in disease enhancement while avoiding any potential complication from cytokine effects on antibody production. Then we sought to determine how the muscle tissue responds to the environment created by these cells.

The hypothesis tested was that innate natural killer cells (NK cells) are the source of the inflammatory cytokine IFN-γ during passive transfer EAMG, the production of which is enhanced in response to IL-12 stimulation. The exacerbation of EAMG by IL-12 and downstream IFN-γ production features inflammation of the muscle tissue, and muscle tissue responds to this inflammation with changes in specific gene expression. We then sought to identify target genes that may later be examined in MG patients and whose expression may be targeted for therapeutic manipulation. Achieving specific elimination of anti-AChR antibodies has proven to be challenging, though strategies such as periodic therapeutic plasma exchange (TPE) in patients who are non-responsive to

immunosuppressive agents do indeed show promise (7). We believed that our approach will yield strategies that may one day complement existing therapies wherein reducing antibody damage may be just as valuable a target as reducing antibody levels in MG.

In order to determine what influence IFN-γ has on passive disease induced with mAb D6, we administered IL-12 and mAb D6 in order to induce passive disease in B6 and IFN-$\gamma^{-/-}$ mice. Our goal was to clarify whether or not functional IFN-γ presence was able to worsen passive disease in combination with mAb D6 immunization. Next, in order to establish what affects IL-12 may directly have on skeletal muscle tissue, the effects of IL-12 treatment on muscle tissue and the disease process were further examined in PBS control and IL-12 treated B6 and IFN-$\gamma^{-/-}$ mice by performing histology and immunofluorescence on mouse diaphragm muscle samples. In this way we attempted to determine whether or not IL-12 treatment, via IFN-γ production, was able to exacerbate passive disease through mechanisms that directly influence the extent of antibody and complement binding to the neuromuscular junction.

To determine what role NK cells play in exacerbation of passive transfer EAMG in response to IL-12, we first examined the effect of IL-12 treatment on passive transfer EAMG in NK cell-depleted C57BL/6J (B6) mice. The aim of these experiments was to ultimately clarify if NK cells are the source of disease enhancing IFN-γ. This was accomplished through depletion of NK cells by administration of the mouse anti-NK1.1 monoclonal antibody, mAb PK136. Next, we administered IL-12 and mAb D6 in order to passively induce EAMG and performed bleeding and serum harvesting on individual mice within these groups in order to measure serum IFN-γ levels using 96-well plate

ELISA assays. Finally, analysis of IL-12 effects on muscle tissue and the disease process were further examined in control and NK cell-depleted mice by performing histology and immunofluorescence on mouse diaphragm muscle samples.

To determine what role T cells and NKT cells play in exacerbation of passive transfer EAMG in response to IL-12, we first examined the effect of IL-12 treatment on passive transfer EAMG in TCRβ/TCRδ double knock-out (KO) mice (TCRβδKO). In this way, we attempted to clarify whether other Th1 cells, possibly NKT cells ($CD3^+$ $NK1.1^+$ cells), are the source of disease enhancing IFN-γ or if NK cells ($CD3^-NK1.1^+$ cells) are the source the IFN-γ. TCRβδ double KO mice ($TCR\beta\delta^{-/-}$ mice) are known to produce normally functioning B cells and NK cells but lack any functioning T cells, including $NK1.1^+$ T cells, which are also known as NKT cells (8). To do so, we first administered IL-12 and mAb D6 to $TCR\beta\delta^{-/-}$ mice in order to induce passive EAMG. Again, these mice were subjected to bleeding and serum harvesting for the purpose of measuring serum IFN-γ levels via 96-well plate ELISA assays. From there, analysis of IL-12 effects on muscle tissue and the disease process were further examined in control and NK cell-depleted mice using histology and immunofluorescence on mouse diaphragm muscle samples harvested from the treated mice.

Our next approach involved attempts to determine the effects of IL-12 and IFN-γ on gene expression in muscle tissue *in vivo* and to examine changes that correlate with the level of antibody pathogenicity. This was done by performing gene array analysis of whole muscle responses in B6 mice differentially treated with either PBS, IL-12, PBS + mAb D6, or IL-12 + mAb D6. The resulting gene array data was then analyzed with a

particular emphasis given to gene products that are known to participate in pathogenesis of MG such as classical complement pathway inhibitory genes, skeletal muscle-specific genes, natural killer cell-specific genes, and chemotactic genes (various chemokine and chemokine receptor genes). This experimental process involved first inducing passive disease with IL-12 and mAb D6 in conjunction with treatment controls and then harvesting diaphragm muscle in order to isolate and purify whole RNA from the individual mouse diaphragm muscle samples. The gene array analysis, performed at the Cleveland Clinic's Lerner Research Institute Genomics Core, allowed us to analyze 23,000 different genes and implement a "fishing" approach in hopes that this analysis would yield potential "hits" (genes with 2X up/down changes in expression) that could serve as to identify additional genes correlating with disease that can later be confirmed by real time RT-PCR.

1.2 Myasthenia gravis (MG) and experimental autoimmune myasthenia gravis (EAMG):

Myasthenia gravis (MG) is an autoimmune disease caused by the production of antibodies to the nicotinic acetylcholine receptor (AChR). The binding of anti-AChR antibodies to their targets at the post-synaptic membrane of the neuromuscular junction (NMJ) results in muscular weakness due to decreased neuromuscular transmission. MG is one of the best characterized and prototypical antibody-mediated autoimmune diseases as the target antigen, the nicotinic acetylcholine receptor, has been well defined (2). Experimental autoimmune myasthenia gravis (EAMG) in B6 mice, induced by repeatedly immunizing with *Torpedo* AChR (TAChR) in complete Freund's adjuvant (CFA), has

proven to be particularly useful for studying the pathogenic mechanisms that cause MG in humans (9, 10). Interestingly, it was shown that the dominant *Torpedo* AChR T cell epitope does not cross react with the dominant mouse AChR T cell epitope, whereas the same is not true for the main immunogenic region (MIR) of TAChR recognized by mouse B cells in which cross reactivity is seen (11). The main pathogenic processes thought to be involved are summarized in Figure 1 and are as follows: (a) binding of specific antibody and activation of complement at the NMJ; (b) accelerated degradation of AChR molecules cross-linked by anti-AChR antibodies (known as "*antigenic modulation*"); and (c) functional blockade of the AChR (known as "*steric hindrance*") (1).

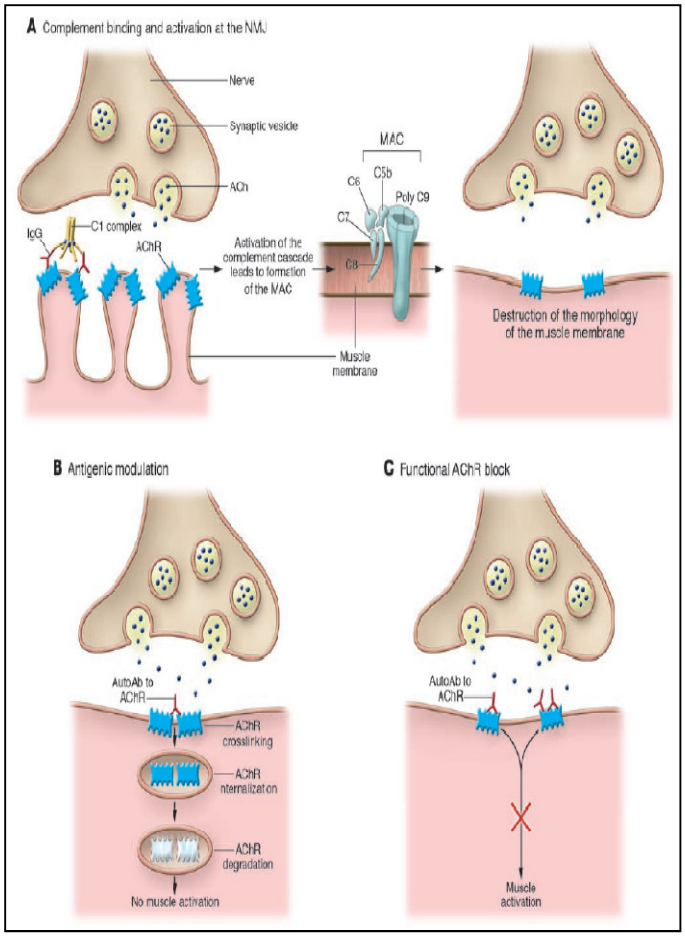

Figure 1: Effector mechanisms of anti-AChR antibodies (1)

1.3 Passive transfer EAMG model using the anti-AChR monoclonal antibodies mAb 35 and mAb D6:

Many of the findings referenced in this introduction have been derived from EAMG studies involving immunization with purified, whole *Torpedo* AChR known as "active induction". In this manner, the development of disease presents with a biphasic autoimmune response, where an early acute phase ("induction phase") is followed by a chronic phase ("effector phase") (12). In mice, EAMG induction using the active induction method requires multiple injections of TAChR to induce antibody production and disease. A proposed reason for this is the inherently high "safety factor" known to be possessed by mice as compared to humans and rats (6, 13, 14). The "safety factor" is a mechanism intended to protect neuromuscular transmission and is defined as the measured excess of released neurotransmitter over that required to trigger an action potential (13).

Due to the large safety factor observed in mice during active EAMG, most studies involving "passive transfer" of anti-AChR antibodies have been performed in rats. Passive transfer of autoimmune serum containing anti-AChR antibodies was shown to induce EAMG in rats, though this passive transfer method did not induce endogenous antibody production or chronic autoimmune disease (12). It has also been described that the passive transfer of antibodies targeting the main immunogenic region (MIR) were capable of generating a disease state very similar to that seen when immunizing with whole, purified AChR (15). In regards to mouse models, additional passive transfer experiments have been performed in which serum IgG from human MG patients (16) or serum from diseased mice (17) has been injected ("transferred") into healthy mice that result in disease. Taken together, the passive transfer of anti-AChR antibodies serves as an appropriate method for studying EAMG and its pathogenic mechanisms.

Previous research from our lab has focused on developing a simplified system to study EAMG pathogenesis by incorporating passive transfer immunization of anti-AChR antibodies specific to the main immunogenic region (MIR), the alpha subunit, of the acetylcholine receptor. Originally this was performed using a fixed amount of the rat anti-AChR monoclonal antibody, mAb 35. MAb 35 is a rat IgG1 that recognizes the main immunogenic region of the AChR α-subunit (18). MAb 35 does not block binding of agonists to the AChR or inhibit the function of the receptor (19) and therefore is commonly used for passive transfer to rats (20, 21) and to mice (22). Due to the high safety factor attributed to mice, it was initially thought that this disease induction regimen required additional priming with the *Torpedo* AChR α-chain sequence 146-162, known to be the dominant T cell recognition epitope. It was shown by Sunghan Yim, a previous member of the Katherine A. Wall Laboratory at the University of Toledo, that upon immunization of B6 mice with the *Torpedo* α146-162 peptide and mAb 35 that these mice exhibited EAMG symptoms as measured by a reduction in their individual hang times (23). Therefore, mAb 35 was proven to be a useful and effective tool for use in the immunization of mice for the purpose of studying EAMG development.

Since mAb 35 is a rat monoclonal antibody, it was possible that the results observed in previous studies were due to a xenogeneic effect and were not representative of an endogenously produced anti-AChR antibody. In order to circumvent this possibility, we attempted to locate a mouse monoclonal anti-AChR antibody and were able to obtain the mouse anti-human AChR hybridoma D6 from Dr. Angela Vincent (The University of Oxford, Oxford, England) (24). As I show in the Results section, I have performed passive transfer experiments in C57BL/6 mice using the mouse D6

monoclonal antibody. MAb D6, which is also identified as mAb399, is a mouse IgG2a antibody made against human AChR that binds strongly to mouse AChR (24). The monoclonal D6 antibody has been shown to bind to the muscle AChR of mice and cause limb weakness with loss of endplate AChR, which is thought to be caused by antigenic modulation and complement activation. It was shown to bind to the alpha subunit of the AChR in a region similar to the MIR defined by rat monoclonal anti-AChR antibodies (the α1 subunit). Interestingly, while mAb D6 has been shown to compete for binding to human AChR with antibodies from the serum of myasthenia gravis patients, it fails to inhibit toxin or agonist binding to the AChR (24). Therefore, mAb D6 is a superior antibody for performing passive transfer EAMG studies in mice as it is derived from the same species and specifically and firmly binds to the MIR of the AChR to facilitate the development of disease symptoms. By incorporating passive transfer using mAb D6 into our EAMG studies, we can effectively study the "effector phase" of the disease while using a fixed amount of antibody and avoiding any added complications from cytokine effects on antibody production. Simplifying the system in this manner will allow us to determine what cells are involved in the exacerbation of disease and ultimately identify targets that could lead to the development of novel therapeutic strategies for the treatment of human myasthenia gravis.

1.4 Antibody characteristics of myasthenia gravis MG and EAMG:

Over half of the anti-AChR antibodies produced in MG and EAMG are directed against the extracellular end of the AChR α1-subunits, the location designated as the MIR. When bound to the MIR, these anti-AChR antibodies do not interfere with

acetylcholine binding or AChR functionality, however they do elicit the binding of early complement components and instigate antigenic modulation (25). Diagnosis of human MG is frequently delayed or missed by practitioners due its rarity in the population and the often fluctuating levels of muscular weakness seen in patients (1). These fluctuating episodes of MG can be aggravated by simultaneous infections and their subsequent generation of inflammatory cytokines, which have been shown to increase the titers of anti-AChR antibodies in infected MG patients.

However, our previous research has shown that inflammatory cytokines can increase disease even when a fixed amount of antibody is used. As I show in the Results section, IFN-$\gamma^{-/-}$ mice fail to exhibit passive disease when pre-treated with IL-12 and passively immunized with a fixed amount of antibody. This same disease-induction regimen produces considerable disease in normal B6 mice. Therefore, the presence of IFN-γ is necessary in disease induction and can influence the environment of the muscle to tailor the disease process by increasing the pathogenesis of a bound antibody. By determining how the muscle is responding in this manner and working to inhibit this response, novel therapeutic targets could be developed with the ultimate goal of designing treatments designed for these novel targets. In this way, a clinician could bypass the current approaches of attempting to limit anti-AChR antibody production and instead reduce the negative impact that these antibodies will generate at their target sites.

1.5 Cytokines: Bridging the gap between innate and adaptive immunity:

As part of the innate resistance mechanisms of the immune system, interleukin-12 (IL-12) plays a central role in the immune response to a variety of microorganisms (26).

Known as a cytokine capable of bridging the early responses of the innate immune system with the more highly developed responses of the adaptive immune system (27), IL-12 was also shown to be important during the later stages of an autoimmune response in a mouse model of inflammatory colitis (28). While IL-12 is produced mainly by activated monocytes, the cytokine can also be produced by activated dendritic cells, B cells, and keratinocytes. Once secreted, IL-12 has been shown to enhance the activation, proliferation, IFN-γ secretion level, and cytolytic activity of natural killer (NK) and T cells (29).

As interferon-gamma (IFN-γ) is known to have a very short half-life in circulation, it is much easier to indirectly induce IFN-γ production *in vivo* by treating mice with IL-12, which has a long half-life in circulation. However, since a number of cells are known to be affected by IL-12 treatment, it is essential to determine the definitive cell type responsible for disease enhancement. To accomplish this, we have utilized mice treated to selectively eliminate different cell populations prior to disease induction. By comparing paralleled elimination of potential disease-enhancing cell types, we were able to ultimately identify the cell population responsible for the enhancement of disease seen. From there, this outcome allowed us to study the reasons for disease enhancement more specifically.

1.6 T-helper type 1 (Th1) cells and IL-12 in MG and EAMG:

Interleukin 12 (IL-12) is a heterodimeric cytokine which plays a pivotal role in promoting type 1 T helper cell (Th1) responses. The primary role of IL-12 in the immune system revolves around its ability to polarize T cell responses towards the Th1

phenotype. These Th1 cells, characterized by their ability to secrete interferon-gamma (IFN-γ), promote the synthesis of complement-fixing antibody isotypes and the elimination of intracellular pathogens (30). In addition to inflammatory colitis (28), treatment with IL-12 has also been shown to enhance disease in autoimmune disease models of collagen-induced arthritis (31), experimental autoimmune encephalomyelitis (32), and insulin-dependent diabetes mellitus (33, 34). In accordance with these findings, our lab and others have shown that IL-12 treatment has the ability to enhance disease in EAMG (5, 6). In addition, IL-$12^{-/-}$ mice are resistant to EAMG development (6, 35), further emphasizing the role IL-12 plays in disease enhancement. These studies have focused on the effect that IL-12 treatment has on Th1 cell responses and antibody production during the induction phase of the disease. One study revealed that upon immunization with protein antigens, IL-12 facilitated an increase in the *in vivo* synthesis of complement-fixing IgG subclasses (36).

The role of T cells as key players in human MG has been well documented (1), where patients have exhibited functional AChR-specific $CD4^+$ T cells in their blood and thymus (3) with symptom improvement after subsequent thymectomy (37) or anti-CD4 antibody treatment (38). In EAMG, a similar importance for the role of T cells has been elucidated using bm12 mice. The bm12 mouse strain is identical to the B6 mouse strain except for a mutation in the I-A^b β chain gene, with the mutation resulting in a three amino acid substitution in the peptide binding groove of the I-A^b molecule (39). This alteration to the I-A^b biding site changes the dominant T cell epitope repertoire and induces resistance to EAMG development (40-42). However, after strong immunizations,

it was demonstrated that EAMG can be induced in bm12 mice and is accompanied by the generation of anti-AChR antibodies (43).

Others have focused on the role of IL-12 on EAMG induction in the bm12 mouse strain. Pre-treatment of bm12 mice with IL-12 prior to TAChR immunization did not induce disease comparable to that seen in control B6 mice (5). Surprisingly, the study found that the EAMG-resistant bm12 mice produced the same amount and isotype distribution of anti-AChR antibodies as did the EAMG-sensitive IL-12 treated B6 mice. More interestingly, the researchers also observed that even after IL-12 treatment, the bm12 mice produced very little IFN-γ as compared to the B6 mice. This was a possible indication of the importance of IFN-γ levels and their ability to influence how much muscle damage an anti-AChR antibody can generate. While it's entirely possible that the levels of other cytokines were also out-of-balance between the IL-12 treated bm12 and B6 mice, these findings are compelling as they shed light onto the potential impact that downstream Th1 responses can elicit in the presence of bound anti-AChR antibody.

1.7 The role of IFN-γ in MG and EAMG:

Previous research has underlined the importance of the Th1 cytokine IFN-γ in EAMG development. IFN-γ was shown to be required in order to induce EAMG (44) while IFN-γ-deficient (IFN-$\gamma^{-/-}$) mice were shown to be resistant to EAMG development and exhibited greatly reduced levels of both IgG1 and IgG2a antibodies specific for mouse AChR (45). As I show in the Results section, IFN-$\gamma^{-/-}$ mice fail to exhibit passive disease when pre-treated with IL-12 and passively immunized with a fixed amount of

anti-AChR antibody while B6 mice do in fact develop striking sickness. Therefore, the presence of IFN-γ is necessary in disease induction and can clearly increase the pathogenesis of bound antibody. When transgenically expressed at the neuromuscular junction, IFN-γ provoked an autoimmune humoral response similar to myasthenia that included infiltration of mononuclear cells and deposition of autoantibody at the motor end plates (46). However, in this case, there was no detectable presence of mouse AChR-specific antibodies. This finding is extremely interesting in that it showcases the powerful potential of IFN-γ to amplify an autoimmune response within the microenvironment of the NMJ although no specific anti-AChR antibodies were present. It can be rationally suggested that if a Th1-mediated autoimmune episode were initiated in response to anti-AChR antibody, such as in EAMG, that any IFN-γ localized within the NMJ would have profound effects on the severity of disease that mimic that seen in the previously mentioned study.

1.8 Other Th1-linked influences on MG and EAMG: interleukin 18 (IL-18), natural killer (NK) cells, and transforming growth factor-beta (TGF-β):

It should be noted as well that in human MG, in addition to the Th1 cytokine interleukin 18 (IL-18), the levels of IFN-γ in the serum were correlated with disease severity. In general, patients showed more severe disease with elevated serum levels of anti-AChR antibody , IFN-γ, and IL-18 as compared to less severe disease with lower serum levels of anti-AChR antibody, IFN-γ, and IL-18 (47). Significantly, IL-$18^{-/-}$ mice were shown to be resistant to EAMG (48) and this was determined to be due to the absence of a required NK cell-driven Th1 response and anti-AChR antibodies. Treatment

with anti-IL-18 antibodies was also shown to suppress ongoing EAMG in rats (49). IL-18, which was first described in 1989 as "interferon-γ inducing factor" (50), has the ability to induce IFN-γ production primarily in the context of a second signal derived from IL-12 (51-54). Of importance is the fact that IL-12 enhances expression of the IL-18 receptor by NK and T cells and therefore allows greater synergy with IL-18 in terms of IFN-γ production. This heightened effect on IFN-γ production due to IL-18 receptor up-regulation is witnessed more profoundly in NK cells (52, 53, 55-58). In fact, it is thought that T cells, NK cells, and NKT cells are the primary producers of IFN-γ in response to IL-12 (59, 60). Due to the fact that IFN-γ is distinguished as a key mediator of innate immune function (61), it is not surprising that one of the main sources of IFN-γ production in response to IL-12 stimulation are the innate natural killer cells.

There is support for a role played by natural killer cells in human MG, as evidenced by the identification of an expanded and dysfunctional NK cell subset described in an ocular MG patient (62). Interestingly, this patient also exhibited elevated serum IL-18 and IFN-γ and decreased transforming growth factor beta (TGF-β) levels compared to control patients prior to the initiation of immunosuppressive therapy. As mentioned previously, NK cells have also been shown to be involved in EAMG development (48). It was shown that while IL-18$^{-/-}$ mice were resistant to EAMG, this resistance could be reversed by reconstituting the IL-18$^{-/-}$ mice with normally functioning NK cells from RAG-1$^{-/-}$ mice. This reversal was determined to be the result of restored IFN-γ production by the transferred NK cells, as NK cells transferred from RAG-1$^{-/-}$IFN-γ$^{-/-}$ mice could not reverse EAMG resistance. Once again, the EAMG studies previously discussed all relied on immunizing animals with *Torpedo* AChR and studying the disease

during and after the induction phase. It is reasonable to believe that in our passive transfer model, where a precise amount of anti-AChR antibody is administered and the effector phase is the focus, the Th1-driven autoimmune response characteristic of EAMG development may arise from NK cell-derived IFN-γ.

Similar to the case of ocular MG referenced previously (62), Shi et al. (48) found that the level of TGF-β production was reduced in IL-18$^{-/-}$ mice upon reconstitution with normal NK cells and reversal of EAMG resistance. The cytokine TGF-β is essential for the differentiation of regulatory T cells (TRegs) (63-65) and is also known to be a potent inhibitor of Th1 and Th2 cell-mediated responses (66, 67), with TGF-β conferring protection against EAMG development (68). It was shown that IL-2 activated NK cells are able to prevent the development of graft-versus-host disease (GVHD) when transferred into recipient mice prior to allogeneic bone marrow transplant (BMT) (69). This resistance could be overcome by neutralizing *in vivo* TGF-β function by injection of anti-TGF-β antibodies in conjunction with NK cell transfer. It was determined that the protective effect derived from donor NK cells is dependent on localized TGF-β mediation, as systemic administration of exogenous TGF-β separately from NK cell transfer caused more rapid GVHD development. More recently, the tissue-specific homing and *in vivo* expansion of these donor-derived, IL-2-activated NK cells was investigated in a murine BMT model and it was found that NK cells trafficked to both lymphoid and non-lymphoid tissues in a CD62L-dependent manner, while IL-2 enhanced their ability to proliferate within these tissues (70). More interestingly, newly published research described an expanded population of IL-12-dependent NK cells that developed independently of IL-15 signaling (or any other γ_c cytokine) in a mouse cytomegalovirus

(MCMV) model using either IL-15$^{-/-}$IL-15Ra$^{-/-}$ or Rag2$^{-/-}$IL-2Rγ$^{-/-}$ transgenic mice previously thought to fully lack NK cells (71). Taken together, these findings support the idea that in passive transfer EAMG, pre-treatment with IL-12 could lead to a priming and expansion of NK cells, possibly via down-regulation of TGF-β, that are capable of entering the muscle microenvironment and responding quite aggressively to anti-AChR antibody presence by producing IFN-γ or causing antibody-dependent cell-mediated cytotoxicity (ADCC).

1.9 Participation of the target tissue in autoimmune disease:

While often overlooked, the idea of the target tissue playing a role in autoimmune disease progression was supported by the finding that muscle tissue from MG patients showed elevated expression levels of IP-10 and CXCR3 (72). In accordance, human myocytes treated with IFN-γ expressed increased levels of adhesion molecules and MHC molecules (73-75). Similarly, when treated with IFN-γ, rat myocytes responded by producing elevated levels of the chemokines IP-10, MCP-1, and RANTES, the adhesion molecule ICAM-1, and class II MHC molecules (76-78). Rat skeletal muscles cells responded to anti-AChR antibodies by up-regulating expression of MCP-1 both in vitro and in vivo (79). When studying the gene expression effects that anti-AChR antibody can exert on muscle tissue, the researchers failed to investigate genes that may be up-regulated based on the pathogenicity of antibody binding. Instead, they focused on genes that are known to be involved in antigen presentation and T cell recruitment, trafficking, and function. Based on the sum of these findings, it would be ill-advised to think of

muscle tissue as simply an innocent bystander in the disease progression of MG and EAMG.

1.10 The role of complement in EAMG:

The classical complement pathway (CCP) has been identified as the primary component of the complement system in EAMG (80). Mice deficient for complement factors C3, C4, or C5 are resistant to EAMG development (81). This is further supported by research showing that the administration of a soluble complement inhibitor (sCR1) protects against EAMG (82-84). It has also been shown that administration with anti-C6 antibody prevents EAMG development (85). The mechanism of resistance requires that the functioning complement inhibitors be present in the immediate vicinity of the muscle. Mice lacking the complement inhibitor decay accelerating factor (DAF) were shown to be more susceptible to EAMG than control animals (86). EAMG resistance in many knock-out models is associated with decreased production of IL-6 and complement component C3, highlighting their role in the disease process. IL-6 is the main cytokine involved in C3 production in the liver (87), and accordingly, IL-$6^{-/-}$ mice are resistant to EAMG and exhibit reduced C3 production capacity (88). Also of importance, Fc$\gamma$$RIII^{-/-}$ mice are resistant to EAMG and they too display lowered levels of IL-6 and C3 production (83).

Chapter 2

Research Design and Methods

2.1 Mice:

2.1.1 Purchasing of mice and housing

Six to eight week old female C57BL/6 (B6), male and female B6.12957-Ifn-γ^{tm1Ts} (IFN-$\gamma^{-/-}$) mice, and female B6.129P2-Tcrb^{tm1Mom}Tcrd^{tm1Mom}/J (TCR$\beta\delta^{-/-}$) mice were obtained from Jackson Laboratory (Bar Harbor, ME). All mice were maintained in the animal facility at the University of Toledo under specific pathogen-free environment. All mouse experiments were performed under approval of the Institutional Animal Care and Use Committee (IACUC). Mice used in all assays were uniquely and individually identified by ear-punch prior to the start of any experiments.

2.1.2 Outline of mouse groups per assay

1.) IFN-γ role determination assay

- Group 1, [+PBS]: Four male IFN-$\gamma^{-/-}$ mice
- Group 2, [+IL-12]: Three male and three female IFN-$\gamma^{-/-}$ mice

2.) Natural killer cell depletion/ passive EAMG assay

•Group 1, [-NK, +PBS]: Six female B6 mice

•Group 2, [-NK, +IL-12]: Four female B6 mice

•Group 3, [B6, +PBS]: Six female B6 mice

•Group 4, [B6, +IL-12]: Four female B6 mice

•Group 5, [TCRβδ$^{-/-}$, +PBS]: Four female TCRβδ$^{-/-}$ mice

•Group 6, [TCRβδ$^{-/-}$, +IL-12]: Four female TCRβδ$^{-/-}$ mice

1.) Gene expression analysis assay

•Group 1, [+PBS]: Two female B6 mice

•Group 2, [+IL-12]: Two female B6 mice

•Group 3, [+mAb D6]: Two female B6 mice

•Group 4, [+IL-12 & mAb D6]: Two female B6 mice

2.2 Monoclonal antibody production and purification:

2.2.1 Anti-AChR monoclonal antibody D6

The anti-AChR antibody, mAb D6, was prepared from culture medium of D6 producing cells (24) that were obtained from Dr. Angela Vincent (The University of Oxford, Oxford, England) that were subcloned and grown in sterile Corning® 75 cm^2 tissue culture flasks in 1X DMEM (CellGro, Mediatech Inc., Manassas, VA) with 10% FBS (Atlanta Biologicals, Lawrenceville, GA). Prior to usage, culture medium was supplemented with thawed, mixed aliquots of sterile medium additions (6 mg/L of folic acid, 36 mg/L of L-asparagine, 116 mg/L of L-arginine, 216 mg/L of L-glutamine, and 110 mg/L of sodium pyruvate).

2.2.2 Anti-NK1.1$^+$ monoclonal antibody PK136

The anti-NK1.1$^+$ antibody, mAb PK136 (89), was prepared from culture medium of PK136 producing cells that were obtained from Dr. Pippa Marrack (National Jewish Center for Immunology and Respiratory Medicine, Denver, CO). PK136 hybridoma cells were grown in sterile Corning® 75 cm^2 tissue culture flasks in 1X DMEM (CellGro, Mediatech Inc., Manassas, VA) with 10% FBS (Atlanta Biologicals, Lawrenceville, GA). Prior to usage, culture medium was supplemented with thawed, mixed aliquots of sterile medium additions (6 mg/L of folic acid, 36 mg/L of L-asparagine, 116 mg/L of L-arginine, 216 mg/L of L-glutamine, and 110 mg/L of sodium pyruvate).

2.2.3 Antibody isolation

Cell culture supernatants were pooled and transferred to sterile 50 ml conical tubes prior to centrifugation for 10 minutes at 2,250 RPM and 4°C to remove heavier cellular debris. The supernatants were then transferred to sterile 250 ml plastic jars and centrifuged for 20 minutes at 10,000 RPM and 4°C to remove any remaining visible cellular debris. Culture supernatants were then carefully filtered through Corning® 44 mm pre-filters (Corning Inc., Corning, NY) prior to 0.22 µm sterile filtration using a SteriCup® (Millipore, Bedford, MA). Sterile culture supernatants were transferred to sterile culture jars, sealed, and stored at 4°C until affinity column chromatography purifications were performed.

2.2.4 Affinity column chromatography antibody purification

For each antibody, a separate 5 ml Pierce® Protein G Chromatography Cartridge (Pierce Protein Research Products, Rockford, IL) was used to purify the antibody from cell culture supernatants using the buffers and reagents suggested and following the protocol provided with the column. Purified antibody fractions were collected using a

fraction collector and were pooled in sterile 15 ml conical tubes and stored at 4°C. A small sample of the pooled fractions was removed and diluted at 1:10 in PBS and subjected to UV-VIS spectrophotometry (Shimadzu® BioSpec-1601, Shimadzu Scientific Instruments, Columbia, MD) 280nm analysis in order to measure pre-dialysis antibody concentrations.

2.2.5 Dialysis and concentration of purified antibody fractions

Pooled, purified antibody fractions were dialyzed against 1 liter volumes of 1X PBS for two consecutive 24-hour time periods at 4°C. After dialysis, purified mAbs were concentrated in sterile 1X PBS with an Ultrafree-15® centrifugal filter device (Millipore, Bedford, MA). Concentrated antibody volumes were sterilized using 0.22 µm, 25 mm syringe filters (ThermoFisher Scientific Inc., Waltham, MA) and sterile 5 ml syringes (Becton-Dickinson Inc., Franklin Lakes, NJ). Small samples of sterile antibody volumes were removed, diluted at 1:60 in PBS, and their 260nm/280nm ratios were measured using spectrophotometry (Shimadzu® BioSpec-1601, Shimadzu Scientific Instruments, Columbia, MD) to determine antibody purity and quantity. Purified, concentrated antibodies were then aliquoted between sterile 1.5 ml plastic tubes and stored at 4°C until use.

2.2.6 Additional purity and quality assessments

The purity of mAb D6 was kindly tested by Dr. James Slama using SDS-PAGE gel electrophoresis on a 12% gel. Two-fold serial dilutions of mAb D6 were performed and can be seen in the lanes labeled 1-3 of Figure 2. Pierce® Perfect Protein Markers (Pierce Protein Research Products, Rockford, IL) were used to measure antibody product band sizes. Reactivity with their specific cellular targets was verified by flow cytometry using C57BL/6 mouse splenocytes for mAb PK136 and the acetylcholine receptor-expressing TE671 cell culture line (CRL-8805, ATCC, Rockville, MD) for mAb D6.

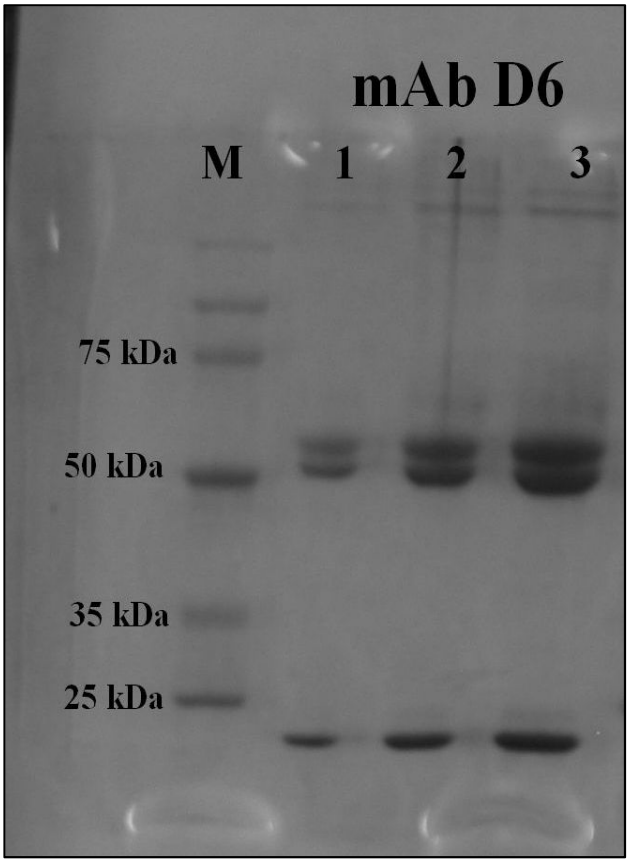

Figure 2: SDS-PAGE gel purity assessment of mAb D6

2.3 IL-12 purification and properties:

Recombinant murine IL-12 (rmIL-12) was purified by a previous member of the Wall Laboratory (Mariola Klis) according to published procedures (90) from transfected Chinese Hamster Ovary (CHO) cells provided by Wyeth Research (Cambridge, MA). Purified rmIL-12 contained only p40 and p35 by SDS-gel electrophoresis and had the

same specific activity as commercial mIL-12 (Atlanta Biologicals, Lawrenceville, GA) in a ConA blast proliferation assay (91).

2.4 Monoclonal antibody PK136-mediated cell depletion:

2.4.1 Injection of mAb PK136

Purified mouse anti-mouse anti-NK1.1 [IgG2a subclass] monoclonal antibody (mAb PK136) from the PK136 hybridoma clone was diluted in sterile PBS to the desired concentrations for individual assays. The monoclonal anti-$NK1.1^+$ antibody (mAb PK136), when used for cell depletion, is known to bind to and cause the destruction of both $CD3^-NK1.1^+$ natural killer (NK) cell and $CD3^+NK1.1^+$ natural killer T (NKT) cells. For pilot cell depletion assays, 200 µl of mAb PK136 [1.5 mg/ml] was injected intraperitoneally into 8 week old, female B6 mice. Control mice received an equivalent volume of sterile PBS via intraperitoneal injection. For the passive EAMG cell depletion assays performed, ten mice received one intraperitoneal injection of 100 µl of mAb PK136 [3 mg/ml] as the "main" injection with two subsequent, spatially timed "booster" intraperitoneal injections of 100 µl of mAb PK136 [1.5 mg/ml]. For all injections, sterile 1 ml syringes (Becton-Dickinson Inc., Franklin Lakes, NJ) and sterile 25G⅝ needles (Becton-Dickinson Inc., Franklin Lakes, NJ) were used. The overall injection timeline containing dosage amounts for each assay is located in further detail in Research Design and Methods, Section 2.8.3.

2.4.2 Measuring mAb PK136-mediated cell depletion efficiency

For all cell depletion assays, spleens were immediately removed from euthanized mice previously treated with mAb PK136 or control mice and homogenized into a cell suspension in cold PBS/BSA [1 mg/ml] using a glass tissue homogenizer. Splenocyte suspensions were appropriately washed and counted prior to transfer into plastic, V-bottomed FACS tubes (Sarstedt AG & Co., Germany) at 10^6 cells per tube. Appropriate washing and staining steps were carried out on an individual basis, as specific staining conditions varied from tube-to-tube. Table 1 shows the staining conditions used during flow cytometry:

Table 1: Staining conditions for cell depletion efficiency flow cytometry assays

Sample	1° Stain	2° Stain
1.) Cells Only	100 µl PBS/BSA	100 µl PBS/BSA
2.) DyLight™488 Control	100 µl PBS/BSA	100 µl DyLight™488 (1:100 dilution)
3.) FITC Mouse IgG2a Isotype Control	100 µl PBS/BSA	100 µl FITC Mouse IgG2a [10 µg/ml]
4.) PE Rat IgM Isotype Control	100 µl PBS/BSA	100 µl PE Rat IgM [1 µg/ml]
5.) In-House mAb PK136 + DyLight™488	100 µl mAb PK136 [10 µg/ml]	100 µl DyLight™488 (1:100 dilution)
6.) eBioscience® FITC anti-NK1.1	100 µl PBS/BSA	100 µl eBioscience® FITC anti-NK1.1 [5 µg/ml]
7.) eBioscience® PE anti-DX5	100 µl PBS/BSA	100 µl eBioscience® PE anti-DX5 [5 µg/ml]
8.) eBioscience® FITC anti-NK1.1 + eBioscience® PE anti-DX5 Dual Stain	100 µl eBioscience® FITC anti-NK1.1 [5 µg/ml]	100 µl eBioscience® PE anti-DX5 [5 µg/ml]

In regards to splenocyte staining, cell surface protein markers tested for included CD49b (α2 integrin) and NK1.1 (the target of mAb PK136). In general, CD49b was used as a marker for NK cells. PE-conjugated anti-DX5 monoclonal rat IgM antibody, from hybridoma clone DX5, was used to confirm CD49b expression (eBioscience™ Inc., San Diego, CA). PE-conjugated Rat IgM (eBioscience™ Inc., San Diego, CA) was used as an isotype control for the PE-conjugated anti-DX5 monoclonal antibody. NK1.1 was also used as a marker for NK cells. In-house PK136 (anti-NK1.1), was used to selectively bind NK1.1. DyLight™ 488-conjugated AffiniPure Goat Anti-Mouse IgG, Fc_γ Subclass 2a Specific monoclonal antibody (DyLight™488, Jackson ImmunoResearch Laboratories, Inc., West Grove, PA) was used to confirm PK136 binding to NK1.1 and also as a control.

PE-conjugated stains were run in the FL2-H channel, while FITC-conjugated stains and DyLight™488 were run in the FL1-H of a Becton-Dickinson® FACSCalibur™ flow cytometer (Becton-Dickinson Inc., Franklin Lakes, NJ). The same flow cytometer channel setting values were used from assay-to-assay in order to maintain consistency. These were as follows: for forward scatter (FSC) - E02/2.80/Linear scale; for side scatter (SSC) – 459/1.00/Linear scale; for FL1 – 665/-/Log scale; and for FL2 – 745/-/Log scale. A total of 125,000 counts were compiled for each sample tube tested during both mAb PK136-mediated cell depletion efficiency flow cytometery assays performed.

2.4.3 Flow cytometry image and data generation

All flow cytometry images and corresponding data were generated using CellQuest® software (Becton-Dickinson Inc., Franklin Lakes, NJ) and imported into

Microsoft® Word or Microsoft® PowerPoint software programs (Microsoft Corp., Redmond, WA). The percentage of $NK1.1^+$ and $CD49b^+$ cells were calculated by analyzing a specific region uniformly applied to all corresponding histograms. Average fluorescence intensity for each stain was derived from the geometric mean fluorescence data obtained using the same regions. Differences in expression levels were quantified by subtracting the background expression levels generated by the isotype controls for each staining series.

2.5 Injection of IL-12:

A frozen aliquot of concentrated sterile recombinant murine interleukin 12 (rmIL-12) was removed from storage at -80°C and diluted in sterile PBS with 1% normal syngeneic mouse serum (PBS/NMS) to the needed concentration in a bulk volume. In order to minimize activity loss of the stock rmIL-12, the large diluted volume was then sterily aliquoted at the volumes needed for injection and re-frozen at -80°C. Prior to injection, frozen "ready to use" aliquots were removed from storage at -80°C, thawed, and re-suspended. Mice received daily intraperitoneal injections of 100 µl of rmIL-12 [10 µg/ml] over a span of five consecutive days using sterile 1 ml syringes (Becton-Dickinson Inc., Franklin Lakes, NJ) and sterile 25G⅝ needles (Becton-Dickinson Inc., Franklin Lakes, NJ). Control mice received five corresponding intraperitoneal injections of 100 µl of sterile PBS/NMS. In order to minimize the risk of cross-contamination, the sterile needles used for injecting were replaced with fresh needles after each mouse group was injected. Mice weights were recorded using an electronic balance prior to the first IL-12 and PBS/NMS injections and on each day during the IL-12 treatment regimen.

2.6 Injection of mAb D6:

Stock volumes of the mouse anti-human AChR [IgG2a subclass] monoclonal antibody D6 (mAb D6) were removed from storage at 4°C and diluted to the desired concentration using sterile PBS. For all assays, mice received one 100 µl injection of mAb D6 [30 mg/ml] intraperitoneally using sterile 1 ml syringes (Becton-Dickinson Inc., Franklin Lakes, NJ) and sterile 25G⅝ needles (Becton-Dickinson Inc., Franklin Lakes, NJ).

2.7 IFN-γ role determination assay:

2.7.1 Injection timeline for IL-12 treatments

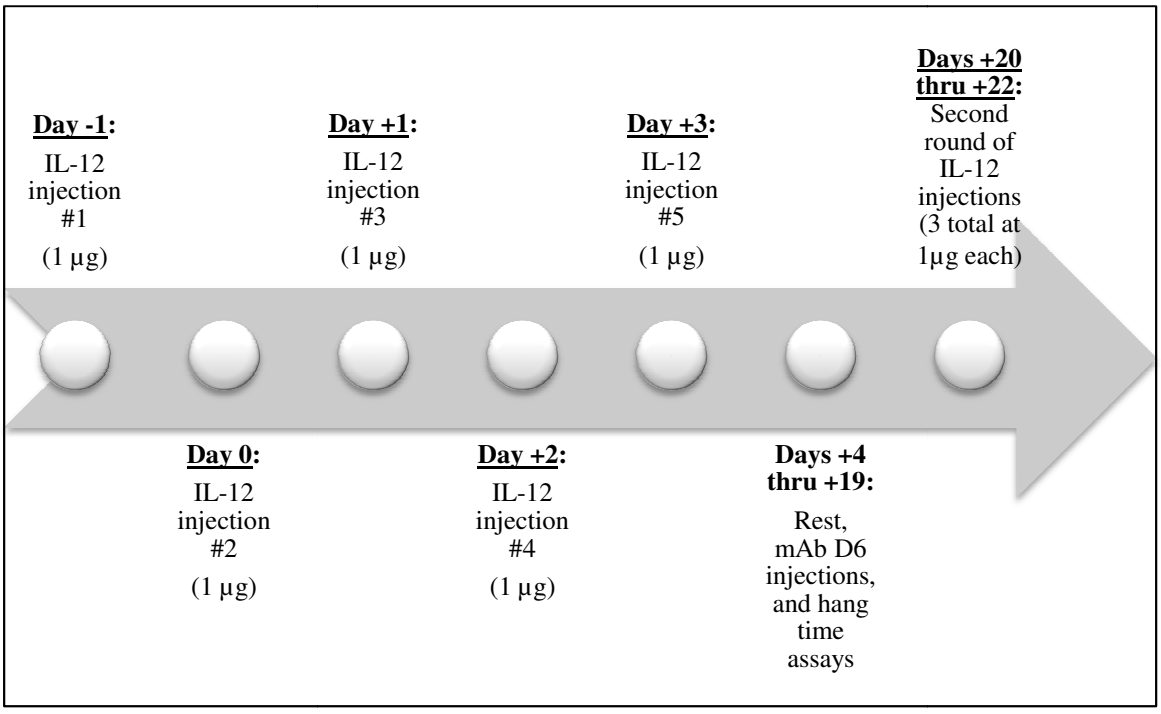

Figure 3: Timeline of all IL-12 injections performed during IFN-γ role determination assay

As can be seen in Figure 3, all mice received the first of five consecutive IL-12 injections (1 µg) on Day -1, with the remaining IL-12 injections occurring every 24 hours on Days 0 thru +3. Therefore, the last injection of IL-12 on Day +3 marked the conclusion of the first IL-12 treatment round of the overall assay. Control mice in received corresponding injections at all time points consisting of an equivalent volume of PBS/NMS. The second round of IL-12 treatments occurred on Days +20 thru +22 and consisted of one daily injection of IL-12 (1 µg) spanned out over three total days. Therefore, mice received three additional injections of either IL-12 or PBS during the second IL-12 treatment round on Days +20 thru +22. The purpose of this second round of IL-12 treatments was to examine the effects of additional IL-12 treatment on the passive EAMG disease process.

2.7.2 Injection timeline for mAb D6 immunization

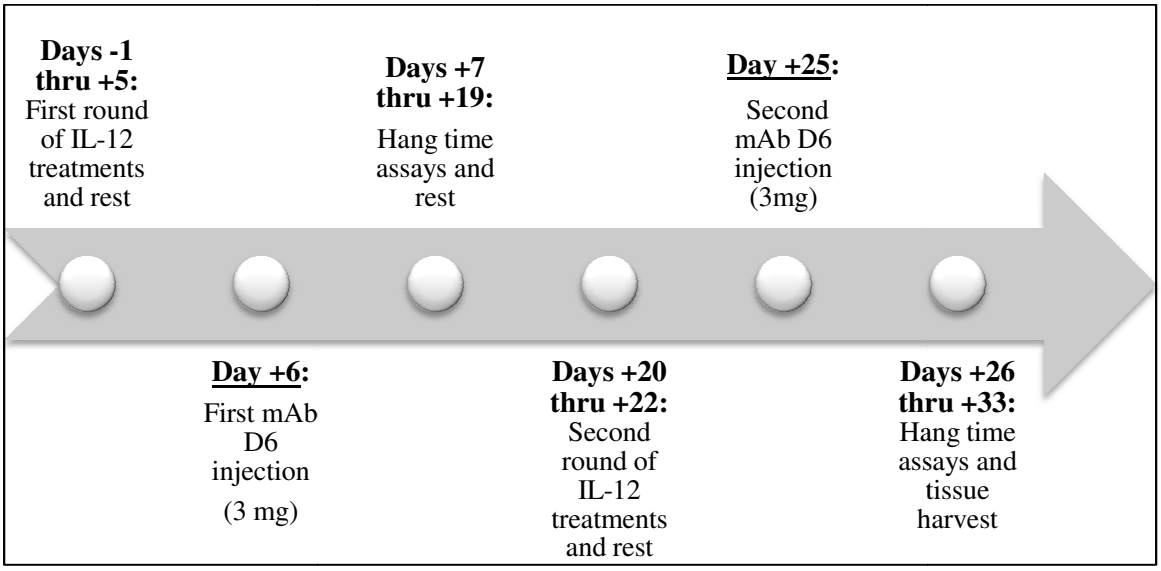

Figure 4: Timeline of passive mAb D6 immunizations performed during IFN-γ role determination assay

As can be seen in Figure 4, mice immunized to induce passive transfer EAMG received a single injection of mAb D6 (3 mg) on Day +6 and an additional single injection of mAb D6 (3 mg) on Day +25. During this assay, all mice in both the IL-12 and PBS-treated groups were immunized with an equal amount of mAb D6 at the Day +6 time point. No vehicle control injections were performed. Immunization with mAb D6 was performed in this manner as the purpose of the overall experiment was to compare the effects of IL-12 treatment versus PBS treatment on passive EAMG induction across the conditionally different mouse groups tested.

2.7.3 Injection of pancuronium bromide

Pancuronium bromide (0.03 mg/kg) in 100 µl PBS was injected i.p. into all mice on days 27, 28, 29, and 30 in order to transiently enhance muscle weakness according to published protocols (92).

2.8 Natural killer cell depletion passive EAMG induction assay:

2.8.1 Injection timeline for mAb PK136

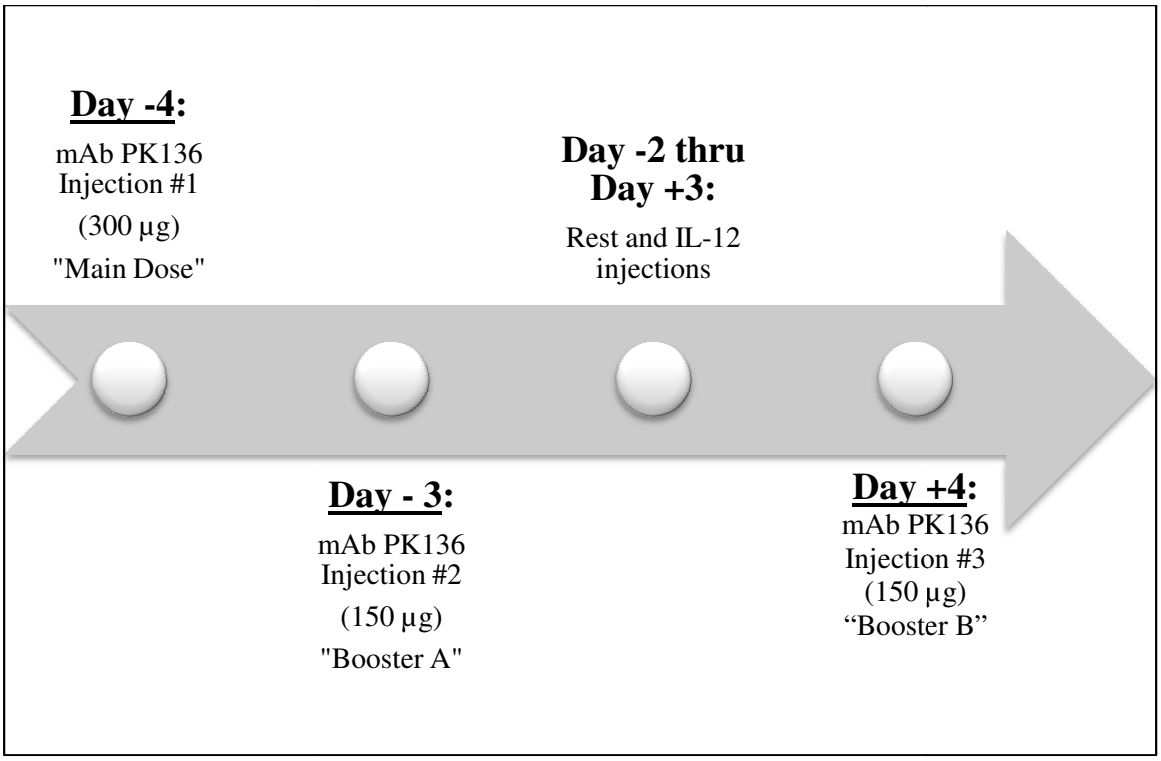

Figure 5: Timeline of all mAb PK136 injections performed

As can be seen in Figure 5, mice received the first and largest injection of either mAb PK136 (300 µg) or PBS on Day -4, which marks the beginning day of the overall assay. The second, smaller injection of either mAb PK136 (150 µg) or PBS follows on Day -3 and serves as a follow-up booster (labeled "Booster A" in Fig. 5) to the first injection, therefore maximizing cell depletion and clearance prior to the start of the IL-12 treatments. The third and final injection, containing 150 µg of mAb PK136 and administered to all mice who received the first injection, is performed on Day +4 and serves as the additional maintenance booster (labeled "Booster B" in Fig. 5). As can be seen, the third injection is incorporated into the assay on the day immediately following the end of the IL-12 treatments. This second booster injection of 150 µg of mAb PK136 is intended to ensure that maximal cell depletion remains consistent prior to passive

immunization with the anti-AChR mAb D6 on Day +6. In this manner, any passive disease that develops due to passive mAb D6 immunization thereafter is not attributable to NK or NKT cell presence or influence.

2.8.2 Injection timeline for IL-12 treatments

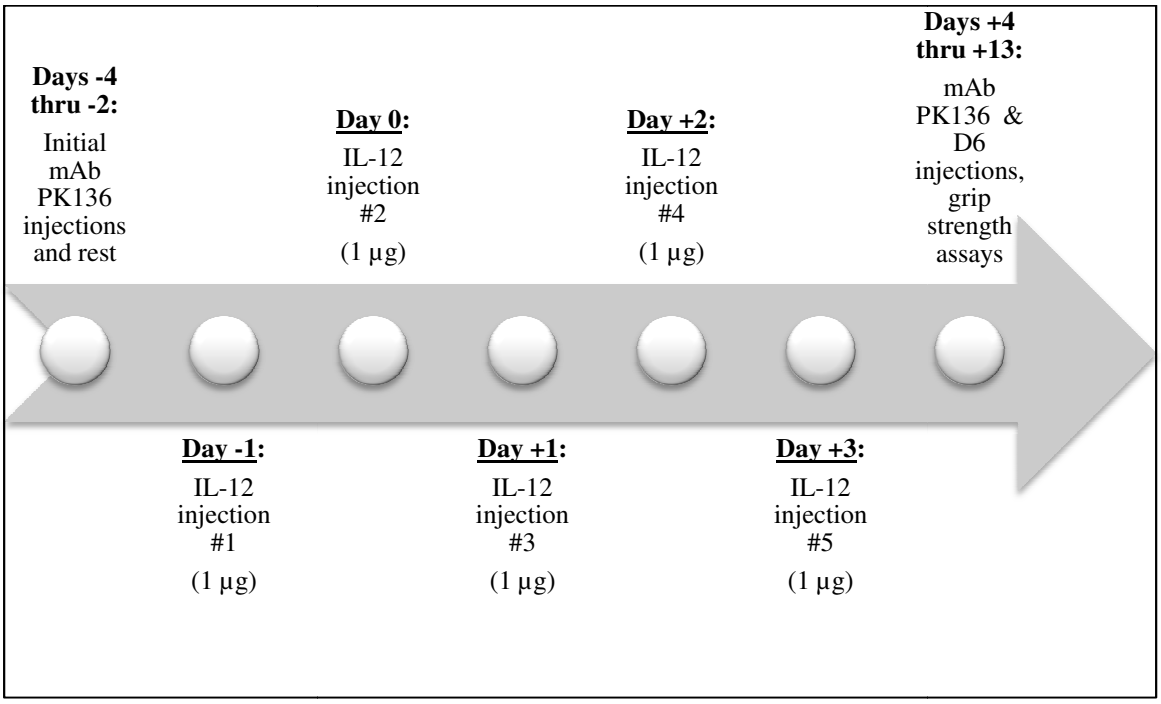

Figure 6: Timeline of all IL-12 injections performed during natural killer cell depletion passive EAMG induction assay

As can be seen in Figure 6, mice received the first of five consecutive injections of either IL-12 (1 µg) on Day -1, with the remaining IL-12 injections occurring every 24 hours on Days 0 thru +3. Therefore, the last injection of IL-12 on Day +3 marked the conclusion of the IL-12 treatment phase of the overall assay. Control mice received corresponding injections at all time points consisting of an equivalent volume of PBS/NMS.

2.8.3 Injection timeline for mAb D6 immunization

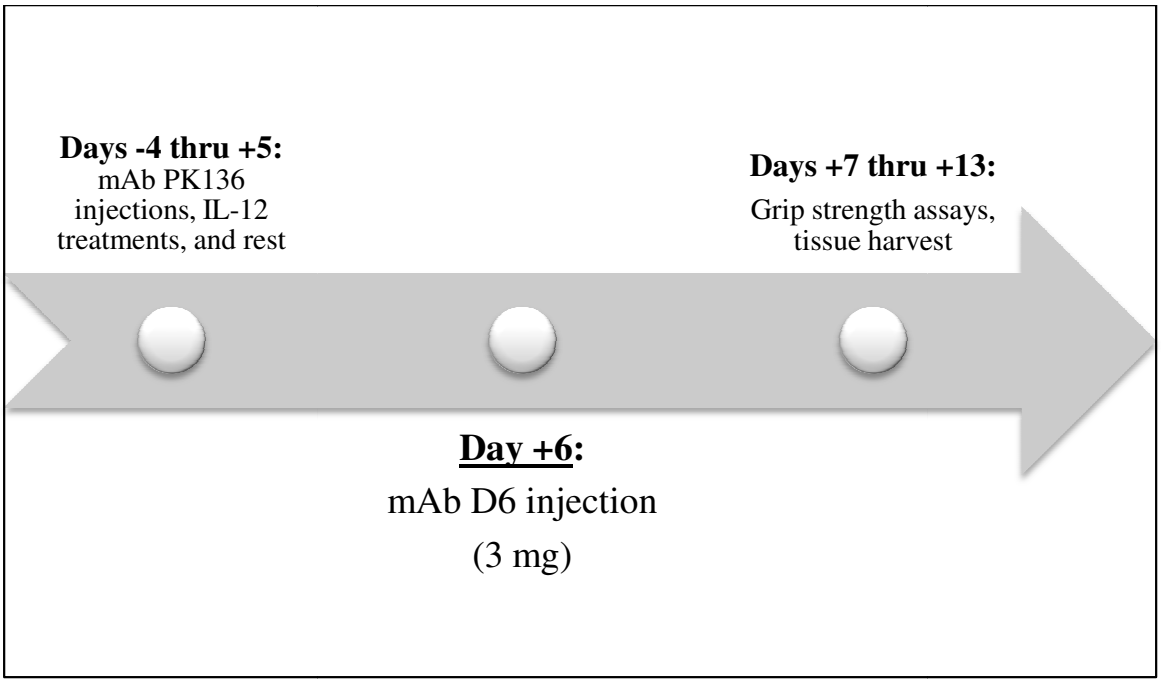

Figure 7: Timeline of passive mAb D6 immunization performed during natural killer cell depletion passive EAMG induction assay

As can be seen in Figure 7, mice immunized to induce passive transfer EAMG received a single injection of mAb D6 (3 mg) on Day +6. During this assay, all mice in both the IL-12 and PBS-treated groups were immunized with an equal amount of mAb D6 at the Day +6 time point. No vehicle control injections were performed as others have shown that injection of an isotype control murine antibody (MAR 18.5) did not cause muscle weakness (personal communication, Dr. Ellen Kraig, University of Texas Health Science Center, San Antonio, TX). Immunization with mAb D6 was performed in this manner as the purpose of the overall experiment was to compare the effects of IL-12 treatment versus PBS treatment on passive EAMG induction across the conditionally different mouse groups tested.

2.9 Clinical evaluation of EAMG:

2.9.1 Hang time assay

During the IFN-γ role determination assay, clinical EAMG was quantitated by measuring the amount of time a mouse could hang vertically suspended from a wire grid. In twenty-four hour intervals post-mAb D6 injection, mice were removed from their cages and placed on a vertical wire-mesh grid (10 cm x 8 cm) in a clean plastic chamber. The plastic chamber was approximately 35 cm tall and contained 75 ml of deionized water in an inverted 96-well plate lid in order to discourage the mouse from jumping off the wire-mesh grid down to the bottom of the chamber. Individual mouse hanging times were measured using a digital timer, where individual mice were allowed to hang for up to 14 minutes prior to being removed and placed back into their cage. A healthy mouse had no trouble hanging 14 minutes without falling, whereas a sick mouse may fall at any point during the 14 minutes hanging round.

To ensure that mice were actually falling due to weakness, and not simply jumping, initial and cumulative hanging times were determined. After the first fall, a mouse was immediately placed back on the grid to measure the cumulative hanging time. Initial hanging time (time of the first fall) and the cumulative hanging time (time of the first fall plus the time to the second fall, if mice were unable to hang more than thirty seconds) were measured and averaged to get the actual hang time data. If the time to the second fall was more than thirty seconds, the time of this second fall would then become the initial hang time and a new cumulative hang time would be measured. Once the hang time assay was completed for an individual mouse, the wire-mesh grid and chamber were

wiped clean using 70% ethanol and the water in the 96-well plate lid was exchanged with 75 ml of fresh deionized water prior to performing another hang time assay.

For all hang time data obtained, variability is expressed as the standard error of the mean for a specific mouse group. Figures of hang time data were generated using GraphPad® Prism5 (GraphPad Software Inc., La Jolla, CA). Statistical significance of the differences among hanging times of groups of mice was calculated within the GraphPad® Prism5 program using One-way ANOVA and Tukey's Multiple Comparisons Post Test. A difference was considered significant when $P < 0.05$.

2.9.2 Injection of pancuronium bromide

In some experiments performed during the IFN-γ role determination assays, clinical EAMG was quantitated by the pancuronium bromide sensitized hang time assay (92). Immediately prior to performing the hang time assays, mice were injected i.p. with 0.03 mg/kg pancuronium bromide in PBS to transiently enhance muscle weakness. Pancuronium treatment was not required in some experiments. Healthy mice could routinely hang > 14 minutes even with pancuronium bromide injection. Mice without pancuronium bromide also hang without falling for more than 14 minutes.

2.9.3 Grip strength apparatus set-up

For the natural killer cell depletion passive EAMG assays, a single-stand model grip strength apparatus and digital force gauge were purchased as a kit from Columbus Instruments® (Columbus Instruments, Columbus, Ohio). The digital grip strength meter was assembled as directed and thoroughly sanitized using Clidox-S® spray (Pharmacal Research Laboratories, Inc., Naugatuck, CT) and sterile 70% alcohol prep pads (Professional Disposables International, Inc., Orangeburg, NY) prior to its placement in the animal handling facility.

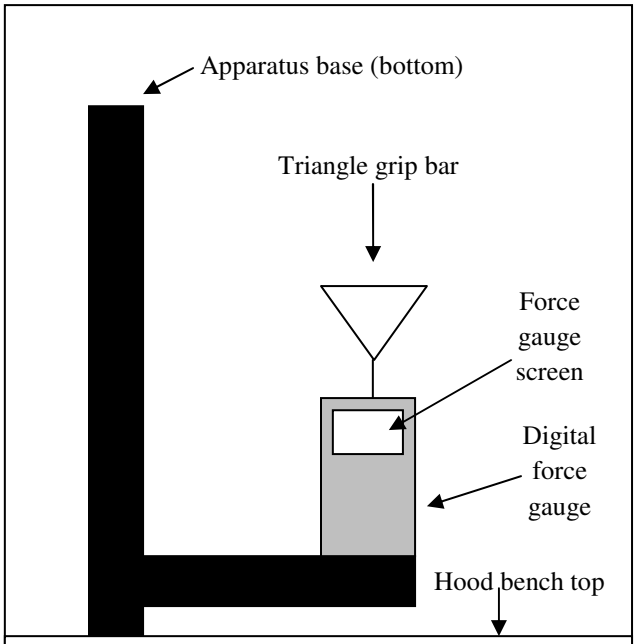

Figure 8: Digital grip strength meter set-up

The triangle bar provided with the grip strength meter was mounted to the digital force gauge and the grip strength apparatus was flipped 90° onto its side so that it sat vertically. Figure 8 above shows the orientation of the grip strength meter apparatus prior to assaying the grip strength of individual mice. Grip strength was measured in grams of force (gf) under the "tension peak" (T-PK) setting of the digital force gauge.

2.9.4 Cage pull procedure for measuring grip strength

Clinical EAMG was quantified by measuring the forelimb grip strength of every mouse immunized with mAb D6 every twenty-four hours following immunization for a period of up to +168 hours post-immunization. Individual mice were subjected to three

consecutive rounds of grip strength measurement consisting of a brief exercise period followed by a series of three measurements. Mice were exercised by gently pulling each mouse backwards across the top of the cage bars while allowing the mouse to grip the bars as it was pulled. The number of tail pulls was reduced during each measurement round, where each mouse was pulled 20 times during the first exercise round, 16 times during the second exercise round, and 12 times during the third exercise round. In total, each mouse was subjected to 48 cage pulls and 9 individual grip strength measurements, in succession, on each assay day.

Upon completion of each exercise round, mice were immediately lowered by their tails and allowed to grip the triangle bar with both forelimbs before being gently pulled upward until they let go. The grip strength measurement, as displayed on the grip force gauge screen in grams of force, was recorded after the mouse could no longer grip the triangle bar. A high value was indicative of normal forelimb muscle strength whereas a lowered value indicated forelimb muscle weakness. This process was repeated twice for a total of three grip strength measurements before moving on to the next exercise round. The digital force gauge was zeroed prior to the first grip strength measurement and again after each individual measurement in a series. A measurement value was thrown out and the grip strength measurement repeated in cases where a mouse failed to grip the bar with both forelimbs.

2.9.5 Analysis of grip strength measurement data

Grip strength data for all mice tested was compiled using Microsoft® Excel software (Microsoft Corp., Redmond, WA). Two methods of compiling and analyzing the grip strength measurement data were used. The first method consisted of summing all

nine individual grip strength measurements for a mouse on a given assay day and dividing the total by nine to generate the mean grip strength value for that mouse on that specific assay day. The other method involved singling out the highest value, termed the "peak value", in each of the three measurement rounds for a mouse on a given assay day and averaging the three peak values to generate single grip strength values for that mouse on that specific assay day. Figures comparing grip strength data between different mouse groups were generated using GraphPad® Prism5 software (GraphPad Software Inc., La Jolla, CA). Statistical significance of data used in these figures was calculated within the GraphPad® Prism5 program using Two-way ANOVA using repeated measures, Two-way ANOVA and Bonferroni's Post Test, or One-tailed paired t-Tests. A difference was considered significant when $P < 0.05$.

2.10 Serum IFN-γ measurements:

2.10.1 Mouse bleeding timeline

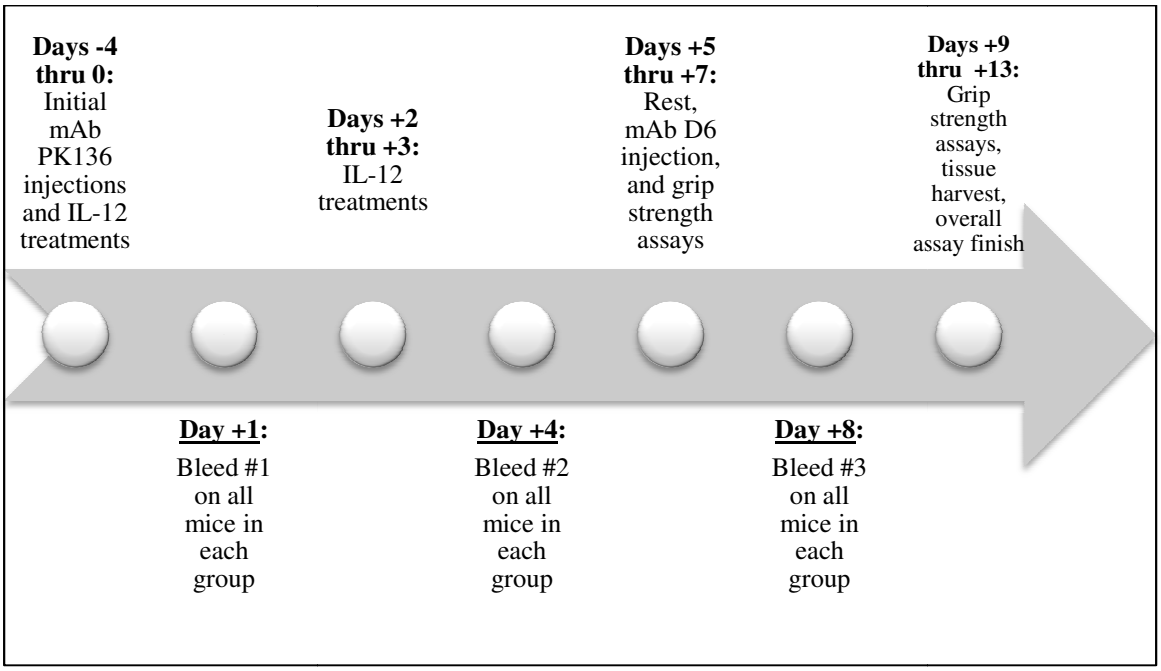

Figure 9: Timeline of mouse bleedings performed

As can be seen from Figure 9, all mice were lancet bled on Day +1 (during IL-12 treatment), Day +4 (after IL-12 treatment), and Day +8 (after mAb D6 immunization).

2.10.2 Lancet bleedings

Blood samples were collected from individual mice using Goldenrod® animal lancets (Medipoint Inc., Mineola, NY) and pooled for each individual group. Approximately 300-400 µL per group was collected per bleed into BD Microtainer® SST™ tubes (Becton-Dickinson and Company, Franklin Lakes, NJ), allowed to sit for thirty minutes at room temperature to permit clotting, and then centrifuged at 12,000 RPM for three minutes to separate sera from other blood components. Sera were then carefully extracted using gel loading pipette tips, transferred to sterile, labeled 1.5 ml Eppendorf tubes, and frozen at -20°C until analysis.

2.10.3 Serum IFN-γ ELISA assays:

Serum INF-γ levels were determined using the Mouse IFN-γ ELISA Ready-Set-Go!™ Kit (eBioscience Inc., San Diego, CA). Anti-mouse IFN-γ monoclonal antibody was used to coat 96-well plates provided with the kit and allowed to incubate overnight at 4°C. Wells were blocked using 200 µl of blocking solution provided in the kit and incubated for one hour at room temperature. All samples were serially 5-fold diluted (at 1:5, 1:25, and 1:125), added in 100 µl volumes, and incubated overnight in sealed plates at 4°C. In addition, the IFN-γ standards were serially 2-fold diluted as directed in the kit protocol, added in 100 µl volumes, and incubated in the same sealed plates at 4°C. Each plate assayed received its own individual IFN-γ standards. The detection antibody, biotin-conjugated anti-mouse IFN-γ, was added at 100 µl per well and the plate was incubated

at room temperature for one hour. The detection enzyme, avidin-HRP, was added at 100 µl per well and incubated at room temperature for thirty minutes. Washing with 0.1% Tween-20 in 1X PBS was done after each of the previously mentioned steps. The substrate solution, 1X TMB, was added at 100 µl per well and the plate was incubated at room temperature for fifteen minutes. The stop solution, 2N H_2SO_4, was then added at 50 µl per well. The absorbance of each well of each 96-well plate was measured at 450 nm and 570 nm on a SpectraMax™ Plus spectrophotometer (Molecular Devices, Sunnyvale, CA).

2.10.4 Analysis of serum IFN-γ ELISA assay data

The 450 nm and 570 nm values measured on the spectrophotometer were transferred to and compiled using the Microsoft® Excel software program (Microsoft Corp., Redmond, WA). For each assay well, the 570 nm value was subtracted as background from the 450 nm value to generate the final raw value for that well. Standard curves, ($y = mx+b$) slope equations, and R^2 best-fit line values for each 96-well plate were generated using the IFN-γ standards data gathered from the absorbance measurements specific to these respective plates. The data was then converted into picogram per serum milliliter (pg/ml) values based on the standard curve slope equations. Compiled data was transferred to GraphPad® Prism5 (GraphPad Software Inc., La Jolla, CA) software in order to generate figures. Statistical significance of the data used in these figures was determined within the GraphPad® Prism5 software program using One-way ANOVA and Tukey's Multiple Comparisons Post Test. A difference was considered significant when $P < 0.05$.

2.11 Immunohistochemical analysis of complement levels:

2.11.1 Tissue harvesting procedural strategy for IFN-γ role determination assay

On Day +10 (+96 hours post mAb D6 injection), one mouse from Group 1 and one mouse from Group 3 were arbitrarily selected for euthanasia and tissue harvesting after hang time assays were performed. The following day (Day +11), the remaining mice in Groups 1-4 were euthanized and tissue harvesting was performed upon completion of the hang time assays. Mice were euthanized by first incapacitating using gaseous CO_2 followed by cervical dislocation prior to tissue harvesting.

2.11.2 Tissue harvesting procedural strategy for natural killer cell depletion passive EAMG assay

The two sickest mice from each mouse group, based on that day's grip strength assay results, were euthanized on Day +12 upon completion of the grip strength assays in order to perform tissue harvesting. The remaining two mice in each group were then assayed for grip strength and euthanized the following day (Day +13) and tissue harvesting was performed. This method was employed in order to spread the tissue harvesting over a two day period as it was impossible to harvest tissues from all mice involved in the assay in a 24-hour time period. Mice were euthanized by first incapacitating using gaseous CO_2 followed by cervical dislocation prior to tissue harvesting.

2.11.3 Tissue harvesting and histological procedures

For each mouse, whole diaphragm muscle and bulk leg muscle (extensor digitorum longus [EDL] and soleus muscles combined) from both hindlimbs was quickly removed immediately following euthanasia. Individually harvested muscles were placed

on small pieces of cut wooden tongue depressors and immediately embedded in Tissue-Tek® O.C.T. Compound (Miles, Inc., Elkhart, IN) prior to snap freezing in isopentane over liquid nitrogen. Once thoroughly frozen through (approximately 20 seconds in isopentane), the muscle samples were individually placed in sterile, labeled 12x75mm tubes and transferred to storage at -80°C until needed further. Mouse diaphragm muscle samples were sectioned at 10 μm on a H/I Bright® OTF5000 cryostat (H/I Bright Instrument Company Ltd, Huntingdon, England). Prepared tissue sections were adhered to pre-cleaned Fisherbrand® Superfrost Plus® microscope slides (ThermoFisher Scientific Inc., Waltham, MA), placed in foam-lined Fisher® Durable Slideboxes (ThermoFisher Scientific Inc., Waltham, MA), and stored at -20°C until stained.

2.11.4 Staining and imaging of prepared slides for IFN-γ role determination assay

Tissue staining was performed using AlexaFluor®594-labeled α-Bungarotoxin (Molecular Probes, Eugene, OR), Cy™2-conjugated AffiniPure Mouse Anti-Rat IgG [H+L] (Jackson ImmunoResearch Laboratories, Inc., West Grove, PA), and FITC Goat IgG Anti-Mouse Complement C3 (MP Biomedicals, Aurora, OH). Sample slides were allowed to stain for 18-24 hours per stain before being washed and mounted in Gel Mount™ Aqueous Mounting Medium (Sigma-Aldrich, Inc., St. Louis, MO). Stained slides were viewed on an Olympus IX71 Inverted Microscope (Olympus America Inc., Center Valley, PA) or and images were captured using an attached Photometrics® Quantix® camera (Roper Scientific, Inc., Germany). Stained slides were also viewed on a Nikon® ECLIPSE TE2000-U Inverted Microscope (Nikon Corporation Co., Ltd., Kawasaki, Japan) and images were captured using an attached Photometrics® CoolSNAP EZ Turbo 1394 camera (Roper Scientific, Inc., Tucson, AZ). Images captured using this

microscope-camera combination were viewed and digitized using MetaMorph® 7 (Molecular Devices Corporation, Downingtown, PA).

2.11.5 Analysis of C3 deposition levels for IFN-γ role determination assay

Each slide image was quantified for fluorescence intensity using a MATLAB 7.1 (The MathWorks, Inc., Natick, MA) image analysis program created by Dr. S. C. Molitor (Department of BioEngineering, University of Toledo). For each image, the co-localized fluorescent signal present in all neuromuscular junctions was measured after performing threshold elimination of non-specific background in the red channel.

2.11.6 Staining and imaging of prepared slides for natural killer cell depletion passive EAMG assay

Muscle sample tissue dual staining was performed using AlexaFluor®594-labeled α-Bungarotoxin (Molecular Probes, Eugene, OR) and FITC Goat IgG Anti-Mouse Complement C3 (MP Biomedicals, Aurora, OH). Sample slides were allowed to stain for 24 hours per stain before being washed in PBS and mounted in Gel Mount™ Aqueous Mounting Medium (Sigma-Aldrich, Inc., St. Louis, MO). Stained slides were viewed on a Nikon® ECLIPSE Ti-E inverted microscope (Nikon Corporation Co., Ltd., Kawasaki, Japan) and images were captured using an attached Photometrics® CoolSNAP™ ES^2 high-performance interline CCD camera (Roper Scientific, Inc., Tucson, AZ). Images captured were viewed and digitized using MetaMorph® v. 7.6.5.0 (Molecular Devices Corporation, Downingtown, PA).

2.11.7 Analysis of C3 deposition levels for natural killer cell depletion passive EAMG assay

For each image, the co-localized fluorescent signal present in all neuromuscular junctions was measured after performing threshold elimination of non-specific background in the red channel (α-Bungarotoxin binding) using the MetaMorph® v. 7.6.5.0 software. To do so, an arbitrarily-sized box was drawn around a full, stained neuromuscular junction in the red channel and specific parameter measurements (overall area, average pixel intensity, and integrated pixel intensity) of that box were recorded and compiled using Microsoft® Excel software (Microsoft Corp., Redmond, WA). An identically sized box was drawn in an area where no junctional staining occurred to generate background levels and the same data was recorded and compiled for this background box. In many cases, an identically sized box was applied to multiple junctions in the red channel of an image (where each stained junction would fit into the box area wholly) while a single, identically sized box was used as the background box for those junctions. Each junction isolated and recorded was carefully labeled in Excel in order to keep from missing or doubling junction measurements. For each mouse sample slide, a single Excel worksheet was created that combined all of the date compiled from multiple images taken of that slide.

Once all the neuromuscular junctions that were stained in the red channel (α-Bungarotoxin binding) of a specific image were cataloged, measured, and recorded in Excel, the same junctional and background boxes for the red channel image were copied and pasted into their corresponding positions within the green channel (FITC anti-C3 binding) image. Once in position within the green channel image, the same specific parameter measurements of each labeled box were recorded and compiled within the same Excel worksheet.

A final co-localized fluorescent signal value for each specific neuromuscular junction was obtained by first subtracting out the background average pixel intensity from the junctional average pixel intensity for both the red and green channel data. From there, a specific neuromuscular junction's green-to-red staining ratio was calculated by dividing the background-subtracted green channel value by the background-subtracted red channel value. The individual green/red staining ratio for all of the recorded neuromuscular junctions within an image were then averaged to generate the overall green/red staining ratio for that image. Statistical significance was generated for each mouse diaphragm muscle sample image by compiling the individual junctional green-to-red ratio values in the GraphPad® Prism5 (GraphPad Software Inc., La Jolla, CA) software program and performing statistical analysis using the unpaired Two-tailed T-test. As several different images were made for each mouse sample slide and analyzed within the same Excel worksheet, the overall green/red staining ratios for all of the analyzed images were then averaged in order to generate the final green-to-red staining ratio value for a given mouse sample slide. In this manner, the level of complement component C3 deposited at each neuromuscular junction analyzed was accounted for and ultimately factored in to determine the overall level of C3 deposition for a given mouse within a specific group. The entire staining and image analysis procedure was performed on muscle sample slides derived from multiple mice within a group, so overall mouse group C3 deposition levels reflected the average of those multiple mice analyzed.

2.12 Whole genome expression analysis assays:

2.12.1 Outline of assay mouse groups

•Group 1, [+PBS]: Two female B6 mice

•Group 2, [+IL-12]: Two female B6 mice

•Group 3, [+mAb D6]: Two female B6 mice

•Group 4, [+IL-12 & mAb D6]: Two female B6 mice

2.12.2 Timeline of IL-12 treatments and mAb D6 immunization

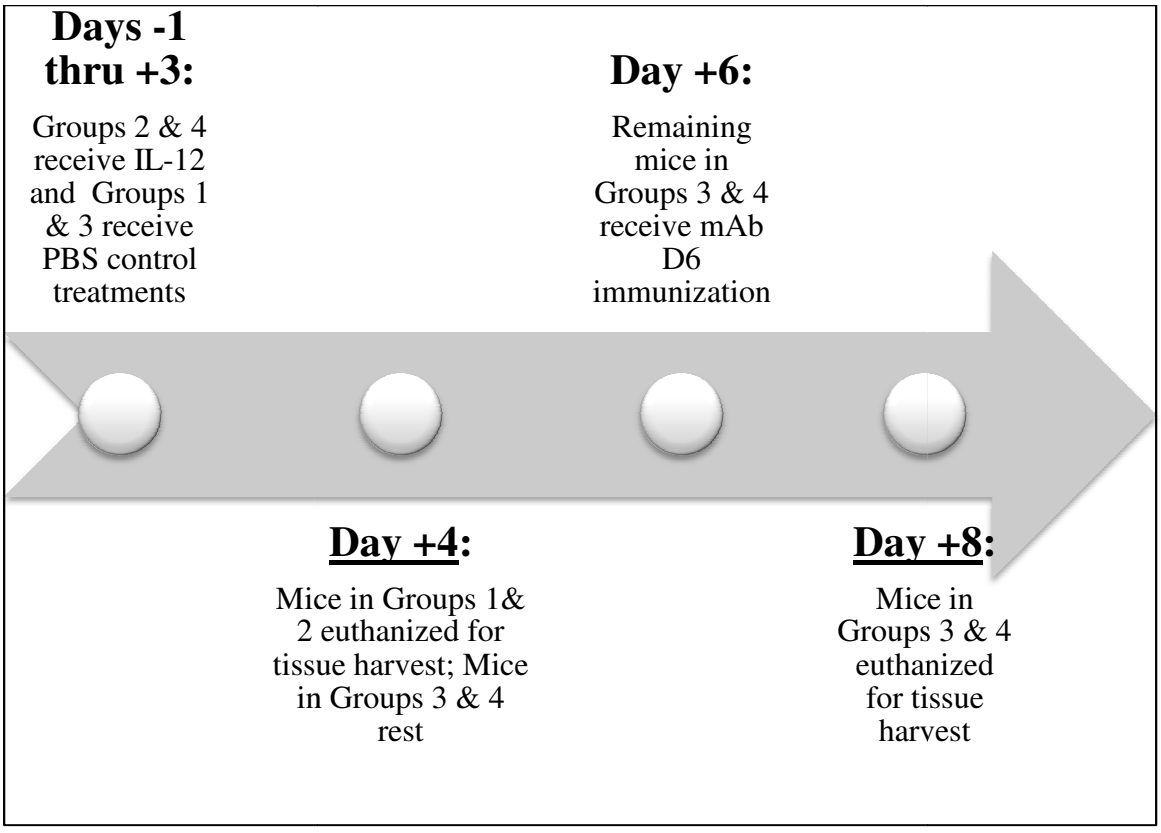

Figure 10: Timeline of the IL-12 treatments and mAb D6 immunization performed during the whole genome expression analysis

As can be seen in Figure 10, mice in Groups 2 and 4 (four mice total) received the first of five consecutive IL-12 injections (1 µg) on Day -1, with the remaining IL-12 injections occurring every 24 hours on Days 0 thru +3. Control mice in Groups 1 and 3 (four mice total) received corresponding injections at all time points consisting of an equivalent volume of PBS/NMS. Therefore, the last injection of IL-12 or PBS/NMS on

Day +3 marked the conclusion of the IL-12 treatment phase of the overall assay. On Day +4, the two mice in Group 1 (PBS/NMS treated) and the two mice in Group 2 (IL-12 treated) were euthanized and tissue harvesting was performed, whereas the mice in Groups 3 and 4 were allowed to rest. On Day +6, the mice in Groups 3 and 4 (four total mice) received a single injection of mAb D6 (3 mg). On Day +8, On Day +4, the two mice in Group 3 (PBS/NMS + mAb D6 treated) and the two mice in Group 4 (IL-12 + mAb D6 treated) were euthanized and tissue harvesting was performed.

2.12.3 Tissue harvesting procedures

For each mouse, whole diaphragm muscle and bulk leg muscle (extensor digitorum longus [EDL] and soleus muscles combined) from both hindlimbs was quickly removed immediately following euthanasia. Individually harvested muscles were immediately rinsed in ice cold, sterile 1X PBS, blot-dried on a fresh Kimwipe® (Kimtech Scientific, Kimberley-Clark Global Sales, Inc., Roswell GA), and weighed. Immediately after weighing, muscle samples were cut into smaller portions which were then immersed in an appropriate volume (based on individual sample weight) of RNAlater® Solution (Applied Biosystems/Ambion, Inc., Austin, TX) within a sterile 1.5 ml plastic tube. Sample tubes were then immediately transferred to a -20°C freezer for long term cold storage until needed further.

2.12.4 RNA isolation, purification, and assessment

For each mouse, RNA was isolated and purified from harvested diaphragm muscle tissue using the reagents and protocol of the Qiagen® RNeasy® Fibrous Tissue Mini Kit (Qiagen Incorporated – USA, Valencia, CA). For each attempted purification, diaphragm muscle sample portions were removed from cold storage at -20°C and

weighed. Approximately 20 mg of diaphragm tissue was used per purification attempt. Working quickly, the diaphragm tissue sample portions were transferred to fresh, sterile 12x75 mm plastic tubes containing 300 µl of 1% β-Mercaptoethanol (β-ME) containing lysis buffer (as directed in the kit protocol). The diaphragm muscle samples were efficiently disrupted and homogenized using a PowerGen® 125 Rotor Stator tissue homogenizer (ThermoFisher Scientific Inc., Waltham, MA) and 7x110 mm, RNAse/DNAse-free plastic disposable rotor stator PowerGen® Generators (ThermoFisher Scientific Inc., Waltham, MA).

Once the diaphragm muscle samples were fully disrupted and homogenized, they were processed further using the reagents, equipment, and procedures contained in the Qiagen® RNeasy® Fibrous Tissue Mini Kit. Isolated and purified RNA was eluted from spin columns in 30 µl volumes of RNAse-free water during two separate elution rounds for a total of 60 µl of purified RNA solution. A small sample of each purified RNA solution was removed, diluted at 1:20 in 10 mM Tris-HCl (pH 7.5), and the 260nm/280nm ratio was measured using spectrophotometry (Shimadzu® BioSpec-1601, Shimadzu Scientific Instruments, Columbia, MD) to determine the level of RNA purity and quantity as directed by the kit protocol. The absorbance at 320 nm (OD320) was also measured and used to determine any background contaminant presence and was found to be negligible for all samples analyzed. The spectrophotometric RNA purity and quantity assessments were performed for each purified RNA sample obtained from an individual mouse diaphragm muscle sample. In general, a range of 11.7 – 16.3 µg of RNA with 260nm/280nm purity ratios of approximately 2.1 was achieved for each mouse diaphragm sample subjected to RNA isolation and purification. Once the RNA purity and

quantity of a sample was assessed, the sample was transferred to cold storage at -80°C until needed further.

2.12.5 Shipment and gene expression analysis at the Cleveland Clinic

Purified RNA samples were removed from cold storage at -80°C, thawed, and diluted from their stock concentrations to 0.1 µg/µl in 20 µl volumes (2 µg of total purified RNA per sample) using DEPC water prior to being transferred to storage at -20°C as directed by staff of the Genomics Core of the Cleveland Clinic's Lerner Research Institute (The Cleveland Clinic, Cleveland, OH). The following day, the diluted samples of pure RNA were removed from cold storage, prepared as directed by the Genomics Core, and overnight-shipped on dry ice via the United Parcel Service to the Genomics Core of the Cleveland Clinic's Lerner Research Institute. An Illumina® Mouse RefSeq-8® BeadChip Gene Expression Chip (Illumina Inc.,San Diego, CA) capable of measuring the expression level of 23,000 individual known and suspected genes was purchased from the Genomics Core. Full-service gene expression analysis was purchased for eight total samples (those diluted and shipped one sample per mouse) from the Genomics Core. The samples were handled, prepared, and loaded on the Mouse RefSeq-8 BeadChip by the Genomics Core staff and assayed on the Illumina® Beadstation platform (Illumina, Inc., San Diego, CA). Data compilation was performed using Microsoft® Excel software (Microsoft Corp., Redmond, WA) by the Genomics Core manager, Dr. Pieter Faber, and compiled data was downloaded from the Cleveland Clinic server. Dendrograms comparing overall gene expression changes between different mouse samples analyzed were generated by Dr. Pieter Faber of the Genomics Core using

Illumina® GenomeStudio™ Gene Expression Module v1.0 software (Illumina Inc.,San Diego, CA).

Chapter 3

Results

3.1 Examining the role of IFN-γ in passive EAMG

3.1.1 Interleukin-12 (IL-12) enhances passive EAMG upon immunization with the mouse anti-AChR monoclonal antibody D6

The downstream IL-12 injection strategy was adapted from previous work by Buchanan et al (93). The requirement for IL-12 in active EAMG induction is well documented (5, 6, 35), though these experiments incorporated IL-12 treatment during the T cell priming phase of disease induction. However, it was determined that T cell priming by injection of the *Torpedo alpha146-162* peptide (Tα146-162) in Complete Freund's adjuvant (CFA) in conjunction with IL-12 treatment was not required to induce passive disease (23). Instead, passive disease was shown to be inducible in B6 mice using only the combination of IL-12 treatment followed by subsequent mAb D6 immunization. Therefore, during these assays we performed the IL-12 injections following the same

chronological experimental pattern as in (93), only in the absence of any simultaneous T cell priming using Tα146-162 peptide.

Originally, the process of active immunization, in which mice were immunized using purified whole *Torpedo californica* AChR, was thought to be necessary to induce EAMG. Later, it was shown that passive transfer of anti-AChR containing serum (12, 94) or monoclonal antibody (20) could also induce disease, though this process was thought to require additional T cell priming. As mentioned previously, experiments performed in the Wall Laboratory determined passive disease was inducible in B6 mice using only the combination of IL-12 treatment followed by subsequent mAb D6 immunization. Where our immunization protocol differs from that seen in (93) is in the timing of the immunization with anti-AChR antibody via intraperitoneal injection. Our passive EAMG induction protocol here employs two singular, chronologically spaced intraperitoneal injections of mAb D6 on Days +6 and +25 of the overall assay, approximately 72 hours after the conclusion of each IL-12 treatment round.

B6 mice were pre-treated with 5 daily injections of IL-12 or PBS on Days -1 thru +3 and on Day +5 the hang time of each mouse was measured. All mice had hang times of ≥ 14 minutes prior to the mAb D6 immunization. On Day +6, 3 mg of mouse monoclonal antibody D6 was injected into all of the mice. The individual hang times of mice in each group were measured once daily in 24-hour intervals post-immunization with mAb D6 and the results can be seen in Figure 11. While the PBS treated mice (○) had hang times of ≥ 14 minutes post-immunization, the IL-12 treated mice (♦) began to exhibit signs of muscle weakness at 48 hours post-immunization, with hang times reduced to a mean of 4.4 minutes by the 72-hour time point. These hang time differences

were statistically significant at the 72, 96, and 120-hour time points (P= <0.05). By the 192-hour time point, the IL-12 treated mice had essentially returned to normal strength. Surprisingly, weakness was so pronounced that no pancuronium bromide injection was required to overcome the high numbers of mouse AChRs and observe weakness in the IL-12 treated mice. This result is in contrast to those derived from studies involving the use of the rat anti-AChR mAb35 antibody, in which injection of pancuronium bromide was required in order to quantify clinical EAMG.

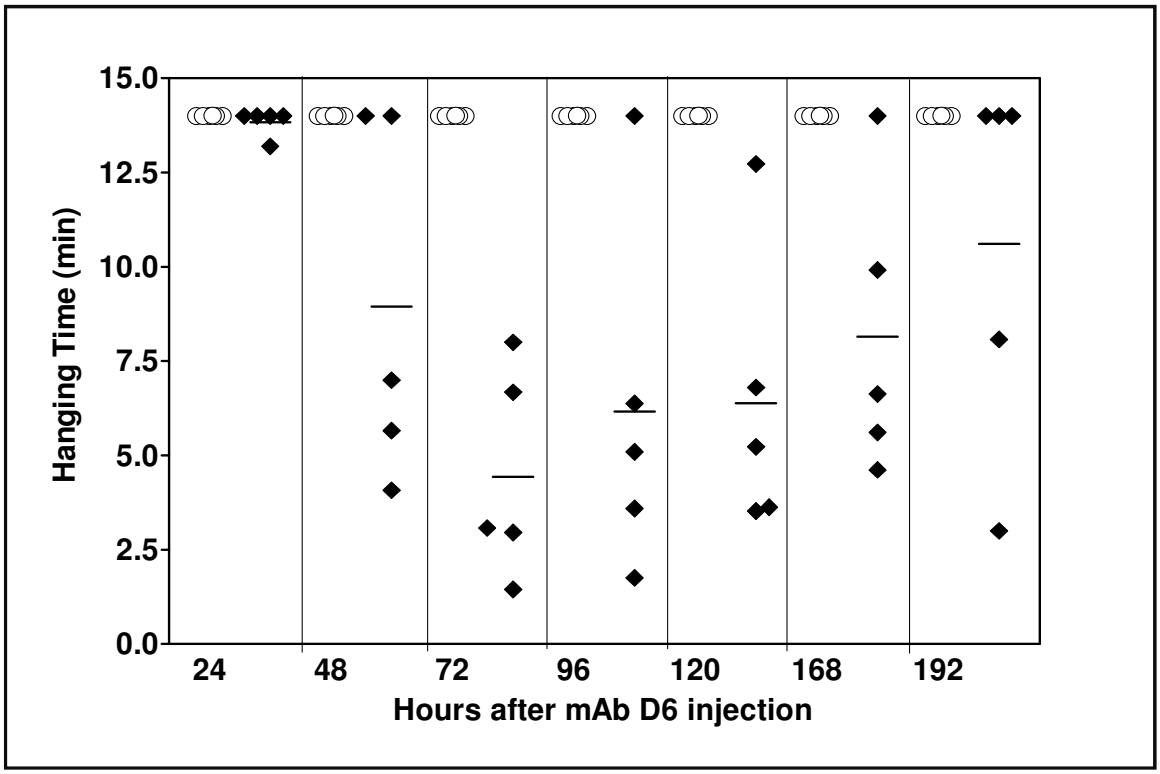

Figure 11: IL-12 enhances passive EAMG in B6 mice after one injection of mouse monoclonal antibody D6. B6 mice received daily i.p. injections of either IL-12 (1 µg) or PBS on Days -1 thru +3 and a single i.p. injection of mAb D6 (3 mg) on Day +6. Individual hang times of mice in the PBS (○) and IL-12 (♦) treated groups were measured daily in 24-hour intervals on Days +7 thru +13. Once a mouse hung for 14 minutes, the measurement was stopped.

The B6 mice from Figure 11 were treated with i.p. injections of IL-12 or PBS again on Days +20 thru +22 and received a second immunization with 3 mg of mAb D6 on Day +25. The hang times of each mouse were again measured on Day +24 pre-immunization, with no muscle weakness being observed, and once daily at 24-hour intervals post-immunization as before. As shown in Figure 12, the mice treated with IL-12 (♦) showed markedly enhanced muscle weakness with their hang times dropping to an average of 3.8 minutes at the 24-hour time point. Four of the five IL-12 treated mice were deceased by the 72-hour time point, whereas the PBS-treated mice (○) that were immunized with mAb D6 had average hanging times of 12.3 at 72 hours post-immunization. Once again, there was no requirement for pancuronium bromide injection in order to observe muscle weakness. These results demonstrate that the enhancement of weakness by IL-12 is not due to a xenogeneic effect, as is a possibility with the rat anti-AChR mAb35, but rather is more pronounced with the usage of the murine anti-AChR antibody, mAb D6.

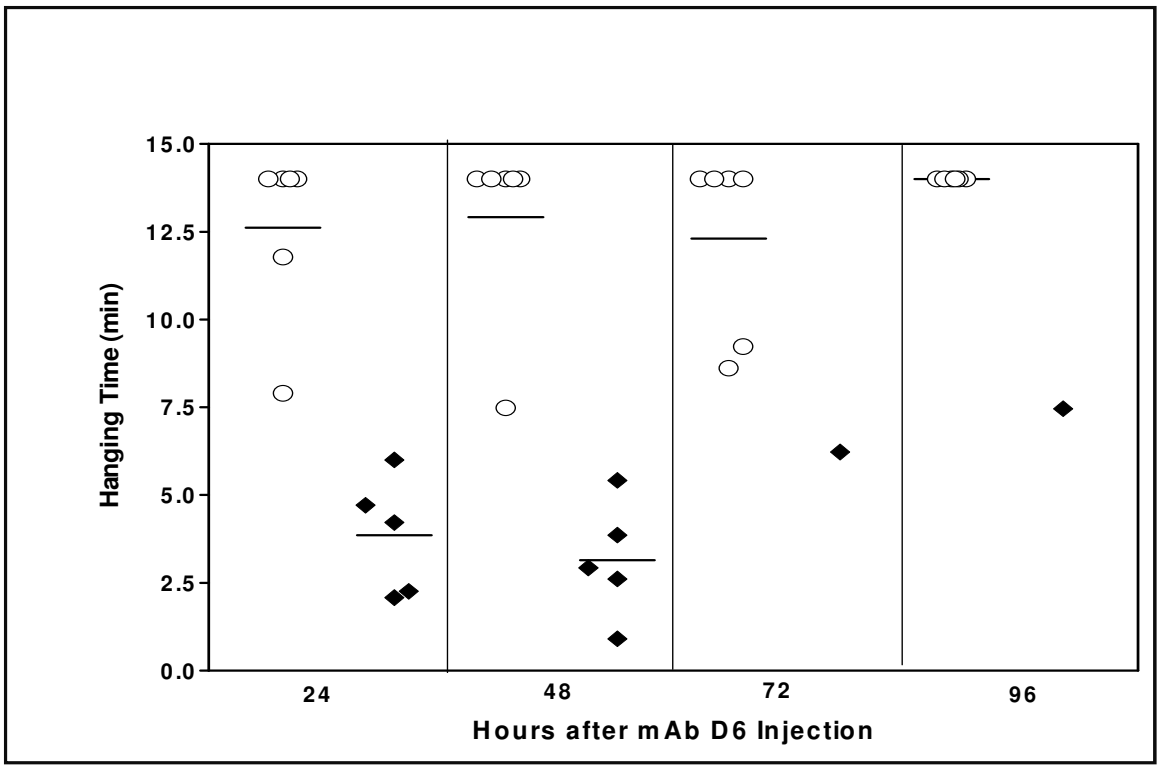

Figure 12: Passive EAMG is severely accelerated in B6 mice by additional IL-12 treatments and mAb D6 immunization. B6 mice received daily i.p. injections of either IL-12 (1 µg) or PBS on Days +20 thru +22 and a single i.p. injection of mAb D6 (3 mg) on Day +25. Individual hang times of mice in the PBS (○) and IL-12 (♦) treated groups were measured daily in 24-hour intervals on Days +26 thru +29. Once a mouse hung for 14 minutes, the measurement was stopped.

3.1.2 Interferon-gamma (IFN-γ) is required for development of passive transfer EAMG upon immunization with mAb D6

The individual treatment conditions, number, sex, and strain of mice used in each assay group are highlighted in the following outline:

- Group 1, [+PBS]: Four male IFN-$\gamma^{-/-}$ mice
- Group 2, [+IL-12]: Three male & three female IFN-$\gamma^{-/-}$ mice

Five daily i.p. injections of either PBS or IL-12 were administered to the B6 and IFN-$\gamma^{-/-}$ (95) mice on Days -1 thru +3 as described in the above outline, with an i.p. injection of mAb D6 being administered to all mice on Day +6. Individual hang times of each mouse were measured once daily in 24-hour intervals post-immunization. Figure 13 shows the results of the hang time assays for all IFN-$\gamma^{-/-}$ mice in which pancuronium bromide was not used.

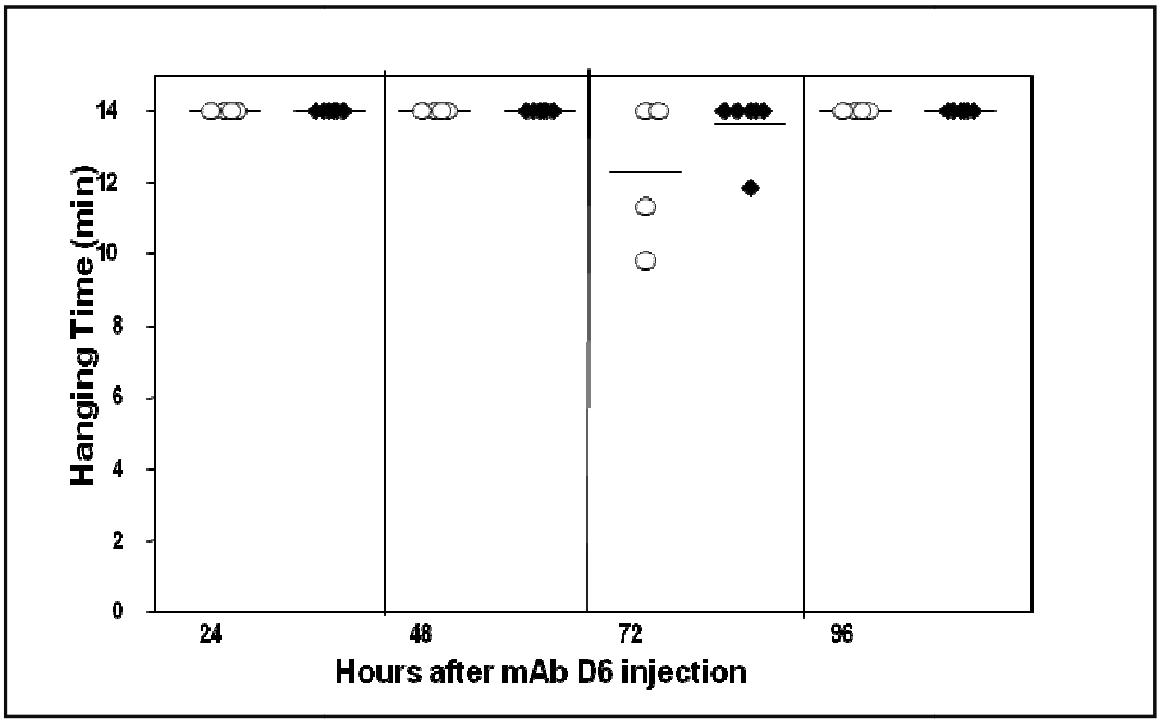

Figure 13: IFN-$\gamma^{-/-}$ mice are resistant to passive EAMG induction. IFN-$\gamma^{-/-}$ mice received daily i.p. injections of either IL-12 (1 µg) or PBS on Days -1 thru +3 and a single i.p. injection of mAb D6 (3 mg) on Day +6. Individual hang times of mice in the PBS (○) and IL-12 (♦) treated groups were measured daily in 24-hour intervals on Days +7 thru +10. Once a mouse hung for 14 minutes, the measurement was stopped.

As can be seen in Figure 13, the mice show no overt signs of muscle weakness, with only slight reductions in average hang times seen in both the PBS-treated (○) and IL-12-treated (♦) groups at the 72-hour time point. In Figure 14 on the following page,

the same IFN-$\gamma^{-/-}$ mice from Figure 13 were injected with pancuronium bromide beginning at the 48-hour time point and their individual hang times were re-measured. In contrast to the results seen in Figure 13, upon administration of pancuronium bromide (an AChR antagonist) the hang times of both groups of mice were similarly and noticeably reduced.

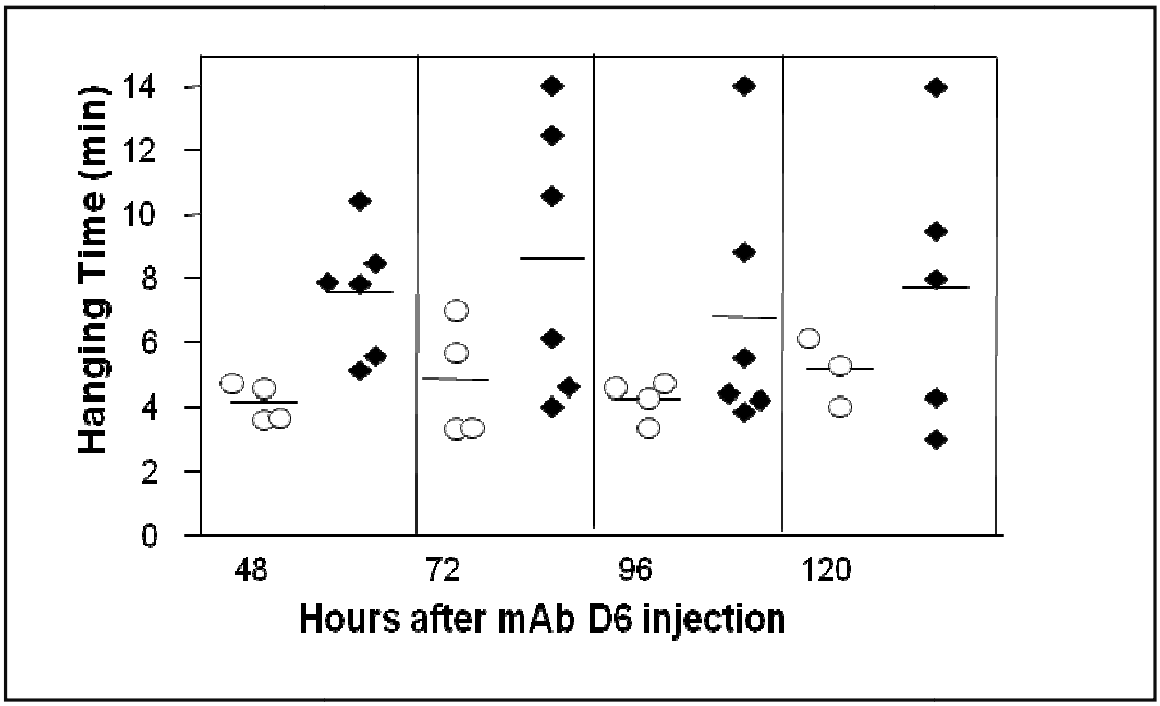

Figure 14: IL-12 treatment reduces muscle weakness due to pancuronium bromide administration in IFN-$\gamma^{-/-}$ mice. IFN-$\gamma^{-/-}$ mice received daily i.p. injections of either IL-12 (1 µg) or PBS on Days -1 thru +3 and a single i.p. injection of mAb D6 (3 mg) on Day +6. Immediately prior to measuring individual hang times at each post-mAb D6 immunization time point, each mouse received a single i.p. injection of pancuronium bromide (0.03 mg/kg). Individual hang times of mice in the PBS (○) and IL-12 (♦) treated groups were measured daily in 24-hour intervals on Days +7 thru +10. Once a mouse hung for 14 minutes, the measurement was stopped.

However, there seemed to be a slight protective effect derived from IL-12 treatment of the IFN-$\gamma^{-/-}$ mice (♦) as compared to the PBS-treated group (○). The mean hanging time of IL-12-treated IFN-$\gamma^{-/-}$ mice was significantly longer than that of PBS

treated mice at all time points. This reversal of hang times in the IL-12 treated mice was never observed with B6 mice. This suggests that IFN-γ is the key facilitator for IL-12 enhancement of muscle weakness as IL-12 treatment in the absence of IFN-γ presence provides a slightly protective effect. The weakness observed after pancuronium treatment suggests that some damage to the neuromuscular junction is occurring in IFN-$\gamma^{-/-}$ mice, although not to the extent observed in B6 mice.

3.1.3 Complement bound to AChRs at the neuromuscular junction is elevated in IL-12 treated B6 mice

In this assay, IL-12 or PBS was administered i.p. once daily to B6 mice on Days -1 thru +3 and again on Days +20 thru +22, while the *Torpedo* α146-162 peptide (11, 42) was administered once on Day 0 with a booster injection on Day +21 via s.c. tail base injection. On Day +25, 3.5 mg of the rat anti-mouse AChR monoclonal antibody mAb 35, shown to induce EAMG, was administered to the mice via i.p. injection (23) and all mice were euthanized two days later. MAb 35 is a rat IgG1 that recognizes the main immunogenic region of the AChR α-subunit (18) and does not block binding of agonists to the AChR or inhibit the function of the receptor (19). The extensor digitorum longus (EDL) muscle was harvested from each mouse and prepared slides were stained with AlexaFluor594-α-Bungarotoxin and either Cy2-mouse anti-rat IgG or FITC-anti-C3 stains and imaged using a fluorescent microscope. As can be seen in Figure 15 (**a**) and (**b**) on the following page, the mAb 35 is effectively reaching and binding to the AChRs in both PBS-treated and IL-12 treated B6 mice as evidenced by the Cy2-mouse anti-rat IgG signal in the green channel. Figure 15 (**c**) and (**d**) show that both the PBS-treated and IL-12 treated mice have complement component C3 bound to their AChRs. While not

visually discernable based on simply viewing the images, when quantified, the level of C3 bound to the AChRs of the sick IL-12 treated mice (1.63 ± 0.08) is approximately twice that of the healthy PBS-treated mice (0.70 ± 0.16). The whole-image quantification was performed using MATLAB software with the assistance of Dr. Scott Molitor (Department of BioEngineering, University of Toledo) and the data is summarized in Table 2.

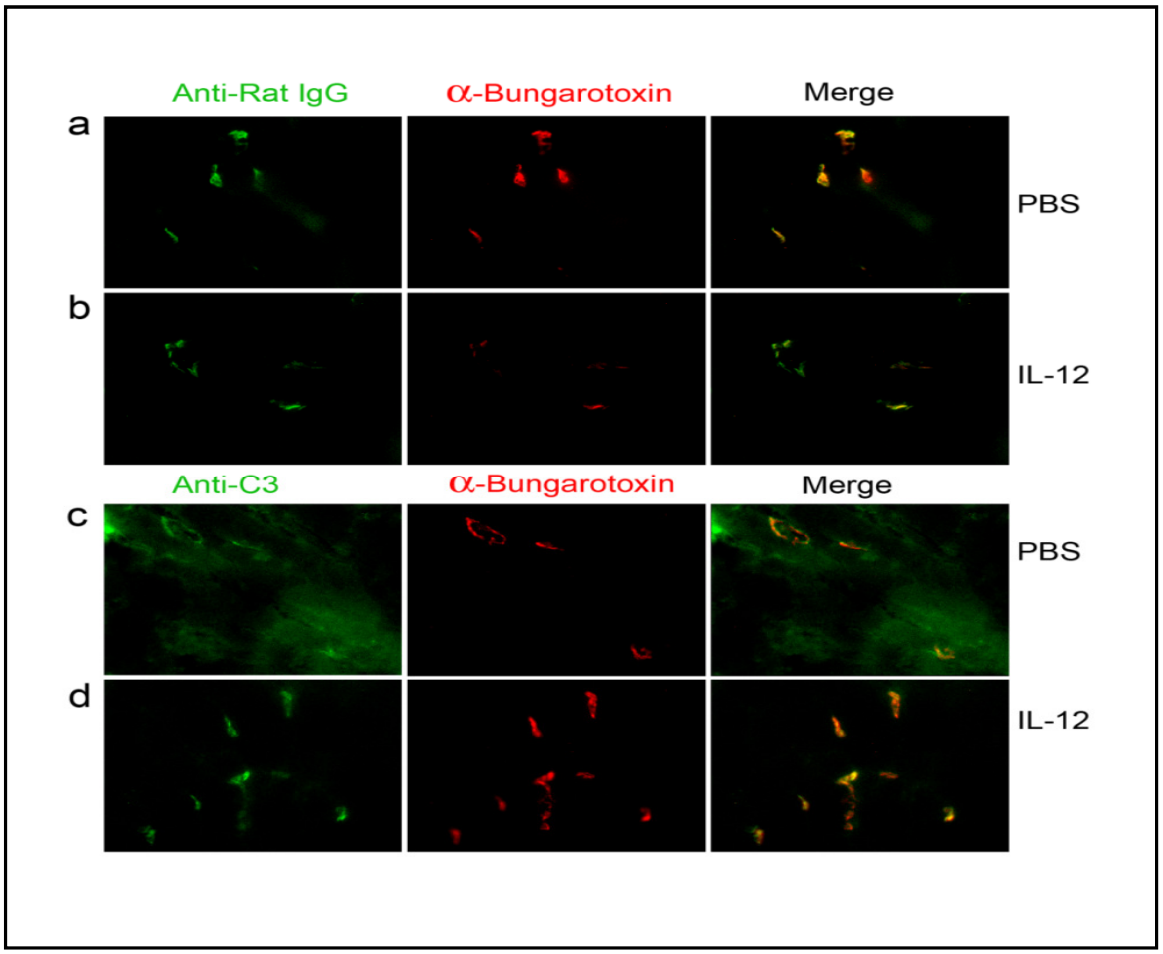

Figure 15: Presence of complement and mAb 35 at the neuromuscular junctions of IL-12 treated B6 mice. B6 mice received daily i.p. injections of IL-12 (1 µg) or PBS on Days -1 thru +3 and again on Days +20 thru +22. All mice received a single s.c. tail base injection of the *Torpedo* α146-162 peptide (1.7 µg in 50 µl CFA with PBS) on Day 0 and again on Day +21. On Day +25, all mice received a single i.p. injection of rat anti-AChR mAb 35 (3.5 mg). Mice were euthanized on Day +27 and EDL muscle was harvested and sectioned. Tissue sections from IL-12 and PBS treated mice were stained with

AlexaFluor594-α-Bungarotoxin and Cy2-mouse anti-rat IgG (a+b) or AlexaFluor594-α-Bungarotoxin and FITC-anti-C3 (c+d).

Table 2: Quantified fluorescent values of images in Figure 15

	PBS Treated	**IL-12 Treated**	**P Values**
Anti-IgG Average Value	0.52 ± 0.07	0.69 ± 0.15	P= 0.3343
Anti-C3 Average Value	0.70 ± 0.16	1.63 ± 0.08	P= 0.002

3.1.4 Complement binding levels do not confer EAMG resistance in IFN-$\gamma^{-/-}$ mice

In the same manner as described for Figure 15, EDL muscle was harvested from all mice treated with once daily i.p. injections of IL-12 at Days -1 thru +3 and again on Days +20 thru +22. The *Torpedo* α146-162 peptide was administered once on Day 0 with a booster injection on Day +21via s.c. tail base injection. On Day +25, all mice received an i.p. injection of 3.5 mg of rat mAb 35 and the mice were euthanized 7 days later (on Day +32). The EDL muscle slices were stained in an identical manner as those described in Figure 15. As can be seen in Figure 16 on the next page, both the mAb 35 (**a**+**b**) and C3 (**c**+**d**) are effectively reaching and binding to the AChRs in both the IL-12 treated B6 and IFN-$\gamma^{-/-}$ mice. Interestingly, when quantified in Table 3, the levels of mAb 35 and C3 bound to the AChRs of the EAMG-resistant IFN-$\gamma^{-/-}$ mice are very similar to the levels of mAb 35 and C3 bound to the AChRs of the sickened B6 mouse. This result indicates that the resistance to EAMG development that IFN-$\gamma^{-/-}$ mice display is not due to a reduction in the capacity of antibody or complement to effectively bind to the AChR. When taken

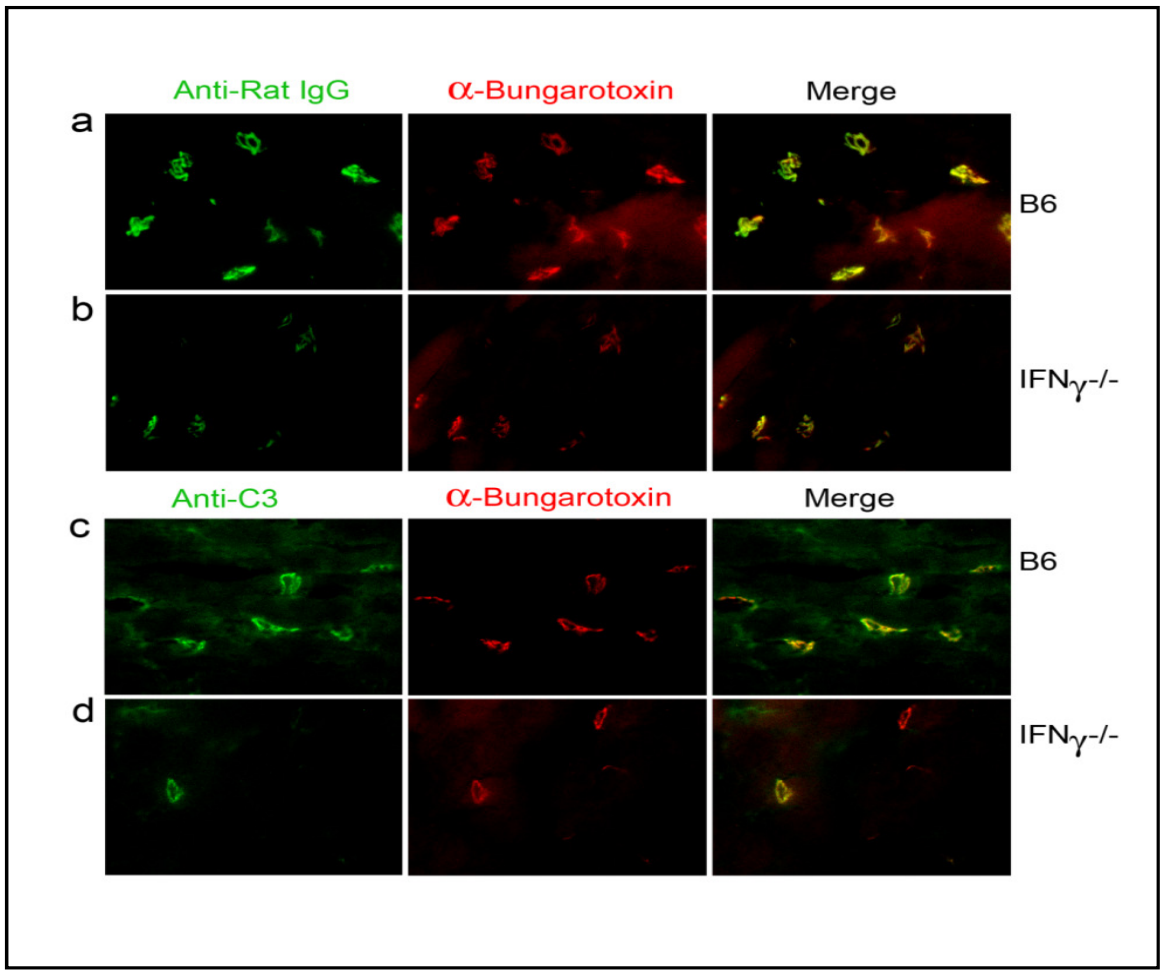

together this suggested that IL-12, through IFN-γ, may increase susceptibility to EAMG through mechanisms downstream of antibody and complement C3 binding.

Figure 16: Presence of complement and mAb 35 at the neuromuscular junctions of IL-12 treated IFN-$\gamma^{-/-}$ mice. B6 and IFN$\gamma^{-/-}$ mice received daily i.p. injections of IL-12 (1 µg) on Days -1 thru +3 and again on Days +20 thru +22. All mice received a single s.c. tail base injection of the *Torpedo* α146-162 peptide (1.7 µg in 50 µl CFA with PBS) on Day 0 and again on Day +21. On Day +25, all mice received a single i.p. injection of rat anti-AChR mAb 35 (3.5 mg). Mice were euthanized on Day +27 and EDL muscle was harvested and sectioned. Tissue sections from IL-12 treated B6 and IFN$\gamma^{-/-}$ mice were stained with AlexaFluor594-α-Bungarotoxin and Cy2-mouse anti-rat IgG (a+b) or AlexaFluor594-α-Bungarotoxin and FITC-anti-C3 (c+d).

Table 3: Quantified fluorescent values of images in Figure 16.

	B6 Mice	IFN-$\gamma^{-/-}$ Mice	P Values
Anti-IgG Average Value	1.42 ± 0.12	1.23 ± 0.08	P= 0.2506
Anti-C3 Average Value	1.09 ± 0.17	1.02 ± 0.12	P=0.7575

3.2 Natural killer cell depletion efficiency assays

3.2.1 Natural killer cell depletion efficiency assay #1

The individual treatment conditions, number, sex, and strain of mice used in each assay group are highlighted in the following outline:

- Group 1, [-NK, +PBS]: Six female B6 mice
- Group 2, [-NK, +IL-12]: Four female B6 mice
- Group 3, [B6, +PBS]: Six female B6 mice
- Group 4, [B6, +IL-12]: Four female B6 mice
- Group 5, [TCRko, +PBS]: Four female TCR$\beta\delta^{-/-}$ mice
- Group 6, [TCRko, +IL-12]: Four female TCR$\beta\delta^{-/-}$ mice

Our mAb PK136 (from hybridoma clone PK136) injection strategy was adapted from previous work by Shi et. Al (48). Based on the results of our pilot assays, we aimed to ensure full clearance of both NK and NKT cells prior to the start of the IL-12 treatments. We incorporated an additional "booster" injection of 150 µg of mAb PK136

prior to the start of the IL-12 treatments in order to achieve this. As detailed previously in Research Design and Methods, Sections 2.4.2 and 2.4.3, mAb PK136 cell depletion efficiency was assayed by flow cytometry using splenocytes derived from mice in both treatment and control groups. In total, this procedure was performed twice at different assay time points.

During the natural killer cell depletion passive EAMG assays, one NK cell-depleted B6 mice from Group 1 (+PBS) and one wild type B6 mouse from Group 3 (+PBS) were euthanized and their spleens were removed and prepared for flow cytometric analysis on Day +3. For each sample tube, 10^6 bulk splenocytes were stained with fluorescently-conjugated monoclonal antibodies against the natural killer cell surface protein markers NK1.1 (FITC-anti-NK1.1 stain derived from hybridoma clone PK136) and CD49b (PE-anti-DX5 stain derived from hybridoma clone DX5). While the NK1.1 (also known as CD161) protein is known to be expressed on the cell surface of both NK and NKT cells in C57BL/6 mice, the CD49b (also known as integrin $\alpha 2\beta 1$) protein is thought to be specific to only NK cells in these mice. Therefore, anti-NK1.1 staining will show the presence of both NK and NKT cells whereas anti-DX5 staining has the ability to detect only NK cell presence. Figure 17 shows histograms of the anti-NK1.1 and anti-DX5 staining results generated from the flow cytometry data compiled for both individual mice.

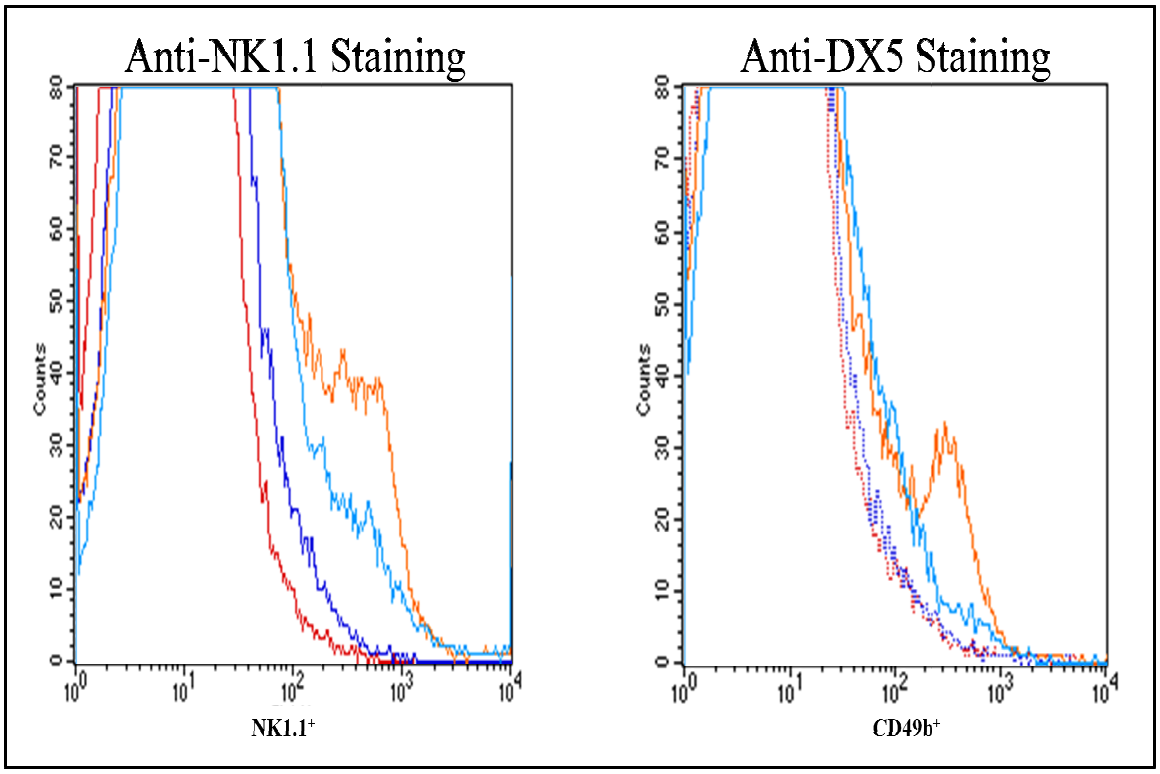

Figure 17: The NK1.1$^+$ and DX5$^+$ splenocyte populations remain depleted on Day +3, seven days after the initial injections of mAb PK136. B6 mice received an i.p. injection of either mAb PK136 (300 µg) or PBS on Day -4 and a booster injection of either mAb PK136 (150 µg) or PBS on Day -3. On Day +3, mice receiving mAb PK136 (+PK136) or PBS (-PK136) were euthanized and their spleens were removed. For the Anti-NK1.1 staining figure at left, splenocytes (10^6 per sample tube) from each mouse were stained as follows: -PK136, DyLight488 isotype control (red); +PK136 DyLight488 isotype control (blue); -PK136, anti-NK1.1 (orange); and +PK136, anti-NK1.1 (cyan). For the Anti-DX5 staining figure at right, splenocytes (10^6 per sample tube) from each mouse were stained as follows: -PK136, PE Rat IgM isotype control (red); +PK136, PE Rat IgM isotype control (blue); -PK136, PE anti-DX5 (orange); and +PK136, PE anti-DX5 (cyan).

As can be seen from Figure 17, the initial bulk mAb PK136 injection on Day -4 and first booster injection on Day -3 resulted in both the NK1.1$^+$ and CD49b$^+$ (DX5$^+$) splenocyte populations remaining depleted seven days later on Day +3. While not 100% depleted, the NK1.1$^+$ population is clearly smaller in the mAb PK136 injected mouse (+PK136) as evidenced by the difference in anti-NK1.1 staining between the +PK136

mouse (light blue line) and the mouse not receiving mAb PK136 (-PK136, orange line) when viewing the anti-NK1.1 staining histogram at left in Figure 17. The level of population reduction is even more pronounced when viewing the anti-DX5 staining histogram at right in Figure 17, in which the +PK136 mouse (light blue line) exhibits a clearly lowered level of DX5 expression versus the –PK136 mouse (orange line). A gate highlighting the location of positive cell populations was applied to both the anti-NK1.1 and anti-DX5 staining histograms shown in Figure 17 in order to generate statistical expression level data of all the staining conditions (both stains of interest and isotype controls). The percentage of positive cells in the isotype controls were subtracted from the percentage of positive cells in the samples of interest in order to calculate the overall percentage of $NK1.1^+$ and $DX5^+$ cells for each mouse. Table 4 summarizes the results of the percentage of positive cells calculations for both mice assayed.

Table 4: Quantified percentage of positive cells for histograms in Figure 17

Mouse	Stain	% Positive Cells	% Positive Cells Above Background
-PK136 (no depletion)	DyLight488 Isotype Control	0.37	7.42
	Anti-NK1.1 + DyLight488	7.79	
	PE Rat IgM Isotype Control	0.92	3.13
	PE anti-DX5	4.05	
+PK136 (NK cell depleted)	DyLight488 Isotype Control	1.21	3.37
	Anti-NK1.1 + DyLight488	4.58	
	PE Rat IgM Isotype Control	0.96	1.22
	PE anti-DX5	2.18	

As can be seen from the expression level percentage values in Table 4, the cell depleted mouse (+PK136) had a 4.05% (7.42% minus 3.37%) lower percentage of $NK1.1^+$ cells correlating to a 54.6% efficiency of depletion as compared to the non-depleted –PK136 control mouse seven days post-injection of mAb PK136. This decrease can be attributed to the depletion and clearance of both NK and NKT cells that arises from treatment with the anti-NK1.1 monoclonal PK136 antibody as described previously. More specifically, in regards to specific NK cell depletion as measured by anti-DX5 staining, the cell depleted +PK136 mouse had 1.91% (3.13% minus 1.22%) fewer $DX5^+$ cells correlating to a 61.0% efficiency of depletion of specifically NK cells as compared to the non-depleted –PK136 control mouse seven days post-injection of mAb PK136. These results show that the level of NK and NKT cells were definitively lowered prior to, during, and after the IL-12 treatments as a result of the initial bulk injection (300 µg on Day -4) and booster injection (150 µg on Day -3) of mAb PK136 performed early on during the overall assay. Therefore, any effects seen on the serum IFN-γ levels of blood samples taken from mAb PK136 injected mice (Groups 1 and 2) during and immediately after the IL-12 treatment round will reflect the mAb PK136-mediated depletion of NK and NKT cells.

3.2.2 Natural killer cell depletion efficiency assay #2

During the natural killer cell depletion passive EAMG assays, one NK cell-depleted B6 mice from Group 1 (+PBS, +PK136) and one wild type B6 mouse from Group 3 (+PBS, -PK136) were euthanized and their spleens were removed and prepared for flow cytometric analysis on Day +9. The mouse from Group 1 had received the second booster i.p. injection (previously labeled “Booster B”) of mAb PK136 on Day +4.

Both mice received an i.p. injection of the anti-AChR mAb D6 on Day +6, and therefore Day +9 represented the +72-hour post-mAb D6 passive immunization time point. Mice were subjected to exercise and grip strength measurement analysis as normal prior to their euthanasia and spleen removal. Splenocyte samples from both mice were processed and stained identically to those analyzed and described above for the natural killer cell depletion efficiency assay #1. Figure 18 shows dot plot comparisons of anti-NK1.1 and anti-DX5 dual-stained sample tube results generated from the flow cytometry data compiled for both individual mice.

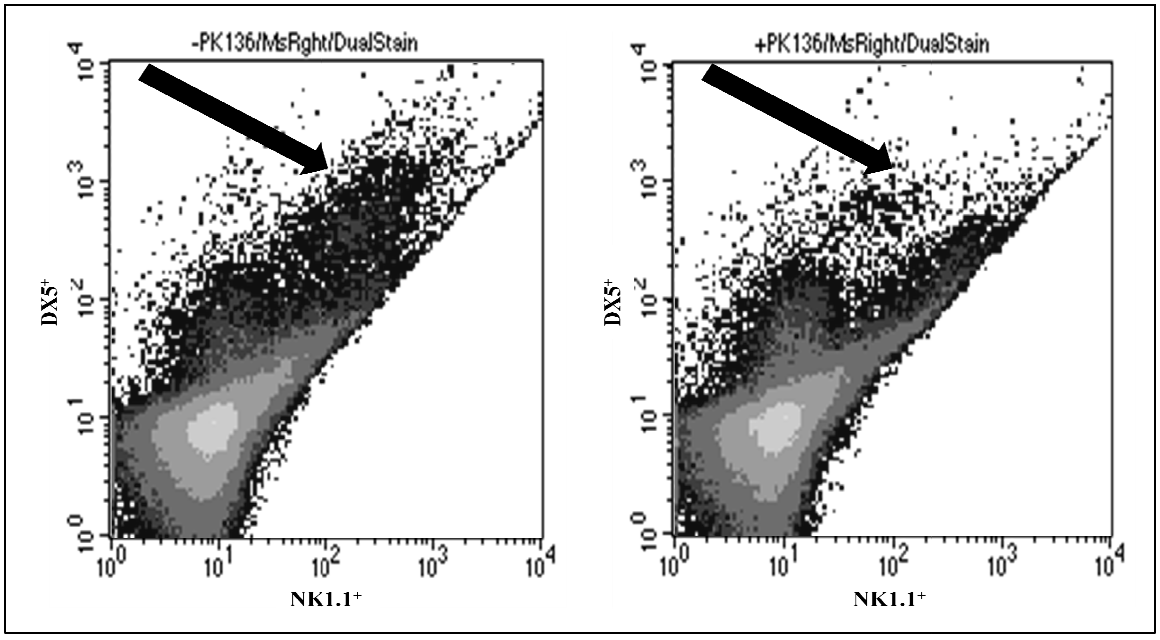

Figure 18: The NK1.1$^+$DX5$^+$ splenocyte population remains depleted on Day +9, five days after the second booster injection of mAb PK136. B6 mice received an i.p. injection of either mAb PK136 (300 µg) or PBS on Day -4 and a booster i.p. injection of either mAb PK136 (150 µg) or PBS on Day -3. On Day +4, mice received a second booster i.p. injection of either mAb PK136 (150 µg) or PBS. On Day +9, mice receiving mAb PK136 (+PK136) or PBS (-PK136) were euthanized and their spleens were removed. For each dot plot, splenocytes (10^6 per sample tube) from each mouse were dual stained with FITC anti-NK1.1 and PE anti-DX5. The large black arrow in each dot plot highlights the presence or absence of a distinctly NK1.1$^+$DX5$^+$ dual stained splenocyte population.

As can be seen from Figure 18, the $NK1.1^{+}DX5^{+}$ splenocyte population remains depleted in the +PK136 mouse on Day +9, five days after the second booster mAb PK136 injection on Day +4. This is evidenced by the visible lack of a well-defined $NK1.1^{+}DX5^{+}$ splenocyte population in the +PK136 mouse. The thick black arrow in the control -PK136 mouse dual-stained dot plot to the left of Figure 18 shows the presence of a rounded, well-defined $NK1.1^{+}DX5^{+}$ splenocyte population that is not present in the +PK136 mouse dual stained dot plot. This confirms once again that the administration of mAb PK136 via i.p. injection is sufficient to effectively deplete available NK and NKT cell populations in the spleen that are able to respond to the IL-12 and mAb D6 treatments. In an identical manner to the procedures performed in order to generate Table 4, a uniform gate highlighting the location of positive cell populations was used on the natural killer cell depletion efficiency assay #2 anti-DX5 staining histogram (not shown) for the purpose of calculating the percentage of positive cells. Table 5 summarizes the results of the percentage of positive cells calculations for both mice assayed.

Table 5: Quantified percentage of positive cells for euthanized Day +9 mice

Mouse	Stain	% Positive Cells	% Positive Cells Above Background
-PK136 (no depletion)	PE Rat IgM Isotype Control	1.08	3.14
	PE anti-DX5	4.22	
+PK136 (NK cell depleted)	PE Rat IgM Isotype Control	1.06	1.24
	PE anti-DX5	2.30	

As can be seen from the expression level percentage values exhibited in Table 5, the cell depleted +PK136 mouse had 1.9% (3.14% minus 1.24%) fewer $DX5^{+}$ cells surface protein correlating to a 60.5% efficiency of depletion of specifically NK cells as

compared to the non-depleted –PK136 control mouse five days post-injection of mAb PK136. This confirms once again that the administration of mAb PK136 via i.p. injection is sufficient to effectively deplete and clear the available NK and NKT cell populations in the spleen that are able to respond to the IL-12 and mAb D6 treatments. In this case, NK and NKT cells still remained depleted to a large extent five days after the injection of mAb PK136. Therefore, at the Day +9 time point +72 hours after mAb D6 passive immunization, any effects seen on passive EAMG induction and muscle weakness in mAb PK136 injected mice (Groups 1 and 2) will reflect the mAb PK136-mediated depletion of NK and NKT cells.

3.3 Grip strength measurements

During the natural killer cell depletion passive EAMG assays, all mice in Groups 1 thru 6 received a single i.p. injection of 3 mg mAb D6 on Day +6. The grip strength of each mouse within these groups was then analyzed once daily every 24 hours post-mAb D6 immunization after the mice were individually subjected to three brief but intensive exercise periods. For a given assay time point, an overall grip strength value was generated for each mouse by averaging the peak grip strength measurements recorded during each of three measurement rounds for a single mouse. The averaged peak grip strength value for each mouse in a group was then plotted and used to generate a mean peak grip strength value for that assay group. The results of the grip strength assays performed on all six groups of mice can be seen in Figure 19.

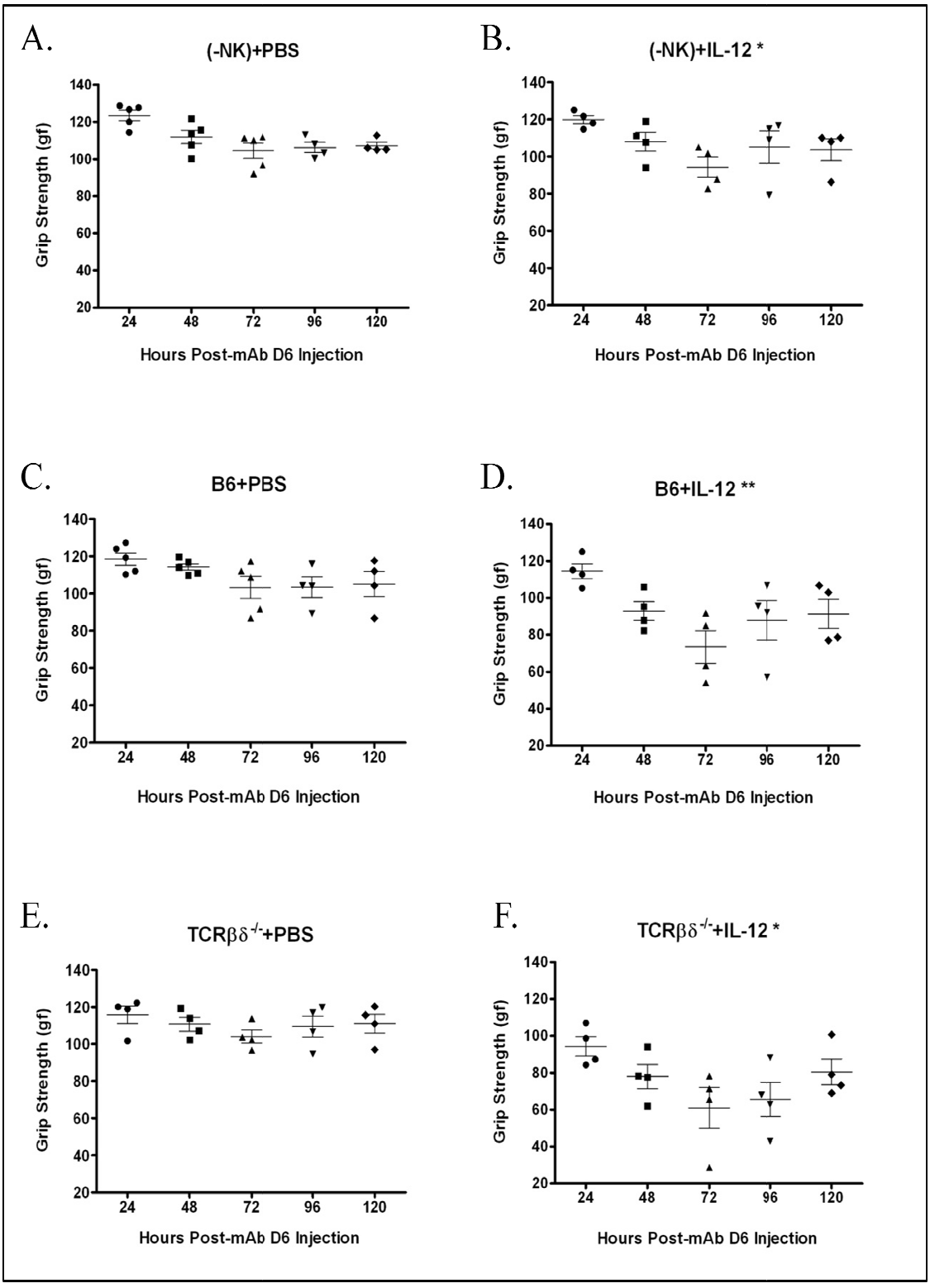

Figure 19: Post mAb D6 immunization grip strength measurements performed every twenty-four hours on Days +7 thru +11. All mice in the -NK+PBS (**A**), -NK+IL-12 (**B**), B6+PBS (**C**), B6+IL-12 (**D**), TCRβδ$^{-/-}$+PBS (**E**), and TCRβδ$^{-/-}$+IL-12 (**F**) groups

received daily i.p. injections of IL-12 (1 μg) or PBS on Days -1 thru +3. On Day +6, all mice received a single i.p. injection of mAb D6 (3 mg). Individual mouse grip strength (in grams of force) was measured daily in 24-hour intervals on Days +7 thru +11 using a digital grip strength meter. Statistical significance of data was assessed using Two-way ANOVA with repeated measures. *$p < 0.05$ and **$p < 0.01$ versus PBS control treatment group for each treatment series.

As can be seen in Figure 19, there was no significant reduction in overall grip strength at any time point in any of the PBS-treated assay groups that received mAb D6 passive immunization (Fig 19 A, C, and E). However, IL-12 treated B6 mice (Fig 19D) showed significant reductions in peak grip strength measurements when compared to their PBS treated counterparts ($p< 0.01$). When examining the trajectory of muscle weakness in these two mouse groups it becomes evident that the PBS treated B6 mice (Fig 19C) remain consistently healthy and do not display extensive negative effects from the administration of mAb D6. The same cannot be said of the IL-12 treated mice B6 (Fig 19D), where muscle weakness begins to appear at 48-hours post-mAb D6 passive immunization, peaks at +72-hours, and has not reversed to healthy grip strength levels by the +120-hour time point.

As can be seen, the peak grip strength averages of the NK cell depleted, PBS-treated mice (Fig 19A) remain consistently high while those of the NK cell depleted, IL-12 treated mice (Fig 19B) exhibit only slight reductions in grip strength, suggesting that NK cell depletion blocks the exacerbation of muscle weakness previously documented in IL-12 and mAb D6 treated B6 mice. This trend of resistance to development of muscle weakness was not witnessed in either the IL-12 treated B6 (Fig 19D) or the IL-12 treated TCR$\beta\delta^{-/-}$ (Fig 19F) assay groups. In these groups, treatment with IL-12 and mAb D6

resulted in noticeable development of muscle weakness that was not witnessed in their PBS and mAb D6 treated counterparts.

Interestingly, the trajectory of muscle weakness development was strikingly more fast-paced in the IL-12 treated TCR$\beta\delta^{-/-}$ mice (Fig 19F) as compared to IL-12 treated NK cell depleted mice (Fig 19B), where muscle weakness was detectable and significantly different than PBS-treated control TCR$\beta\delta^{-/-}$ mice (Fig 19E) as early as the 24-hour post-mAb D6 passive immunization time point. The peak grip strength measurements of the IL-12 treated TCR$\beta\delta^{-/-}$ mice were significantly lower than their PBS-treated counterparts as well ($p<0.05$) [Fig 19E and F]. The difference in overall grip strength reduction between IL-12 treated B6 (Fig 19D) and NK cell depleted (Fig 19B) mice was found to be statistically significant using the Two-way ANOVA with repeated measures analysis ($p<0.01$). The same was true when using this statistical analysis method to compare the difference in IL-12 treatment in the B6 (Fig 19D) and TCR$\beta\delta^{-/-}$ (Fig 19F) mouse groups ($p<0.05$). Figure 20 emphasizes the differences in peak grip strength measurements seen between the IL-12 treated NK cell-depleted, wild-type B6, and TCR$\beta\delta^{-/-}$ mouse assay groups seen in Figure 19B, D, and F.

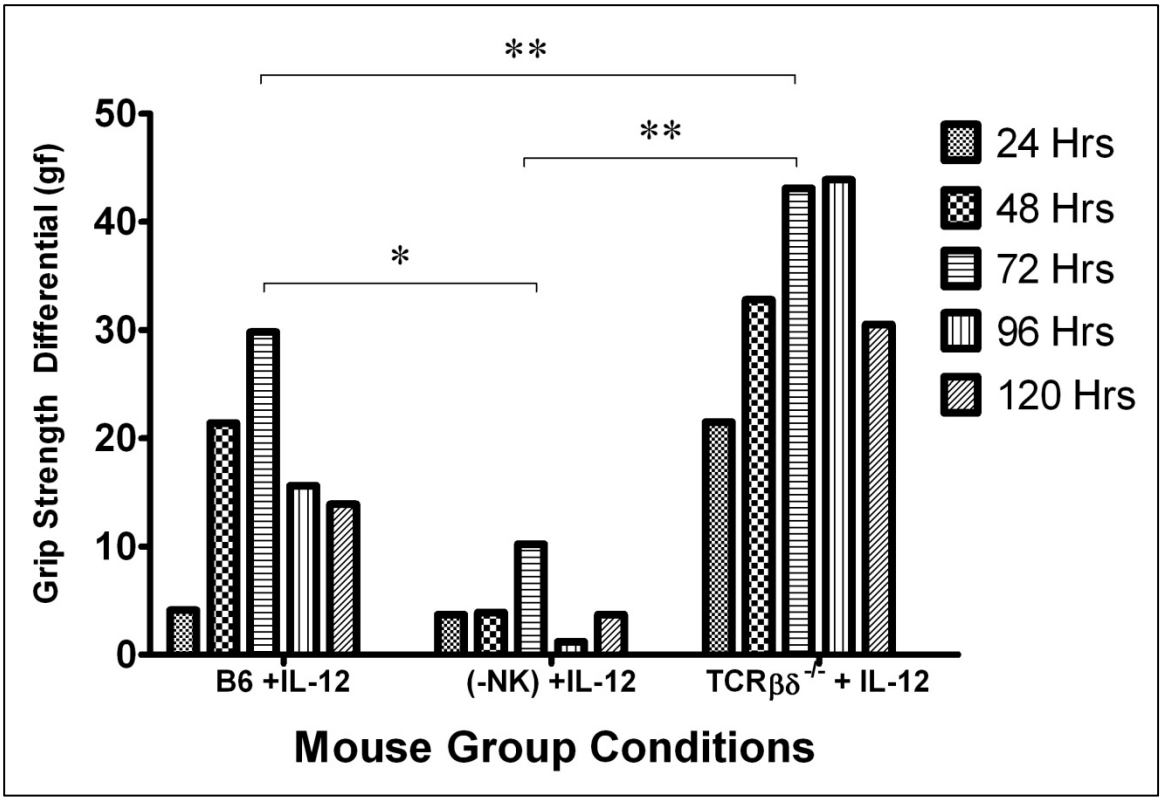

Figure 20: Comparison of the effect of IL-12 treatment on assay group peak grip strength differentials. Data gathered from the grip strength assays for all mouse in the groups seen in Fig. 19 was analyzed and a mean grip strength differential (in grams of force) was determined for each by subtracting the mean grip strength value of the IL-12 treated group from the mean grip strength value of the control PBS treated group at each assay time point. Statistical significance of data was assessed using One-tailed paired t-Tests. *$p < 0.05$ and **$p < 0.01$ comparing IL-12 treatment groups shown in brackets.

As can be seen in Figure 20, there are noticeable differences in the grip strength differential between the IL-12 treated NK cell-depleted, wild-type B6, and TCR$\beta\delta^{-/-}$ mouse assay groups. The peak grip strength differential for each mouse assay group at a given time point was determined by subtracting the IL-12 treated group's peak grip strength average from the PBS-treated group's peak grip strength average. In this manner, it is clear that the trend in passive EAMG severity throughout the grip strength measurements is highest in the TCR$\beta\delta^{-/-}$ mice and lowest in the NK cell–depleted mice,

with wild-type B6 mice showing mid-level sickness. These results were found to be significant using the One-tailed paired t-Test statistical assay. While not shown, statistical significance was also seen when using One-Way ANOVA and Tukey's Multiple Comparisons Post-Test in order to compare the peak grip strength differential of the IL-12 treated TCR$\beta\delta^{-/-}$ versus that of the IL-12 treated B6 ($p < 0.05$) and –NK ($p < 0.001$) mouse groups. Therefore, passive EAMG severity during these assays is as follows: TCR$\beta\delta^{-/-}$ mice > wild-type B6 mice > NK cell depleted mice. The climax of disease in all three IL-12 treated mouse groups appears to occur around the +72-hour post-mAb D6 immunization time point (Day +9), though muscle weakness remains substantially higher and declines much less rapidly in the IL-12 treated TCR$\beta\delta^{-/-}$ mice over the remaining two days of grip strength measurements.

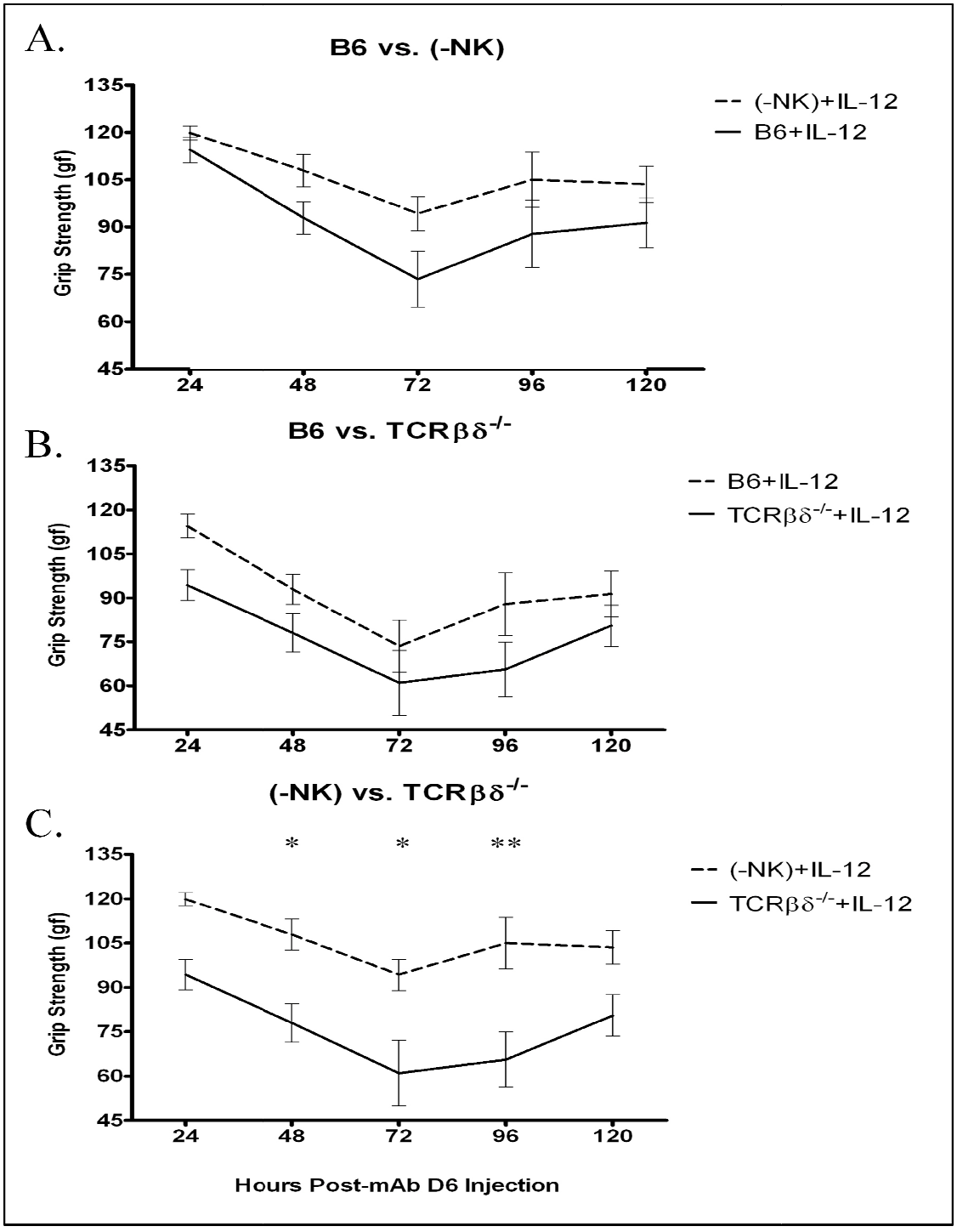

Figure 21: Effect of IL-12 treatment on peak grip strength measurements of individual treatment groups. Data gathered from the grip strength assays for all mouse in the groups seen in Fig. 19 was analyzed and the mean grip strength (in grams of force) for the IL-12 treated groups were plotted in comparison to one another. Statistical significance of data was assessed using Two-way ANOVA and Bonferroni's Post Test. *$p < 0.05$ and **$p < 0.01$ versus compared IL-12 treatment group.

As can be seen in Figure 21A, the IL-12 treated wild-type B6 mice display reduced peak grip strength as compared to the IL-12 treated NK cell-depleted mice. When comparing the differences in peak grip strength values seen in the TCRβδ$^{-/-}$ mouse strain to those in the B6 wild-type (Fig 21B) and NK cell depleted mice (Fig 21C), it becomes more evident that the IL-12 treated TCRβδ$^{-/-}$ mice exhibited a higher degree of sickness. In general, the IL-12 treated B6 and TCRβδ$^{-/-}$ mice showed a similar slope of disease development towards the +72-hour minimum, though the TCRβδ$^{-/-}$ mice were noticeably weaker during this time frame (Fig 21B). However, the IL-12 treated TCRβδ$^{-/-}$ mice showed a lag in their pace of recovery from the +72-hour disease climax point that the wild-type B6 mice did not (Fig 21B). This phenomenon becomes more pronounced when comparing the slope of disease development between the IL-12 treated NK cell-depleted and TCRβδ$^{-/-}$ mice (Fig 21C), where the NK cell-depleted mice show more resistance to disease development. Additionally, the IL-12 treated NK cell-depleted mice displayed a faster-paced recovery from the +72-hour disease climax point (Fig 21C). In fact, the differences in peak grip strength measurements between IL-12 treated TCRβδ$^{-/-}$ and NK cell-depleted mice are statistically significant at the +48, +72, and +96-hour time points. All in all, these results suggest that IL-12 treated TCRβδ$^{-/-}$ mice develop more severe passive EAMG symptoms earlier and take longer to recover from them than either IL-12 treated wild-type B6 or NK cell-depleted mice.

3.4 Serum IFN-γ ELISA assay

The rationale for harvesting and pooling blood serum from each mouse group involved in the overall passive EAMG assay stemmed from our desire to monitor the

serum IFN-γ concentrations of these groups at certain time points throughout the assay. While IL-12 treatment is known to facilitate IFN-γ production, the extent and duration of IFN-γ production remained unknown, especially in our passive transfer EAMG disease model. By performing the serum harvests and measuring the IFN-γ concentration via cytokine-specific enzyme-linked immunosorbent assays (ELISAs), we hoped to determine what the systemic levels of IFN-γ were at crucial time points throughout the assay. Mainly, these time points were segregated into three questions we hoped to answer:

1.) What is the systemic serum IFN-γ level during IL-12 treatment (mid-way through the IL-12 treatments, after two IL-12 injections, on Day +1 of the assay)?
2.) What is the systemic serum IFN-γ level immediately after the conclusion of IL-12 treatment but prior to immunization with mAb D6 (24 hours after the last IL-12 injection was administered, on Day +4 of the assay)?
3.) What is the systemic serum IFN-γ level post-mAb D6 immunization (48 hours after mAb D6 was administered, on Day +8 of the assay)?

By performing the serum harvests at these time points and measuring the serum IFN-γ concentration via ELISA, we hoped to determine how much of an impact IL-12 treatment had on overall IFN-γ production between different mouse groups, and also what influence on passive disease severity could any remaining serum IFN-γ have upon immunization with mAb D6.

During the natural killer cell depletion passive EAMG assays, all mice in Groups 1 thru 6 were lancet bled on Day +1, Day +4, and Day +8. Blood from individual mice in a group was pooled and allowed to clot before serum was harvested and frozen. Frozen serum samples from each bleeding time point were thawed and serially 5-fold diluted in order to measure serum IFN-γ levels via ELISA. Frozen IFN-γ standard solution was serially 2-fold diluted and measured within the same ELISA assay in order to generate a standard curve for downstream data analysis of diluted serum sample IFN-γ level data. The results of the serum IFN-γ level ELISA assay can be seen in Figure 22. Please note the differences in the pg/ml serum IFN-γ level scales (located on the y-axis) between the Day +1, Day +4, and Day +8 figures.

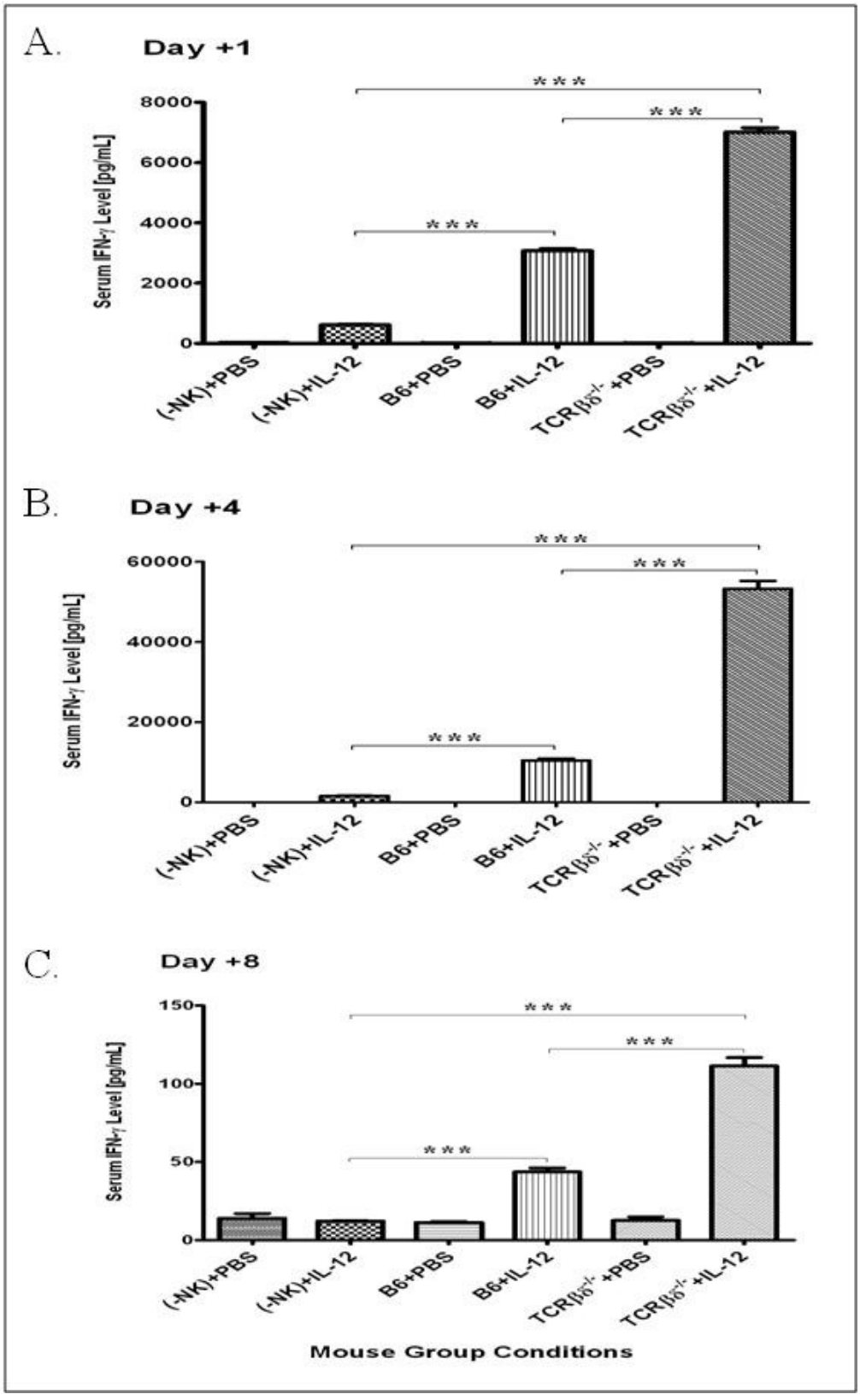
A.
Day +1
Serum IFN-γ Level [pg/mL]
8000
6000
4000
2000
0
* * *
* * *
* * *
(-NK)+PBS
(-NK)+IL-12
B6+PBS
B6+IL-12
TCRβδ-/- +PBS
TCRβδ-/- +IL-12
B.
Day +4
Serum IFN-γ Level [pg/mL]
60000
40000
20000
0
* * *
* * *
* * *
(-NK)+PBS
(-NK)+IL-12
B6+PBS
B6+IL-12
TCRβδ-/- +PBS
TCRβδ-/- +IL-12
C.
Day +8
Serum IFN-γ Level [pg/mL]
150
100
50
0
* * *
* * *
* * *
(-NK)+PBS
(-NK)+IL-12
B6+PBS
B6+IL-12
TCRβδ-/- +PBS
TCRβδ-/- +IL-12
Mouse Group Conditions

Figure 22: Serum IFN-γ levels on Days +1, +4, and +8. Mice in all groups were lancet bled on Days +1, +4, and +8. Blood from individual mice in each group was pooled and serum IFN-γ levels were measured using ELISA. Absorbance was measured at 450 nm and background absorbance, measured at 570 nm, was subtracted out to determine final values. Standard curves for each time point were generated using known concentrations of IFN-γ standards. *Please note the differences in the pg/ml serum IFN-γ level scales (located on the y-axis) between the Day +1, Day +4, and Day +8 figures.* Statistical significance of data was assessed using One-way ANOVA and Tukey's Multiple Comparisons Post Test. ***$p < 0.001$ versus either -NK+IL-12 or B6+IL-12 treatment groups where indicated by brackets.

As can be seen from Figure 22A, the IL-12 treated B6 mice possessed a significantly higher amount of serum IFN-γ than the IL-12 treated NK cell-depleted mouse group. In addition, the IL-12 treated TCRβδ$^{-/-}$ mouse group displayed significantly higher serum IFN-γ levels than all other mouse treatment groups on the Day +1 bleeding time point. In fact, on Day +1 after two i.p. injections of IL-12 were performed the IL-12 treated TCRβδ$^{-/-}$ mice exhibited the highest serum IFN-γ concentration at 7,013 pg/ml. This serum IFN-γ concentration was 11.3-fold higher than that of the IL-12 treated NK cell-depleted mouse group (621 pg/ml) and 2.3-fold higher than the IL-12 treated B6 mouse group (3,074 pg/ml). In all cases on the Day +1 bleeding time point, PBS-treated control mouse groups exhibited very low serum IFN-γ levels that were significantly lower than their IL-12 treated counterparts, reinforcing the fact that IL-12 treatment is necessary for IFN-γ production within the immune system.

Figure 22B shows that the level of serum IFN-γ in IL-12 treated B6 mice is greatly increased by the Day +4 time point, exactly 24 hours after administration of the last IL-12 treatment. Similarly to Day +1, the IL-12 treated B6 mice possessed a significantly higher amount of serum IFN-γ than the IL-12 treated NK cell-depleted mouse group on the Day +4 time point. In fact, the IL-12 treated TCRβδ$^{-/-}$ mice again

exhibited the highest serum IFN-γ concentration at 53,205 pg/ml (Fig 22B). More surprisingly, this serum IFN-γ concentration was 33.1-fold higher than that of the IL-12 treated NK cell-depleted mouse group (1,609 pg/ml) and 5.1-fold higher than the IL-12 treated B6 mouse group (10,427 pg/ml). This dramatic elevation in serum IFN-γ level out-paced that which was occurring in the IL-12 treated wild-type B6 mouse group between Day +1 and Day +4 (a 2.3-fold difference on Day +1 vs. a 5.1-fold higher difference on Day +4). Again, in all cases on the Day +4 bleeding time point, PBS treated control mouse groups exhibited very low serum IFN-γ levels that were significantly lower than their IL-12 treated counterparts.

On Day +8, forty-eight hours after passive immunization with mAb D6, the IL-12 treated B6 mice possessed a significantly higher amount of serum IFN-γ than the IL-12 treated NK cell-depleted mouse group. In accordance with results seen on Days +1 and +4, the IL-12 treated TCR$\beta\delta^{-/-}$ mice still exhibited the highest serum IFN-γ concentration at 111.4 pg/ml (Fig 22C), though this serum IFN-γ level was substantially lower than those previously seen on Days +1 and +4. While quite reduced, this serum IFN-γ concentration was 9.0-fold higher than that of the IL-12 treated NK cell-depleted mouse group (12.3 pg/ml) and 2.5-fold higher than the IL-12 treated B6 mouse group (43.6 pg/ml). Again, in all cases on the Day +8 bleeding time point, PBS treated control mouse groups exhibited very low serum IFN-γ levels that were significantly lower than their IL-12 treated counterparts except in the NK cell-depleted mouse groups. Table 6 summarizes the serum IFN-γ concentrations for each mouse group at each bleeding time point as shown in Figure 22. It is important to note that all PBS treated mouse groups had

very similar basal levels of serum IFN-γ at the Day +1, Day +4, and Day +8 bleeding assay time points.

Table 6: Mean serum IFN-γ concentrations (in pg/mL) for all groups assayed in Figure 22

Mouse Group	Day +1	Day +4	Day +8
(-NK) +PBS	22	14	14
(-NK) +IL-12	621	1,609	12
(B6) +PBS	15	12	11
(B6) +IL-12	3,074	10,427	44
(TCRβδ$^{-/-}$) +PBS	14	10	13
(TCRβδ$^{-/-}$) +IL-12	7,013	53,205	111

The results of the serum IFN-γ ELISA assays performed suggest that the absence of NK and NKT cells (in NK cell depleted mice) dramatically blunts the IL-12-induced IFN-γ production that is seen in the IL-12 treated B6 mice on Days +1 and +4. More so, the extremely high levels of serum IFN-γ in the IL-12 treated TCRβδ$^{-/-}$ mice, which possess only NK cells, on Days +1 and +4 compared to the other IL-12 treated groups suggests that innate NK cells are the primary source of IFN-γ in response to IL-12 within the immune system. In addition, all IL-12 treatment groups exhibited dramatically reduced serum IFN-γ levels that approached baseline control levels by the Day +8 time point, 120 hours after the last injection of IL-12 was administered and 48 hours post-mAb

D6 immunization. This observation suggests that serum IFN-γ levels drop upon cessation of IL-12 treatment and that additional IFN-γ production due to mAb D6 treatment, if any, is minor at best. Therefore, the trend in overall IFN-γ production between the different IL-12 treated mouse groups is as follows: TCRβδ$^{-/-}$ mice > B6 mice > NK cell-depleted mice.

3.5 Analysis of neuromuscular junction C3 deposition levels

During the natural killer cell depletion passive EAMG assays, all mice in Groups 1 thru 6 were euthanized between Days +12 and +13 and whole diaphragm muscle was immediately harvested from each mouse. Tissue slides were generated from frozen diaphragm muscle samples and stained with AlexaFluor®594-labeled α-Bungarotoxin and FITC Goat IgG Anti-Mouse Complement C3. Sample slides were imaged using an inverted fluorescent microscope and captured images were viewed and digitized using MetaMorph® 7. The digital images generated from the fluorescently stained diaphragm muscle samples can be seen in Figures 23 and 24.

For each image in Figures 23 and 24, individual neuromuscular junctions were quantified for average intensity using MetaMorph® 7. This was accomplished as previously described using the drawn box method (see Research Design and Methods, Section 2.11.7). Average intensity values were generated for each box drawn. The background average intensity was subtracted from a specific junctional average intensity in order to calculate the overall intensity for that junction, which was then averaged with all other junctions within that image for both the red and green fluorescent channel images. Table 7 on the following pages summarize the results of the individual

neuromuscular junction C3 staining level calculations for each mouse diaphragm sample derived from the images in Figures 23 and 24.

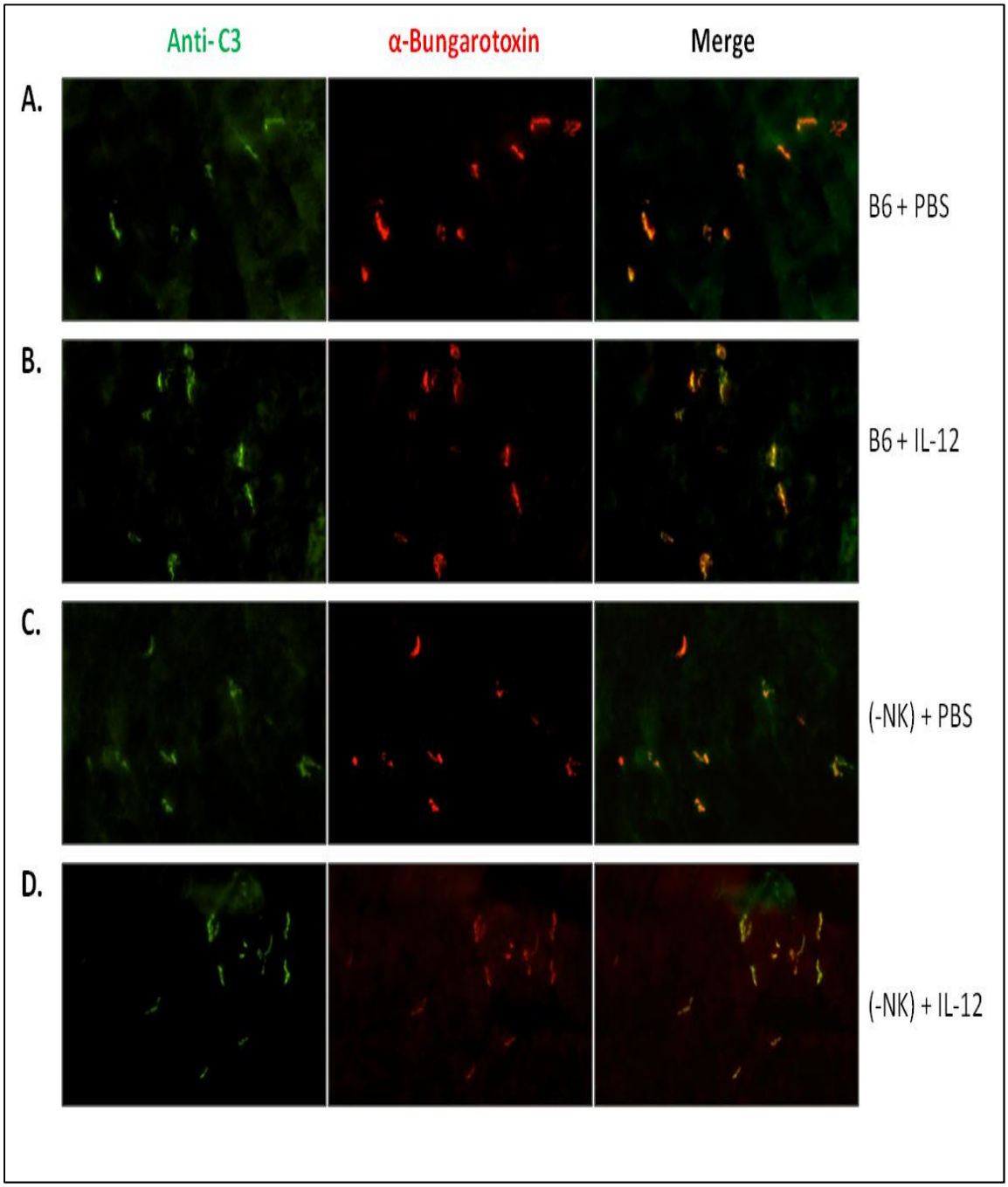

Figure 23: Presence of C3 at the neuromuscular junctions of PBS and IL-12 treated B6 and NK cell-depleted mice. B6 mice received an i.p. injection of either mAb PK136 (300 µg) or PBS on Day -4 and a booster i.p. injection of either mAb PK136 (150 µg) or PBS on Day -3 and again on Day +4 that served to designate them as either –NK (NK

cell depleted) or wild-type B6 mice. On Days -1 thru +3, all mice received daily i.p. injections of IL-12 (1 µg) or PBS. On Day +6, all mice received a single i.p. injection of mAb D6 (3 mg). All mice were euthanized on Days +12 and +13 and diaphragm muscle was removed and cryostat sectioned. Tissue sections were stained with AlexaFluor594-α-Bungarotoxin and FITC-anti-C3. Mouse groups sample staining is shown as follows: B6+PBS (**A**), B6+IL-12 (**B**), -NK+PBS (**C**), -NK+IL-12 (**D**).

As can be seen in Figure 23, all mouse diaphragm samples imaged display the presence of complement component C3 co-localized with the location of neuromuscular junctions. Both the PBS treated B6 (Fig 23A) and NK cell-depleted (Fig 23C) mice exhibit anti-C3 staining in the green channel that co-localizes with the location of neuromuscular junctions in the red channel when merged together. The same is true for the IL-12 treated B6 (Fig 23B) and NK cell-depleted (Fig 23D) mice, where C3 clearly co-localizes with neuromuscular junction presence when merged. In addition, while visually appearing similar in intensity, the levels of C3 deposition at the site of neuromuscular junctions are quite alike when examining the quantified average green-to-red intensity values shown in Table 7 for each individual mouse diaphragm sample within Figure 23.

Table 7: Quantified average green-to-red neuromuscular junction fluorescence intensity values of images in Figures 23 & 24. Green-to-red ratios for each stained and imaged neuromuscular junction were generated as described in Research Design and Methods Section 2.11.7. Statistical significance was determined by comparing the IL-12 and PBS treatment group average green-to-red ratio values using the unpaired Two-tailed T-test.

Mouse Group	Avg. Green/Red Ratio	P Value	IL-12 Treatment Difference: [IL-12]/[PBS]
B6 + PBS	0.44 ± 0.06	0.494	**0.89**
B6 + IL-12	0.39 ± 0.04		
(-NK) + PBS	0.76 ± 0.24	0.544	**0.82**
(-NK) + IL-12	0.62 ± 0.05		
TCRβδ$^{-/-}$ + PBS	0.47 ± 0.05	0.483	**0.89**
TCRβδ$^{-/-}$ + IL-12	0.42 ± 0.05		

When examining the quantified average green-to-red neuromuscular junction fluorescence intensity values seen in Table 7 for all four mouse diaphragm samples

within Figure 23 it becomes evident that the individual sample average intensity values are quite comparable. For the wild-type B6 assay groups, PBS treated mice (Fig 23A) have an average green-to-red sample ratio value of 0.44 ± 0.06 whereas that of IL-12 treated mice (Fig 23B) is 0.39 ± 0.04. The similar green-to-red ratio values indicate that the IL-12 and PBS treated B6 mice have comparable levels of complement component C3 bound to their neuromuscular junctions. In regards to the effects of NK cell depletion, PBS treated NK cell-depleted mice (Fig 23C) have an average green-to-red ratio value of 0.76 ± 0.24 while that of the IL-12 treated NK cell-depleted mice (Fig 23D) is 0.62 ± 0.05. Here, the slightly smaller green-to-red ratio value indicates that the IL-12 treated NK cell-depleted mice have a somewhat lower level of C3 bound to their neuromuscular junctions on average as compared to their PBS treated counterparts.

The impact of IL-12 versus PBS treatment on specific mouse groups, as shown in Table 7, indicates that the individual neuromuscular junctions of IL-12 treated B6 mice are bound by virtually the same amount of complement component C3 on average as compared to IL-12 treated NK cell-depleted mice. This is evidenced by the results seen when comparing the IL-12-to-PBS treatment differential for the B6 mouse groups (0.89) to that of the NK cell-depleted mouse groups (0.82). The similarity of the IL-12-to-PBS treatment differentials between the B6 and NK cell-depleted groups is telling as it underlines the consistent extent of C3 deposition at the neuromuscular junctions of IL-12 treated B6 mice as compared to their PBS treated counterparts. This highlights that the degree of C3 deposition at the neuromuscular junctions of IL-12 treated NK cell-depleted mice is similar to that seen in the IL-12 treated B6 mice and suggests that depletion of NK and NKT cells has little effect on either C3 production or binding capacity.

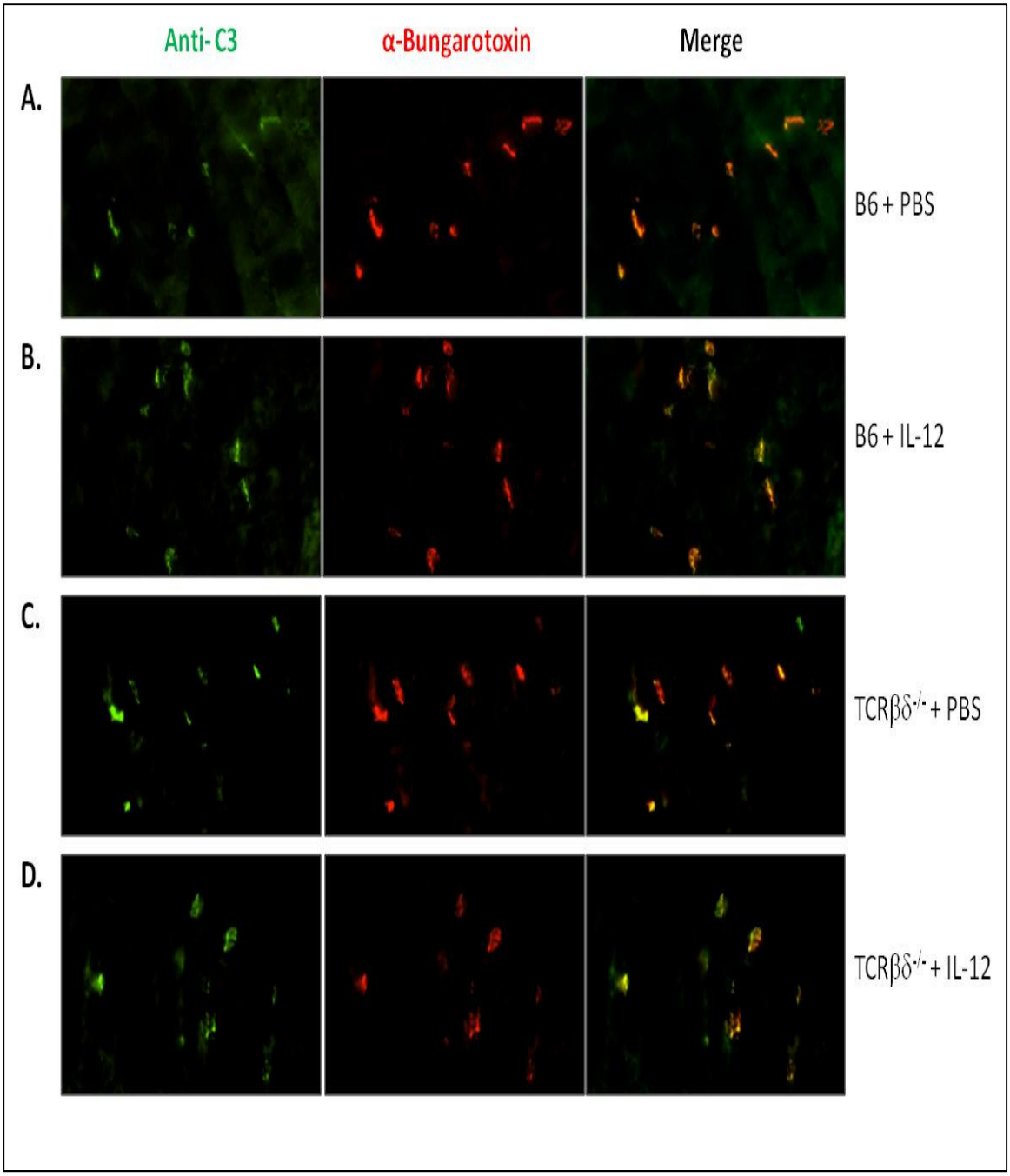

Figure 24: Presence of C3 at the neuromuscular junctions of PBS and IL-12 treated B6 and TCRβδ$^{-/-}$ mice. B6 mice and TCRβδ$^{-/-}$ mice received daily i.p. injections of IL-12 (1 µg) or PBS on Days -1 thru +3. On Day +6, all mice received a single i.p. injection of mAb D6 (3 mg). All mice were euthanized on Days +12 and +13 and diaphragm muscle was removed and cryostat sectioned. Tissue sections were stained with AlexaFluor594-α-Bungarotoxin and FITC-anti-C3. Mouse groups sample staining is shown as follows: B6+PBS (**A**), B6+IL-12 (**B**), TCRβδ$^{-/-}$+PBS (**C**), TCRβδ$^{-/-}$+IL-12 (**D**).

As can be seen in Figure 24, all mouse diaphragm samples imaged display the presence of complement component C3 co-localized with the location of neuromuscular junctions. Both the PBS treated B6 (Fig 24A) and TCRβδ$^{-/-}$ (Fig 24C) mice exhibit anti-C3 staining in the green channel that co-localizes with the location of neuromuscular junctions in the red channel when merged together. The same is true for the IL-12 treated B6 (Fig 24B) and TCRβδ$^{-/-}$ (Fig 24D) mice, where C3 clearly co-localizes with neuromuscular junction presence when merged. Again, while also visually appearing similar in intensity, the levels of C3 deposition at the site of neuromuscular junctions are quite comparable when examining the quantified average green-to-red intensity values shown previously in Table 7 for each individual mouse diaphragm sample within Figure 24.

When examining the quantified average green-to-red neuromuscular junction fluorescence intensity values seen in Table 7 for all four mouse diaphragm samples within Figure 24 it is again evident that the individual sample average intensity values are quite alike. As compared to the B6 mouse groups discussed earlier, for the TCRβδ$^{-/-}$ assay groups, PBS treated mice (Fig 24C) have an average green-to-red sample ratio value of 0.47 ± 0.05 whereas that of the IL-12 treated mice (Fig 24D) is 0.42 ± 0.05. The virtually identical green-to-red ratio value indicates that the PBS-treated TCRβδ$^{-/-}$ mice have nearly the same level of C3 bound to their neuromuscular junctions on average compared to their IL-12 treated TCRβδ$^{-/-}$ counterparts. These findings in the TCRβδ$^{-/-}$ mouse groups are similar to those seen in the B6 and NK cell depleted mouse groups and indicate that the ability of complement component C3 to deposit in the vicinity of the neuromuscular junction in response to IL-12 and mAb D6 treatment is no different than that resulting

from PBS and mAb D6 treatment. While unexpected, as all IL-12 treated mice show more sickness than their PBS treated counterparts during grip strength assays, this suggests that IL-12 treatment fails to enhance complement component C3 binding at the neuromuscular junction during passive transfer EAMG. Conversely, it's also entirely possible that all the IL-12 treated mouse groups display serum C3 levels that saturate the available number of anti-AChR antibody sites and therefore display no detectable difference in bound C3 extent. This can be assayed in the future by performing ELISA assays on harvested mouse serum in order to determine serum C3 concentrations in IL-12 treated mice.

When examining the impact of IL-12 versus PBS treatment on specific mouse groups, as shown in Table 7, the individual neuromuscular junctions of IL-12 treated B6 mice are bound by an identical level of complement component C3 on average as compared to IL-12 treated TCR$\beta\delta^{-/-}$ mice. This is evidenced by the similarity seen when comparing the PBS-to-IL-12 treatment differential for the B6 mouse groups (0.89) to that of the TCR$\beta\delta^{-/-}$ mouse groups (0.89). The similarity of the IL-12-to-PBS treatment differentials between the B6 and TCR$\beta\delta^{-/-}$ groups again highlights the equivalent degree of C3 deposition at the neuromuscular junctions of IL-12 treated B6 mice as compared to their PBS-treated counterparts. The degree of C3 deposition at the neuromuscular junctions of IL-12 treated TCR$\beta\delta^{-/-}$ mice (0.89) is therefore quite consistent with that seen in both the IL-12 treated B6 (0.89) or NK cell-depleted (0.82) mice. This suggests that the high degrees of muscle weakness seen in the IL-12 treated TCR$\beta\delta^{-/-}$ mice during the grip strength assays are unrelated to the levels of C3 deposited at their neuromuscular junctions, and therefore sickness in these mice is manifesting by some other means.

3.6 Gene chip analysis of IL-12 and mAb D6 treatment influence on gene expression of mouse diaphragm muscle

Our previous findings that EAMG-resistant IFN-$\gamma^{-/-}$ mice had levels of complement and antibody bound at the NMJ comparable to sickened B6 mice suggests that IL-12, through IFN-γ, may increase susceptibility to disease through mechanisms downstream of antibody and complement binding. In this scenario, IFN-γ may influence EAMG severity through promoting changes in specific gene expression within muscle tissue affected by anti-AChR binding. Therefore, the purpose of performing the whole genome expression analysis assays was to determine which, if any, genes within mouse muscle tissue may be either positively or negatively influenced singularly by IL-12 treatment, mAb D6 immunization, or by the combination of both. By comparing the gene expression levels in muscle samples from treated mice to those from control mice, we hoped to identify target genes that may shed light onto any role played by muscle tissue itself on the passive EAMG disease process. Any genes clearly determined to influence the pace or severity of disease development, either positively or negatively, could then be further studied as leads for the development of potential new therapies for human MG patients.

On Days -1 thru +3 during the whole genome expression analysis, all of the mice in Groups 2 and 4 received a single daily i.p. injection of IL-12 (1 µg in 100 µl PBS w/ 1% NMS) while all of the mice in Groups 1 and 3 received corresponding control i.p. injections of 100 µl PBS (w/ 1% NMS) at the same time points. On Day +4, the mice in Groups 1 and 2 were euthanized and diaphragm and hind limb muscle tissue samples were harvested prior to storage in RNase inhibiting buffer at -80°C. On Day +6, all of the

mice in Groups 3 and 4 received a single i.p. injection of the mouse anti-AChR mAb D6 (3 mg in 100 µl PBS). On Day +8, approximately 48 hours post-mAb D6 immunization, all of the mice in Groups 3 and 4 were euthanized and diaphragm and hind limb muscle tissue samples were harvested prior to storage in RNase inhibiting buffer at -80°C. Frozen diaphragm muscle samples from each mouse mentioned previously were removed from cold storage and RNase inhibiting buffer prior to rotor-stator tissue homogenization. Individual homogenized tissue sample lysates were processed over RNA purification spin columns, and purified whole RNA was isolated and collected from the processed homogenized tissue lysates.

After spectrophotometric quantification and purity assessments were performed, a purified diaphragm muscle RNA sample from each mouse mentioned previously (eight mice in total @ 2 per group) was subjected to gene chip analysis in order to measure the individual expression levels of approximately 23,000 unique genes across the entire mouse genome. The resulting gene expression data generated from each mouse diaphragm muscle sample was compiled in order to perform further downstream analysis of individual gene expression levels. Table 8 serves as an informational legend detailing how specific genes of interest were categorized into one of five distinct categories based on their known protein product roles: natural killer cell-specific genes [*NK*], chemotactic genes (chemokines, chemokine receptors, and integrins) [*Chemo*], classical complement pathway inhibitory genes [*Comp*], skeletal muscle-specific genes [*SkMusc*], and miscellaneous genes with noticeable changes in expression level [*Misc*].

Table 8: Informational legend outlining selected genes analyzed for changes in overall expression level. Individual genes are ordered in descending alphabetical order with their category classification to the left and their known protein product information to the right of the specific gene name. Gene classification is delineated as follows: natural killer cell-specific genes [**NK**], chemotactic genes (chemokines, chemokine receptors, and integrins) [**Chemo**], classical complement pathway inhibitory genes [**Comp**], skeletal muscle-specific genes [**SkMusc**], and miscellaneous genes with noticeable changes in expression level [**Misc**].

Gene Classification	Gene Name	Known Gene Protein Product
SkMusc	*Acta1*	Actin alpha-1 subunit (skeletal muscle)
Misc	*Alcam*	Activated leukocyte cell adhesion molecule (ALCAM)
Misc	*Bak1*	Bcl-2 antagonist
Chemo	*Ccr5*	Chemokine (C-C motif) receptor 5
Misc	*Cd19*	CD19 antigen (B-cell specific)
Misc	*Cd1d1*	CD1d1 antigen
NK	*Cd244*	CD244 (NK cell receptor 2B4)
Misc	*Cd247*	CD247, CD3 zeta chain (T-cell specific)
Comp	*Cd46*	Complement regulatory protein (CD46 antigen)
Misc	*Cd52*	CD52 antigen
Comp	*Cd55*	Decay accelerating factor [DAF] (CD55 antigen)
Comp	*Cd59a*	Protectin (complement regulatory protein), MIRL, CD59
Misc	*Cd6*	T cell differentiation antigen CD6
Misc	*Cd74*	Invariant polypeptide of major histocompatibility complex class II
SkMusc	*Chrna1*	Nicotinic cholinergic receptor alpha polypeptide 1 (muscle)
Chemo	*Cx3cl1*	Chemokine (C-X3-C motif) ligand 1
Chemo	*Cx3cr1*	Chemokine (C-X3-C motif) receptor 1
Chemo	*Cxcl1*	Chemokine (C-X-C motif) ligand 1
Chemo	*Cxcl10*	CXCL10, IP-10, IFN-γ-induced protein
Chemo	*Cxcl11*	CXCL11, Interferon-inducible T-cell alpha chemoattractant (I-TAC)
Chemo	*Cxcl9*	CXCL9
Chemo	*Cxcr3*	CXCR3
Chemo	*Itga1*	Integrin alpha 1
Chemo	*Itga2*	Integrin alpha 2 (CD49b antigen)
Chemo	*Itga2b*	Integrin alpha 2b
Chemo	*Itgae*	Integrin alpha E (epithelial associated)
Chemo	*Itgb7*	Integrin beta 7
Misc	*Itk*	IL-2-inducible T cell kinase
Misc	*Itm2a*	Integral membrane protein 2A
NK	*Klra1*	Killer cell lectin-like receptor, subfamily A, member 1 (Ly49a)
NK	*Klra16*	Killer cell lectin-like receptor, subfamily A, member 16
NK	*Klra19*	Killer cell lectin-like receptor, subfamily A, member 19

NK	*Klra2*	Killer cell lectin-like receptor, subfamily A, member 2
NK	*Klra7*	Killer cell lectin-like receptor, subfamily A, member 7
NK	*Klrb1b*	Killer cell lectin-like receptor, subfamily B, member 1b
NK	*Klrb1c*	NK1.1 (CD161 antigen)
NK	*Klrb1f*	Killer cell lectin-like receptor, subfamily B, member 1f
NK	*Klrd1*	CD94 antigen
NK	*Klre1*	Killer cell lectin-like receptor, subfamily E, member 1
NK	*Klrg1*	Killer cell lectin-like receptor, subfamily G, member 1
NK	*Klri1*	Killer cell lectin-like receptor, subfamily I, member 1
NK	*Klrk1*	NKG2D (CD314 antigen)
Misc	*Lst1*	Leukocyte specific transcript
Misc	*Ly6a*	Lymphocyte antigen 6 complex, locus A
Misc	*Ly86*	Lymphocyte antigen 86
Misc	*Lyzs*	Lysozyme
Misc	*Mlkl*	Mixed lineage kinase domain-like (protein kinase)
Misc	*Msr2*	Macrophage scavenger receptor 2
SkMusc	*Musk*	Skeletal muscle receptor tyrosine kinase
SkMusc	*Myh1*	Myosin heavy polypeptide 1 (skeletal muscle)
SkMusc	*Myh4*	Myosin heavy polypeptide 4 (skeletal muscle)
SkMusc	*Myl1*	Myosin light polypeptide 1
SkMusc	*Mylpf*	Myosin light chain phosphorylatable (fast skeletal muscle)
Misc	*Ncam1*	Neural cell adhesion molecule 1 (CD56 antigen)
NK	*Nkg7*	G1G1 (G-CSF-induced gene protein 1)
Misc	*Nos1*	Nitric oxide synthase 1
Misc	*Obscn*	Obscurin (cytoskeletal calmodulin and titin-interacting RhoGEF)
Misc	*Phf11*	PHD finger protein 11 (zinc finger)
Chemo	*SELL*	L-Selectin (CD62L)
Chemo	*Selplg*	P-Selectin glycoprotein ligand 1 (CD162 antigen)
Misc	*Sema4a*	Semaphorin-4A

The expression levels of the specific genes of interest listed in Table 8 were then examined and compared between the different assay treatment groups. The genes analyzed in this way were compared for fold changes in expression level between the following three different treatment pairs: a) IL-12 treatment vs. PBS treatment, b) IL-12 + mAb D6 treatment vs. PBS + mAb D6 treatment, and c) PBS + mAb D6 treatment vs.

PBS treatment. The mouse treatment group gene expression level comparisons can be seen in Tables 9, 10, and 11 respectively.

Table 9: Comparison of fold changes in gene expression levels between IL-12 and PBS treated mouse groups. Genes are ordered in descending order with those having the highest fold difference in expression level due to IL-12 treatment being listed first.

Gene Name	PBS Group Avg. Gene Expression	IL-12 Group Avg. Gene Expression	IL-12 vs. PBS Fold Expression Difference
Cxcl9	66.1	10335.6	156.4
Cxcl10	6.0	708.4	118.1
Phf11	6.9	239.3	34.7
Nkg7	13.1	339.1	26.0
Klra7	-3.3	81.9	24.8
Ccr5	9.0	218.6	24.4
Cd6	1.3	28.9	22.2
Cxcr3	-2.1	37.2	17.7
Klra16	1.3	14.3	11.4
Mlkl	26.9	257.9	9.6
Klri1	1.1	9.0	8.1
Lst1	58.3	380.1	6.5
Cd74	2183.3	13499.8	6.2
Ly86	165.3	993.4	6.0
Klrk1	2.5	14.3	5.7
Itgb7	36.2	201.7	5.6
Cd52	511.4	2644.1	5.2
Klrd1	22.9	109.5	4.8
SELL	60.4	274.3	4.5
Klre1	-8.6	38.7	4.5
Ly6a	5432.8	22823.0	4.2
Cxcl1	42.4	163.8	3.9
Klrg1	17.2	57.9	3.4
Cd1d1	124.8	403.3	3.2
Klra2	-8.5	25.5	3.0
Itk	17.8	52.9	3.0
Bak1	12.9	36.8	2.8
Selplg	119.9	336.8	2.8
Sema4a	217.2	605.3	2.8
Cx3cl1	54.8	141.2	2.6
Cx3cr1	22.0	55.1	2.5
Itga1	54.2	114.5	2.1
Itga2b	12.7	25.4	2.0

Itgae	130.9	226.9	1.7
Klrb1b	7.3	11.8	1.6
Lyzs	499.5	777.2	1.6
Klrb1f	-3.2	4.6	1.4
Alcam	14.6	19.4	1.3
Acta1	21372.5	24889.2	1.2
Musk	49.1	54.0	1.1
Mylpf	26766.1	27962.7	1.0
Cd59a	2381.2	2461.4	1.0
Myl1	13441.7	13234.0	1.0
Chrna1	327.2	311.2	1.0
Cxcl11	-6.6	-6.1	0.9
Myh1	6334.0	5619.7	0.9
Ncam1	101.9	76.3	0.7
Cd55	73.5	54.9	0.7
Klra19	72.3	47.1	0.7
Klrb1c	13.1	6.4	0.5
Nos1	20.3	9.4	0.5
Myh4	1599.1	719.0	0.4
Itm2a	704.8	301.4	0.4
Cd19	30.5	12.9	0.4
Cd247	5.4	1.8	0.3
Msr2	94.7	30.0	0.3
Cd244	-4.0	-1.1	0.3
Klra1	-6.5	-1.2	0.2
Itga2	-6.6	-0.8	0.1
Obscn	10.9	-2.3	-0.2
Cd46	1.9	-1.5	-0.8

As can be seen in Table 9, treatment of female B6 mice with IL-12 leads to many substantial changes in the expression of specific genes in comparison to PBS control treatments. In general, a fold expression difference value higher than 1.0 represents a gene whose expression level was upregulated in response to IL-12 treatment whereas a fold expression difference value of 1.0 represents no change in expression and values lower than 1.0 represent a decrease in expression level. Most strikingly, IL-12 treatment

resulted in a 156.4-fold increase in *Cxcl9* gene expression and a 118.1-fold increase in *Cxcl10* gene expression over the levels seen with PBS treatment. The proteins Cxcl9 and Cxcl10 (also known as IP-10) are chemokines whose expression is known to be induced by IFN-γ presence. Along with Cxcl11, whose parent gene expression (*Cxcl11*) is increased 3.9-fold due to IL-12 treatment, they signal through a common chemokine receptor, Cxcr3. Therefore, it is not surprising that the expression level of the *Cxcr3* gene is 17.7-fold higher in IL-12 treated B6 mice as compared to PBS treatment. In addition, the expression level of another chemokine receptor gene, *Ccr5*, is 24.4-fold higher in the IL-12 treatment group. This suggests that mouse diaphragm muscle tissue has the ability to directly participate in the overall immune response to IL-12 treatment by regulating the levels of chemokine and chemokine receptor genes, thus facilitating a "primed" immunological environment within muscle tissue that may assist in downstream effector cell recruitment or functionality. This finding has clear implications in regards to the immunological responses that occur within muscle tissue, whether in response to pathogenic challenge or autoimmune anomalies.

While the increases in the expression levels of specific chemokine and chemokine receptor genes signals that the IL-12 treated mice develop a higher state of immune activation within muscle tissue, the increase in the expression of genes directly related to NK cell function suggests that these cells may be specifically activated (or "primed") in response to IL-12 treatment. For instance, the expression of the *Klra7* gene, whose NK cell-specific protein product is known as killer cell lectin-like receptor, subfamily A, member 7, is 24.8-fold higher due to IL-12 treatment. The same is true for the *Nkg7* gene, whose protein product is known as natural killer cell protein 7, where the expression level

is 26-fold higher upon treatment with IL-12. The same is true for numerous other NK cell specific genes, such as *Klra16* (11.4-fold increase), *Klri1* (8.7-fold increase), *Klrk1* (5.7-fold increase), and *Klrd1* (4.8-fold increase) just to name a few, where IL-12 treatment has caused considerable increases in gene expression over that seen with PBS control treatment.

It is difficult to determine whether the increased expression seen in these genes is occurring within the muscle tissue itself, or if it is the result of mRNA isolated from "primed" NK cells that have infiltrated the muscle tissue environment. However, the gene expression levels of the traditional NK cell markers *Klrb1c* (NK1.1, or CD161) and *Itga1* (CD49b) are not dramatically increased in the IL-12 treated mice, with *Itga1* expression increased 2.1-fold and *Klrb1c* expression decreased 0.5-fold. It is unlikely that the increased expression of the previously mentioned genes is occurring within muscle cells and is more likely the result of NK cell trafficking into the muscle tissue environment, as many of the these genes are NK cell-specific and have been reported as non-existent within skeletal muscle, such as with the *Nkg7* gene (96). Taken together, these results suggest that one of the effects of IL-12 treatment is direct activation of NK cells and that they respond to this cytokine signal by infiltrating the muscle tissue environment. Further testing would be necessary to determine if this infiltration event is specific to muscle tissue or if it occurs indiscriminately throughout the various tissues and organs of the mouse.

It is also important to note that there were very few changes seen in the gene expression levels of major skeletal muscle-specific [*SkMusc*] or classical complement pathway inhibitory genes [*Comp*] between the IL-12 and PBS-treated mouse groups. In

fact, these two categories of selected genes showed fold expression difference values that hovered at or very near to 1.0, suggesting no net change in expression level. For example, the skeletal muscle-specific genes *Acta1* (Actin alpha-1 subunit, 1.2-fold increase), *Chrna1* (Alpha1 subunit of the nicotinic acetylcholine receptor, 1.0-fold increase), *Musk* (Skeletal muscle receptor tyrosine kinase, 1.1-fold increase), *Myh1* (Myosin heavy chain 1, 0.9-fold decrease), and *Myl1* (Myosin light chain 1, 1.0-fold increase) showed little to no change in expression levels. In accordance, the complement inhibitor genes *Cd55* (decay-accelerating factor, 0.7-fold decrease) and *Cd59a* (Protectin, 1.0-fold increase) also did not exhibit distinguishable changes in expression level. However, of interest is the noticeable reduction in expression of the *Cd46* gene (Complement regulatory protein, -0.8-fold decrease) seen upon treatment with IL-12. While not nearly as high of a fold expression difference seen with the *Cxcl9* gene upon IL-12 treatment, the reduction in expression of the complement inhibitory *Cd46* gene upon treatment with IL-12 may have further implications in regards to the elevated muscle weakness seen upon antibody and complement binding during passive EAMG induction using mAb D6 immunization.

Table 10: Comparison of fold changes in gene expression levels between IL-12+D6 and PBS+D6 treated mouse groups. Genes are ordered in descending order with those having the highest fold difference in expression level due to IL-12+D6 treatment being listed first.

Gene Name	PBS+D6 Group Avg. Gene Expression	IL-12 +D6 Group Avg. Gene Expression	IL-12+D6 vs. PBS+D6 Fold Expression Difference
Cd6	-0.4	50.7	126.6
Cxcl9	99.3	4290.0	43.2
Cxcr3	4.6	115.0	25.0
Phf11	3.9	90.8	23.3
Ccr5	9.0	143.2	15.9
Itgb7	18.9	282.3	14.9
Klrd1	9.1	109.0	12.0
Nkg7	32.2	379.3	11.8
Klra16	-1.2	12.4	10.3

Cd52	339.8	3099.9	9.1
Cxcl10	23.0	192.1	8.4
Cd74	1710.4	12165.4	7.1
Ly86	111.9	785.3	7.0
Lst1	57.9	373.3	6.4
Itk	13.0	75.5	5.8
Selplg	80.0	450.0	5.6
Klrk1	1.8	7.9	4.4
SELL	17.5	72.0	4.1
Klrb1f	-1.4	5.5	3.9
Cd247	1.2	4.5	3.8
Cx3cr1	32.7	122.2	3.7
Lyzs	388.4	1441.8	3.7
Klra7	-9.7	35.6	3.7
Cxcl1	39.3	127.3	3.2
Klrg1	21.7	67.5	3.1
Alcam	14.9	40.0	2.7
Klrb1b	6.1	15.7	2.6
Mlkl	30.7	78.4	2.6
Klri1	2.7	6.6	2.4
Sema4a	298.7	711.2	2.4
Ly6a	5649.3	11566.3	2.0
Klra2	-4.6	9.4	2.0
Cd1d1	166.7	331.8	2.0
Cd46	-1.6	3.2	2.0
Klrb1c	8.9	15.6	1.8
Klre1	-11.5	15.4	1.3
Cd19	8.9	11.9	1.3
Itga2b	20.1	25.1	1.2
Cd55	81.3	98.1	1.2
Itgae	104.7	125.9	1.2
Klra1	-2.8	3.1	1.1
Cx3cl1	60.1	64.4	1.1
Acta1	22673.9	23670.9	1.0
Mylpf	26190.2	26576.6	1.0
Myh1	6423.9	6483.7	1.0
Itga1	68.2	68.8	1.0
Myl1	14174.9	14107.0	1.0
Cd59a	2145.0	2068.1	1.0
Cd244	-2.5	-2.2	0.9
Klra19	76.0	61.0	0.8

Itm2a	791.5	610.9	0.8
Chrna1	380.2	293.3	0.8
Musk	52.3	38.9	0.7
Bak1	27.2	17.2	0.6
Itga2	-9.2	-5.0	0.5
Msr2	114.0	58.8	0.5
Ncam1	103.7	51.8	0.5
Nos1	15.6	7.6	0.5
Myh4	2095.5	452.0	0.2
Obscn	10.0	0.4	0.0
Cxcl11	3.4	-7.4	-2.2

As can be seen in Table 10, treatment of female B6 mice with IL-12 and mAb D6 leads to several considerable changes in the expression of specific genes in comparison to PBS and mAb D6 control treatments. A fold expression difference value higher than 1.0 represents a gene whose expression level was upregulated in response to IL-12 treatment whereas a fold expression difference value of 1.0 represents no change in expression and values lower than 1.0 represent a decrease in expression level. Most noticeably, IL-12 and mAb D6 treatment resulted in a 126.6-fold increase in the expression of the *Cd6* gene, whose protein product is the T cell differentiation antigen CD6. While IL-12 treatment alone increased *Cd6* gene expression by 22.2-fold (see Table 9), this further exacerbation in *Cd6* gene expression seen with combined IL-12 and mAb D6 treatment suggests that there is a synergistic effect of IL-12 and mAb D6 on this specific gene's expression level. It has been documented that IFN-γ can enhance the expression of CD6, which is often involved in mature T cell interactions with select non-professional antigen-presenting cells (97). Also, gene expression of *Alcam*, the natural ligand for CD6 known as activated leukocyte cell adhesion molecule (ALCAM), is also increased 2.7-fold over that seen with PBS+D6 control treatment. Therefore, it is plausible that initial IL-12

treatment has the effect of activating T cells while downstream mAb D6 immunization compounds this effect, possibly through further activating these previously "primed" T cells through an antibody recognition event.

Though the mice assayed in Table 10 were euthanized 96 hours (Day +8) after the mice in Table 9 (Day +4), it is clear to see that the effects of IL-12 treatment still remain prominent on the gene expression pattern of mouse diaphragm muscle tissue. Similar to the effects seen with IL-12 treatment alone in Table 9, the IL-12+D6 treated mice exhibit increases in the expression of the same specific chemokine and chemokine receptor genes (*Cxcl9*, *Cxcl10*, *Cxcr3*, and *Ccr5*) compared to the PBS+D6 treated mice. In this same pattern, many identical NK cell-specific genes (for example *Klra16*, *Nkg7*, *Klrd1*, *Klrk1*, and *Klri1*) also remain more highly expressed in the IL-12+D6 treated mice as compared to the PBS+D6 treated mice. Therefore, these results suggest that any activation of NK cells and infiltration into muscle tissue that may occur as a result of initial IL-12 treatment still persists, though at a lowered level, after passive immunization with mAb D6.

Accordingly, the levels of the complement inhibitor genes *Cd46*, *Cd55*, and *Cd59a* remain relatively unchanged in their patterns of expression after IL-12 and mAb D6 treatment, with only the *Cd46* gene again showing any appreciable change in expression. There is also a tendency for a lack of influence on the gene expression pattern of the skeletal muscle-specific genes of interest by IL-12 and mAb D6 treatment, where there is a definitive lack in changes in gene expression above background. This trend becomes apparent when again examining the expression levels of the genes *Acta1* (1.0-fold increase), *Chrna1* (0.8-fold decrease), *Musk* (0.7-fold decrease), *Myh1* (1.0-fold

increase), and Myl1 (1.0-fold increase). Taken together, these results suggest that treatment with IL-12 and mAb D6 does not affect the expression pattern of complement inhibitor and skeletal muscle-specific genes to any appreciable extent over the levels seen in the PBS+D6 control treatment group.

Table 11: Comparison of fold changes in gene expression levels between PBS+D6 and PBS treated mouse groups. Genes are ordered in descending order with those having the highest fold difference in expression level due to PBS+D6 treatment being listed first.

Gene Name	PBS Group Avg. Gene Expression	PBS+D6 Group Avg. Gene Expression	PBS+D6 vs. PBS Fold Expression Difference
Cxcl10	6.0	23.0	3.8
Klra7	-3.3	-9.7	2.9
Nkg7	13.1	32.2	2.5
Klri1	1.1	2.7	2.5
Cxcr3	-2.1	4.6	2.2
Bak1	12.9	27.2	2.1
Itga2b	12.7	20.1	1.6
Cxcl9	66.1	99.3	1.5
Cx3cr1	22.0	32.7	1.5
Itga2	-6.6	-9.2	1.4
Sema4a	217.2	298.7	1.4
Klre1	-8.6	-11.5	1.3
Cd1d1	124.8	166.7	1.3
Myh4	1599.1	2095.5	1.3
Klrg1	17.2	21.7	1.3
Itga1	54.2	68.2	1.3
Msr2	94.7	114.0	1.2
Chrna1	327.2	380.2	1.2
Mlkl	26.9	30.7	1.1
Itm2a	704.8	791.5	1.1
Cd55	73.5	81.3	1.1
Cx3cl1	54.8	60.1	1.1
Musk	49.1	52.3	1.1
Acta1	21372.5	22673.9	1.1
Myl1	13441.7	14174.9	1.1
Klra19	72.3	76.0	1.1
Ly6a	5432.8	5649.3	1.0
Alcam	14.6	14.9	1.0

Ncam1	101.9	103.7	1.0
Myh1	6334.0	6423.9	1.0
Ccr5	9.0	9.0	1.0
Lst1	58.3	57.9	1.0
Mylpf	26766.1	26190.2	1.0
Cxcl1	42.4	39.3	0.9
Obscn	10.9	10.0	0.9
Cd59a	2381.2	2145.0	0.9
Klrb1b	7.3	6.1	0.8
Itgae	130.9	104.7	0.8
Cd74	2183.3	1710.4	0.8
Lyzs	499.5	388.4	0.8
Nos1	20.3	15.6	0.8
Itk	17.8	13.0	0.7
Klrk1	2.5	1.8	0.7
Klrb1c	13.1	8.9	0.7
Ly86	165.3	111.9	0.7
Selplg	119.9	80.0	0.7
Cd52	511.4	339.8	0.7
Cd244	-4.0	-2.5	0.6
Phf11	6.9	3.9	0.6
Klra2	-8.5	-4.6	0.5
Itgb7	36.2	18.9	0.5
Cxcl11	-6.6	3.4	0.5
Klrb1f	-3.2	-1.4	0.4
Klra1	-6.5	-2.8	0.4
Klrd1	22.9	9.1	0.4
Cd19	30.5	8.9	0.3
SELL	60.4	17.5	0.3
Cd247	5.4	1.2	0.2
Cd6	1.3	-0.4	-0.3
Cd46	1.9	-1.6	-0.9
Klra16	1.3	-1.2	-1.0

As can be seen in Table 11, treatment of female B6 mice with mAb D6 alone leads to few sizeable changes in the expression of specific genes in comparison to PBS control treatments. Again, fold expression difference values higher than 1.0 represent genes whose expression level was upregulated in response to IL-12 treatment whereas a

fold expression difference value of 1.0 represents no change in expression and values lower than 1.0 represent a decrease in expression level. In general, the expression levels of the various genes of interest are quite similar, with very few genes showing above a 2.0-fold increase in expression. The largest fold expression difference was seen with the chemokine *Cxcl10* gene, where a 3.8-fold increase in expression was seen in the PBS+D6 group compared to the PBS-treated group. Interestingly, of the six genes exhibiting an increase in expression greater than 2.0-fold in the PBS+D6 treatment group, five are classified as either chemotactic (*Cxcl10* and *Cxcr3*) or NK cell-specific (*Klra7*, *Nkg7*, and *Klri1*) genes. While the changes in the expression of these genes is not massive, this finding suggests that immunization with mAb D6 may in fact lead to an increase in immune effector cell activation or trafficking that is not seen with PBS treatment alone. This is significant in that neither mouse treatment group received any IL-12 treatments, and therefore any changes in gene expression that are consistently seen are solely attributable to an immune response towards mAb D6 presence. Should this be the case, further testing would need to be performed in order to determine if this immune response is initiated in the periphery, as mAb D6 is injected i.p. and can access the bloodstream, or if the event begins at the neuromuscular junction with recognition of AChR-bound antibody.

As was mentioned previously, a majority of the analyzed genes in Table 11 showed little to no change in their expression pattern. This was the case with the skeletal muscle-specific genes (*Acta1*, *Chrna1*, *Musk*, *Myh1*, and *Myl1*) which all showed slightly increased expression in the range of 1.0-1.2-fold. In addition, the complement inhibitory genes (*Cd46*, *Cd55*, and *Cd59a*) also exhibited very small changes in their individual

expression levels. When taken together, these results suggest that treatment with mAb D6, which has been shown to localize within the neuromuscular junction, has little influence on the expression levels of genes that would be directly impacted by any potential damage caused by anti-AChR antibody binding and AChR destruction. This is the most obvious with the *Chrna1* gene, whose protein product is the nicotinic acetylcholine receptor alpha-1 subunit, which also happens to be the main immunological target of mAb D6. Therefore, in passive transfer EAMG incorporating immunization with the anti-AChR monoclonal antibody D6 in the absence of IL-12 treatment, it is likely that any muscle weakness witnessed is not attributable to a deficiency in skeletal muscle, acetylcholine receptor-specific, or complement inhibitor gene expression. The impact of a deficiency in the expression of one of these genes would potentially lead to a distinct and severe exacerbation of passive disease caused by mAb D6 or possibly any other anti-AChR monoclonal antibody. However, it is possible that an increase in extrajunctional AChR numbers may possibly manifest at later time points during active disease.

Chapter 4

Discussion

Interleukin-12 (IL-12), a major inducer of interferon-gamma (IFN-γ) production, has been shown to enhance clinical passive experimental autoimmune myasthenia gravis (EAMG) independently of the level of antibody and complement bound to AChRs. While playing a central role as part of the innate resistance mechanisms of the immune system against microorganisms (26), IL-12 has also been identified as a cytokine capable of bridging the early-responding innate immune system with the adaptive immune system (27) as well as being important during the later stages of an inflammatory autoimmune response (28). During an inflammatory response, cells of the innate immune system produce molecules such as IL-12, which can then act on other cells of the immune system to produce additional cytokines, such as IFN-γ.

The results of other studies have revealed the importance of IL-12 in EAMG development. It has been shown that IL-12 treatment has the ability to enhance disease in EAMG (5, 6), and additionally, that IL-$12^{-/-}$ mice are resistant to EAMG development (6, 35), further emphasizing the role IL-12 plays in disease enhancement. The results of my research support these findings, where IL-12 was shown to enhance passive EAMG in wild-type B6 mice upon immunization with the mouse anti-AChR monoclonal antibody

D6 (Fig 11). Repeated IL-12 and mAb D6 treatments accelerated disease development in B6 mice, leading to the death of 80% of the IL-12 treated mice at the +72-hour post-mAb D6 immunization time point (Fig 12). In fact, for all the assays performed during my research where control mice received PBS instead, the absence of IL-12 conferred resistance to passive EAMG development upon mAb D6 immunization (Figs 11-12, and 19). This suggests that functional IL-12 signaling is essential for the development of passive transfer EAMG using mAb D6.

It is known that the primary role of IL-12 within the immune system is to polarize T cell responses towards the Th1 phenotype, thus stimulating them to produce and secrete IFN-γ. Not surprisingly then, once secreted, IL-12 has been shown to enhance the activation, proliferation, IFN-γ secretion level, and cytolytic activity of NK and T cells (29). In fact, it is thought that T cells, NK cells, and NKT cells are the primary producers of IFN-γ in response to IL-12 (59, 60). The results of other studies have revealed the importance of IFN-γ in EAMG development as well. It has been shown that IFN-γ is required for EAMG development (44) while another study found that IFN-$\gamma^{-/-}$ mice are resistant to EAMG development and had greatly reduced levels of mouse AChR-specific IgG1 and IgG2a antibodies (45). My work clarifies the role of IFN-γ in enhancing disease versus increasing the production of anti-AChR antibodies.

The results of my research support these findings, where the absence of IFN-γ conferred resistance to passive EAMG development. Here, IL-12 treatment of IFN-$\gamma^{-/-}$ mice on the C57BL/6 background failed to accelerate passive disease development upon immunization with mAb D6 (Fig 13). Surprisingly, sensitization of these mice by pancuronium bromide administration suggested that IL-12 treatment of IFN-$\gamma^{-/-}$ mice may

offer slight protection against passive disease development over PBS treatment (Fig 14). However, this may be the effect of immune compensatory mechanisms in the absence of IFN-γ, as IL-12 treatment may trigger negative cytokine feedback reactions from specific immune effector cells, such as that seen by IL-10 production (98), that PBS treatment cannot elicit. Therefore, as compensatory cytokine effects have been documented elsewhere (99), the slight protective effect of IL-12 we have seen here is more likely the result of the experimental treatment conditions incorporated during the assay.

The role of the complement system and the classical complement pathway (CCP) in EAMG is well documented (80), as mice deficient for complement factors C3, C4, or C5 are resistant to EAMG development (81). Mice lacking the complement inhibitor decay accelerating factor (DAF) were shown to be more susceptible to EAMG than control animals (86), while research showing that the administration of a soluble complement inhibitor (sCR1) (82-84) or anti-C6 antibody prevents EAMG development (85). Here I have shown that IL-12 treated, mAb 35-immunized wild-type B6 mice had similar levels of anti-AChR antibody but 2-fold higher levels of complement component C3 bound at their neuromuscular junctions compared to their PBS-treated counterparts (Fig 15 and Table 2). These IL-12 treated mice also exhibited elevated muscle weakness manifesting in reduced hang times (data not shown), further evidencing that complement plays a role in passive EAMG development. In contrast to those results however, when quantified, IL-12 treated EAMG-resistant IFN-$\gamma^{-/-}$ mice had similar levels of anti-AChR antibody and C3 bound to their neuromuscular junctions compared to IL-12 treated EAMG-competent B6 mice (Fig 16 and Table 3). This result indicates that the resistance to EAMG development that IFN-$\gamma^{-/-}$ mice display is not due to a reduction in the capacity

of antibody or complement to effectively bind to the AChR. When taken together this suggested that IL-12, through IFN-γ, may increase susceptibility to EAMG through mechanisms downstream of antibody and complement binding.

As mentioned previously, NK cells have also been shown to be involved in EAMG development (48), where IL-18$^{-/-}$ mice were resistant to EAMG and this resistance could be reversed by reconstituting the IL-18$^{-/-}$ mice with normally functioning NK cells from RAG-1$^{-/-}$ mice. This reversal was determined to be the result of restored IFN-γ production by the transferred NK cells, as NK cells transferred from RAG-1$^{-/-}$IFN-γ$^{-/-}$ mice could not reverse EAMG resistance. Of importance is the fact that IL-12 enhances expression of the IL-18 receptor by NK and T cells and therefore allows greater synergy with IL-18 in terms of IFN-γ production. This heightened effect on IFN-γ production due to IL-18 receptor up-regulation is witnessed more profoundly in NK cells (52, 53, 55-58). Taken together, these findings support the idea that in passive transfer EAMG, pre-treatment with IL-12 could lead to a priming and expansion of NK cells that are capable of responding quite aggressively by producing IFN-γ.

Studies performed in our laboratory have been designed to test whether the innate NK cells, rather than T or NKT cells, are the major producers of IFN-γ in response to IL-12 treatment within the immune system and are therefore responsible for enhancing passive disease. In order to study this, I sought to attempt to induce passive EAMG in wild-type B6 mice, B6 mice devoid of NK cells due to depletion using the anti-NK1.1 monoclonal antibody PK136, and NK cell competent TCRβδ$^{-/-}$ mice. Bred on the C57BL/6 background, TCRβδ$^{-/-}$ mice intrinsically lack a conventional T cell receptor (TCR) and therefore also naturally lack all functional T cell and NKT cell subsets while

still possessing functional B and NK cells (8). These cellular milieu characteristics made them a superior model for this assay compared to the RAG1$^{-/-}$ mouse strain used in many other published reports, which lack all functional B, T, and NKT cell subsets, as results from Haddad et. al suggested the requirement for B cell presence in order to elicit IFN-γ production from NK cells in response to IL-12 treatment (8).

By attempting to induce passive disease in wild-type B6 mice, NK cell-depleted B6 mice, and TCRβδ$^{-/-}$ mice, I hoped to determine if NK cell absence confers protection against passive EAMG development and, conversely, if NK cell predominance confers increased severity of passive EAMG. I hypothesized that if NK cells are the main source of disease-enhancing IFN-γ in response to IL-12 treatment during passive EAMG induction, then their absence should present with decreased IFN-γ production and therefore decreased disease. Conversely, as TCRβδ$^{-/-}$ mice have a preponderance of NK cells, they should exhibit elevated IFN-γ levels and therefore more severe disease upon treatment with IL-12 and passive immunization with mAb D6. This was exactly the effect seen, where IL-12 treated NK cell depleted mice were resistant to passive EAMG development while IL-12 treated TCRβδ$^{-/-}$ mice exhibited severe sickness that significantly surpassed the levels of passive disease seen in the IL-12 treated wild-type B6 mice (Figs 19, 20, and 21). The change in passive EAMG development was much more discernable when comparing the grip strength measurement results of the IL-12 treated TCRβδ$^{-/-}$ and NK cell-depleted B6 mice, where the TCRβδ$^{-/-}$ mice exhibited definitively enhanced disease represented by statistically reduced peak grip strength values as early as 24 hours post-mAb D6 immunization (Fig 21).

The results comparing the effects of NK cell absence versus presence were even more telling when examining data from the serum IFN-γ ELISA assays performed. At all three bleeding time points assayed, the serum IFN-γ level of the IL-12 treated NK cell depleted mouse group was quite significantly lower than that seen in either the IL-12 treated B6 or TCRβδ$^{-/-}$ groups (Fig 22 and Table 6). In fact, the IL-12 treated TCRβδ$^{-/-}$ mouse group displayed greatly elevated serum IFN-γ levels compared to the IL-12 treated B6 mouse group at all three bleeding time points assayed (2.3-fold, 5.1-fold, and 2.5-fold higher respectively). This was in contrast to the PBS treated TCRβδ$^{-/-}$ mouse group, which exhibited background serum IFN-γ levels comparable to the other PBS treated mouse groups, thus eliminating the possibility that TCRβδ$^{-/-}$ mice possess intrinsically higher serum IFN-γ levels in the absence of IL-12 treatment as a result of their NK cell predominance. I also suspect that the reason for serum IFN-γ levels higher than background in the IL-12 treated NK cell-depleted B6 mice reflect the inability to achieve full depletion of NK cells resulting from mAb PK136 administration, where significant depletion efficiencies of 61.0% at +7 days post-immunization and 60.5% at +5 days after final booster immunization with mAb PK136 were achieved (Figs 17-18 and Tables 4-5). When taken together, these results indicate that innate NK cells are the primary cellular source of the disease-enhancing IFN-γ produced upon IL-12 treatment during passive EAMG induction. This finding also identifies NK cells as a potential therapeutic target in treating other diseases that show elevated IFN-γ or enhanced disease upon IL-12 treatment mentioned earlier, such as in inflammatory colitis (28), collagen-induced arthritis (31), experimental autoimmune encephalomyelitis (32), and insulin-dependent diabetes mellitus (33, 34). It is also entirely possible that the innate NK cells may serve as

the sources of cellular damage during antibody-dependent cell-mediated cytotoxicity (ADCC).

Accordingly, it was important to examine the role that the complement system, and more specifically the classical complement pathway, may be playing in each mouse group during our passive EAMG induction assays. I have already shown that the levels of C3 bound to the neuromuscular junctions of IL-12 treated wild-type B6 mice were 2-fold higher than those seen in their PBS treated counterparts (Fig 15 and Table 2), while the levels between IL-12 treated B6 and IFN-$\gamma^{-/-}$ mice were similar (Fig 16 and Table 3), though IFN-$\gamma^{-/-}$ mice were resistant to development of passive EAMG. At best, based on the conflicting results seen in regards to the contributions of complement towards passive disease development, it was necessary to determine the extent of C3 binding to the neuromuscular junctions of the wild-type B6 mice, the NK cell depleted B6 mice, and the TCR$\beta\delta^{-/-}$ mice assayed. Surprisingly, and contrary to my predictions, when quantified the average ratio of C3 bound to the neuromuscular junctions of the highly diseased IL-12 treated TCR$\beta\delta^{-/-}$ mice was virtually identical to that of the less sick IL-12 treated wild-type and NK cell depleted B6 mouse groups (Figs 23-24 and Table 7).

In fact, while all of the IL-12 treated mouse groups had comparable neuromuscular junction C3 binding ratios, the IL-12 treated B6 mice exhibited passive EAMG sickness and serum IFN-γ levels in between those of the IL-12 treated EAMG-resistant NK cell-depleted B6 and disease-afflicted TCR$\beta\delta^{-/-}$ mouse groups. The similarity in C3 binding levels seen during this assay contrasts the two-fold increase in C3 binding seen in the IL-12 treated B6 mice discussed previously. The difference in C3 binding levels in the IL-12 treated B6 mice between the two assays is most likely due to

the differences in the number of IL-12 injections (the previous assay incorporated 3 more injections) and the timing of mouse euthanasia. This finding further supports my hypothesis that the classical complement pathway may simply serve as a bystander in its ability to enhance passive EAMG, where its disease-enhancing capabilities are more directly related to the amount and isotype of anti-AChR antibodies bound to acetylcholine receptors within the neuromuscular junction. It is possible that the levels of complement components such as C3 within the serum are elevated, and therefore saturating, during the passive disease process. The possible elevation of complement components within the serum may result from T cell mediated cytokine signaling that leads to enhanced complement component synthesis within the liver. Therefore, the levels of available complement components that can inflict damage to the neuromuscular junction may surpass the available number of anti-AChR antibody binding sites and may reflect a requirement for full T cell presence and functionality. In such a manner, the levels of passive EAMG seen in IL-12 treated TCR$\beta\delta^{-/-}$ mice are more of a reflection of the extremely high systemic levels of IFN-γ that are potentially able to affect the muscle tissue's response to passively transferred mAb D6, and not responding complement component levels, as functional T cells are absent and antibody levels were kept constant during these assays.

This would not be the case in the IL-12 treated NK cell depleted mouse, where systemic IFN-γ levels are greatly reduced due to NK cell absence yet the presence of all functional T cell subsets allows for the enhancement of complement component synthesis, and therefore complement mediation towards bound anti-AChR antibodies remains intact and results in normal C3 binding. Therefore, the functional T cell subsets

present in IL-12 treated wild-type B6 mice combine the effects of enhanced complement mediation with those seen from regulatory control of NK cell-driven IFN-γ production. This implies that if not for regulation of NK cell-driven IFN-γ production in IL-12 treated wild-type B6 mice, possibly by Tregs, these mice most likely would exhibit more elevated levels of systemic IFN-γ similar to those seen when NK cells are allowed to freely produce IFN-γ in IL-12 treated TCRβδ$^{-/-}$ mice. A good way to test my hypothesis in the future would be to perform simple serum C3 ELISA assays to see what systemic differences, if any, can be detected between the different mouse treatment groups at different time points during the overall assay in an identical manner to those performed to measure serum IFN-γ levels during these experiments. As there could be an enhancement in clearance of neuromuscular junction-bound C3 in the TCRβδ$^{-/-}$ mice, it would also be of interest to examine the binding levels of other complement components (C5 thru C9) or complement inhibitors (DAF or Protectin) over time using immunofluorescence.

Since IFN-γ is a short-lived cytokine in the circulation, its function in exacerbating EAMG would most logically occur in the vicinity of the muscle tissue or NMJ. Long-distance mediation from thymus or lymph node-resident effector cells would require exposure of any IFN-γ to the degradative elements of the blood or lymphatics as it travels to the NMJ, thus reducing its capacity to exert its effect. It is more likely that the effector cells responsible for the production of IFN-γ in EAMG become localized within the muscle tissue microenvironment prior to the release of IFN-γ. While the mechanisms by which naïve T cells migrate from the blood and localize within the secondary lymphoid organs have been well documented (100-103), NK cells circulate throughout the blood but are generally excluded from lymph nodes. However, populations of NK

cells have been detected in the lymph nodes (104, 105) and the mechanism by which they gain entry and localize has been elucidated (106). Chemokines comprise a superfamily of chemoattractant cytokines that mediate leukocyte recruitment into tissues in homeostasis and inflammation (107). Interestingly, it was found that in addition to CD62L, NK cells use the chemokine receptor CXCR3, not the CCR7 receptor used by T cells, to gain entry into the lymph node. Once localized in the lymph nodes, it was also determined that these NK cells provided the initial source of IFN-γ that was necessary for polarization towards a Th1 response (106).

A number of studies have indicated a role for CXCR3 and its chemokine ligands (CXCL9, CXCL10, and CXCL11) in the recruitment of inflammatory cells in several Th1-type autoimmune disease models such as asthma (108) and psoriasis (109, 110). In particular, CXCL10 (also known as IFN-γ-inducible protein 10, or IP-10) was shown to recruit activated T cells into sites of tissue inflammation during studies of rheumatoid arthritis (111) and multiple sclerosis (112, 113). During inclusion body myositis, a rare inflammatory muscle disease, the production of pro-inflammatory chemokines was up-regulated in response to IFN-γ signaling. These chemokines actively contributed to the development of tissue inflammation and recruitment of activated T cells (114). In addition to serving as a highly inducible chemoattractant for activated T cells, IP-10 is also known to stimulate NK cells (115). The observation that IP-10 stimulates NK cells may serve as a possible explanation as to how a Th1-type autoimmune response can be initiated in a tissue that lacks any detectable $CD4^+$ T cell infiltration. Such is the case in MG and EAMG, where infiltrating $CD4^+$ T cells have not been found in the vicinity of the NMJ.

There has been intriguing evidence that chemokines and chemokine receptors may play a role in MG and EAMG. One study found that levels of the chemokine receptor CXCR3 and its ligand, IP-10 (or CXCL10), were over-expressed in the lymph nodes of EAMG rats versus control animals (72). During this study it was discovered that the same trend was evident in thymus and muscle samples from MG patients compared with their age-matched controls. These results demonstrated a positive association between IP-10/CXCR3 signaling and the pathogenesis of MG and EAMG. More recently, it was demonstrated that the suppression of ongoing (established) EAMG could be achieved in rats using two separate approaches: a) blocking the activity of the chemokine IP-10 using IP-10-specific antibodies, and b) inhibiting the CXCR3 chemokine receptor using a small molecule CXCR3 antagonist (known as "T487" from Amgen Inc.) (116). There was also a noticeable reduction in the expression level of cathepsin-1, a lysosomal endopeptidase induced following muscle damage and loss (117, 118), following both suppressive treatments. While this study focused on EAMG during the effector phase, once disease had manifested, it still followed the active *Torpedo* AChR immunization protocol. A future point of interest regarding my research would be to test the effects of blocking IP-10/CXCR3 signaling during passive transfer EAMG both during and after priming with IL-12.

Other studies performed in our laboratory have been designed to test the hypothesis that the major role of IFN-γ in muscle weakness is not restricted to the change of antibody isotype distribution, and that the cellular targets of IFN-γ are not restricted to immune cells. This concept further supports my hypothesis that serum IFN-γ may potentially influence the ability of muscle tissue to respond to downstream anti-AChR

binding within the neuromuscular junction as discussed previously. In order to study this possibility, I incorporated varied singular and combined control, IL-12, and mAb D6 treatments at different passive EAMG disease process time points on female wild-type B6 mice with the intent being to harvest and analyze purified skeletal muscle RNA for changes in specific gene expression between the differentially treated mouse groups. This was performed by means of a whole mouse genome gene array analysis with the assistance of the Cleveland Clinic's Lerner Research Institute Genomics Core staff. In this way, I hoped to be able to detect any significant changes in specific gene expression between PBS, IL-12, PBS+mAb D6, and IL-12+mAb D6 treated groups. This design would then allow me to determine which essential treatment step, either IL-12, mAb D6, or both has the largest influence on gene expression levels that may potentially possess the ability to enhance passive disease.

The results of the whole genome expression analysis assay point to a trend in which IL-12 treatment solely produces the greatest fluctuation in gene expression changes in the skeletal muscle of female wild-type B6 mice (Table 9). Surprisingly, the expression of both B-cell specific (*Cd19*) and T-cell specific (*Cd247*) genes was reduced below baseline levels in the IL-12 treated B6 mice, suggesting that B and T cells are not infiltrating the muscle tissue microenvironment in response to IL-12 treatment alone. The levels of chemotactic and NK cell-specific gene expression were most noticeably increased in the IL-12 treated mice with little influence on the levels of skeletal muscle specific and complement inhibitory gene expression levels. This suggested that IL-12 treatment alone was enough to activate the immune system and "prime" NK cells. When combined with the results seen in the grip strength and serum IFN-γ ELISA assays, this

priming of activated NK cells would explain their propensity to produce high levels of IFN-γ that further exacerbate passive disease and lead to increased muscle weakness upon immunization with mAb D6.

In accordance with published findings regarding CXCR3 and CXCL10 in regards to T cell activation (108-114), NK cell stimulation (115), and involvement in EAMG (72, 116-118) mentioned previously, my results further support these findings in which IL-12 treatment confers more severe passive disease in conjunction with substantially elevated expression levels of both the *Cxcr3* and *Cxcl10* genes. In fact, another chemokine gene in the same C-X-C family, *Cxcl9*, and the chemokine receptor gene *Ccr5* also exhibited highly increased expression levels resulting solely from IL-12 treatment, which correlates well with the findings proposed in other studies (104-107) in regards to chemokine involvement in NK cell trafficking and tissue inflammation. These elevated gene expression levels were paralleled by increased expression levels of NK cell specific genes, shedding further light onto the potential role that NK cells play in the passive EAMG disease process.

In contrast to the findings seen with IL-12 treatment alone, immunization with mAb D6 alone had little effect on overall gene expression levels (Table 11), with very small changes seen in a small subset of selected genes of interest. These small changes were in the chemotactic and NK cell-specific genes and not in skeletal muscle-specific or complement inhibitor genes. This suggests that any muscle weakness occurring with only mAb D6 immunization is most likely due to anti-AChR antibody binding and subsequent AChR clearance, and therefore an overall lowering of the available AChR numbers, and not the result of gene expression level influences resulting from anti-AChR antibody

binding that leads to greater damage to AChRs or the neuromuscular junction itself. This also serves to further explain the results I've presented here where passive disease levels are influenced more dramatically by functional IFN-γ presence and not the levels of complement or antibody bound at the neuromuscular junction. Similar to that seen with IL-12 treatment, the expression of both B-cell specific (*Cd19*) and T-cell specific (*Cd247*) genes was reduced below baseline levels in the mAb D6 treated B6 mice, suggesting that B and T cells are not infiltrating the muscle tissue microenvironment in response to mAb D6 treatment alone.

It was also important to see if there existed any compounding effects of IL-12 and mAb D6 treatment on gene expression levels (Table 10). In general, the overall levels of gene expression seen with IL-12 and mAb D6 treatment remained high but were lower than those seen with IL-12 treatment alone. Of interest, the expression level of both B-cell specific (*Cd19*) and T-cell specific (*Cd247*) genes was increased 1.3-fold and 3.8-fold respectively in the IL-12 and mAb D6 treated B6 mice, suggesting that B cells, and to a larger extent T cells, may potentially infiltrate the muscle tissue microenvironment in response. Also, many of the same chemotactic and NK cell-specific genes remained highly expressed compared to control treatments, however they were reduced compared to the IL-12 treatment alone.

The latter observation involving chemotactic and NK cell-specific genes is most likely due to the difference in tissue harvest timing, where the IL-12+mAb D6 mice were euthanized 96 hours after the IL-12 only mice, and therefore their levels of IFN-γ were greatly reduced, as supported by the serum IFN-γ levels seen for the IL-12 treated B6 mice at Day +8 of the serum IFN-γ ELISA (Fig 22C). In this scenario, the systemic level

of gene expression-influencing IFN-γ would be greatly reduced and this would therefore also be the case in localized tissue microenvironments, for example the skeletal diaphragm muscle. It makes sense then that decreased IFN-γ levels would correlate with reduced expression levels of genes that were much more highly expressed at a time when systemic IFN-γ levels were also much higher, as would be the case with the IL-12 treated group since these mice were euthanized 24 hours after the last IL-12 injection was administered. In further support of this idea, the serum IFN-γ levels of IL-12 treated B6 mice at this time same time point (Day +4) during the serum IFN-γ ELISA assays were at their highest levels seen (Fig 22B).

Another important finding that was not previously highlighted in the Results section is that the expression level of the *Sema4* gene was increased after IL-12 treatment. Expression of the *Sema4* gene, whose known protein product is semaphorin-4A, was increased 2.8-fold after IL-12 treatment (Table 9) and remained 2.4-fold higher in IL-12 treated B6 mice at 48 hours post-mAb D6 immunization (Table 10). While less substantial, mAb D6 treatment alone led to a modest 1.4-fold increase in the expression level of the *Sema4* gene (Table 11) over control PBS treatment. This is relevant as semaphorin-4A, a class IV semaphorin known to be capable of activating T cells (119, 120), belongs to the class IV semaphorin family of soluble and transmembrane proteins that are known to be involved in the guidance of axonal migration during immune responses (121, 122). This finding is of great interest in the passive EAMG arena, as the disease presents with antibodies that affect the acetylcholine receptors within the neuromuscular junction and eventually lead to decreased neuromuscular transmission and junctional remodeling. The potential role that sempahorin-4A could therefore play during

the passive EAMG disease process, whether possibly in junctional destruction or remodeling, remains unclear and needs to be further investigated as the connection between neuronal growth and immune responses is intriguing.

In summary, my results demonstrate that muscle weakness in passive transfer EAMG is enhanced by treatment with IL-12 when mice are able to respond by IFN-γ production. The primary source of disease-enhancing IFN-γ was shown to be the innate NK cells, as NK cell absence conferred resistance to passive EAMG development while specific NK cell predominance conferred increased susceptibility to passive EAMG development. This was evidenced by increased sickness demonstrated by reduced grip strength measurements and drastically elevated serum IFN-γ levels in the EAMG-susceptible IL-12 treated TCRβδ$^{-/-}$ mice. Conversely, resistance to passive EAMG development was demonstrated in IL-12 treated NK cell-depleted B6 mice by lower serum IFN-γ levels and sustained grip strength measurements that paralleled healthy PBS treated controls. No association between disease severity and the levels of C3 deposition at neuromuscular junctions was found, as the highly EAMG-susceptible IL-12 treated TCRβδ$^{-/-}$ mice exhibited the lowest levels of C3 deposition within their neuromuscular junctions.

Treatment with IL-12 alone caused the greatest number of changes in gene expression that serve to activate immune effector cells, especially NK cells, and to facilitate an increased efficiency in their ability to possibly infiltrate skeletal muscle tissue environments by means of increased chemokine signaling. Immunization with mAb D6 alone was not enough to generate significant disease or changes in gene expression levels. Future work in our lab will be directed towards developing a better

understanding of the role that NK cells play in passive disease and identifying genes whose expression is altered in muscle tissue during the passive EAMG disease development process with the intention of developing new therapeutic targets for human MG patients. It will also be of relevance to investigate the role that other identified genes, which showed increased expression after IL-12 treatment but that are not commonly associated with the autoimmune disease process, play in passive EAMG development.

Chapter 5

References

1. Conti-Fine, B. M., M. Milani, and H. J. Kaminski. 2006. Myasthenia gravis: past, present, and future. *J Clin Invest* 116:2843-2854.
2. Drachman, D. B. 1994. Myasthenia gravis. *N Engl J Med* 330:1797-1810.
3. Hohlfeld, R., K. V. Toyka, K. Heininger, H. Grosse-Wilde, and I. Kalies. 1984. Autoimmune human T lymphocytes specific for acetylcholine receptor. *Nature* 310:244-246.
4. Sommer, N., G. C. Harcourt, N. Willcox, D. Beeson, and J. Newsom-Davis. 1991. Acetylcholine receptor-reactive T lymphocytes from healthy subjects and myasthenia gravis patients. *Neurology* 41:1270-1276.
5. Sitaraman, S., D. W. Metzger, R. J. Belloto, A. J. Infante, and K. A. Wall. 2000. Interleukin-12 enhances clinical experimental autoimmune myasthenia gravis in susceptible but not resistant mice. *J Neuroimmunol* 107:73-82.

6. Moiola, L., F. Galbiati, G. Martino, S. Amadio, E. Brambilla, G. Comi, A. Vincent, L. M. Grimaldi, and L. Adorini. 1998. IL-12 is involved in the induction of experimental autoimmune myasthenia gravis, an antibody-mediated disease. *Eur J Immunol* 28:2487-2497.

7. Triantafyllou, N. I., E. I. Grapsa, E. Kararizou, E. Psimenou, A. Lagguranis, and A. Dimopoulos. 2009. Periodic therapeutic plasma exchange in patients with moderate to severe chronic myasthenia gravis non-responsive to immunosuppressive agents: an eight year follow-up. *Ther Apher Dial* 13:174-178.

8. Haddad, E. A., L. K. Senger, and F. Takei. 2009. An accessory role for B cells in the IL-12-induced activation of resting mouse NK cells. *J Immunol* 183:3608-3615.

9. Patrick, J., and J. Lindstrom. 1973. Autoimmune response to acetylcholine receptor. *Science* 180:871-872.

10. Berman, P. W., and J. Patrick. 1980. Experimental myasthenia gravis. A murine system. *J Exp Med* 151:204-223.

11. Wall, K. A., J. Y. Hu, P. Currier, S. Southwood, A. Sette, and A. J. Infante. 1994. A disease-related epitope of Torpedo acetylcholine receptor. Residues involved in I-Ab binding, self-nonself discrimination, and TCR antagonism. *J Immunol* 152:4526-4536.

12. Lindstrom, J. M., B. L. Einarson, V. A. Lennon, and M. E. Seybold. 1976. Pathological mechanisms in experimental autoimmune myasthenia gravis. I. Immunogenicity of syngeneic muscle acetylcholine receptor and quantitative

extraction of receptor and antibody-receptor complexes from muscles of rats with experimental automimmune myasthenia gravis. *J Exp Med* 144:726-738.

13. Wood, S. J., and C. R. Slater. 2001. Safety factor at the neuromuscular junction. *Prog Neurobiol* 64:393-429.

14. Christadoss, P., M. Poussin, and C. Deng. 2000. Animal models of myasthenia gravis. *Clin Immunol* 94:75-87.

15. Conti-Fine, B. M. 1997. *Myasthenia gravis : the immunobiology of an autoimmune disease*. R.G. Landes Co. ;

North American distributor, Chapman & Hall, Austin, Tex.

New York.

16. Toyka, K. V., D. B. Drachman, D. E. Griffin, A. Pestronk, J. A. Winkelstein, K. H. Fishbeck, and I. Kao. 1977. Myasthenia gravis. Study of humoral immune mechanisms by passive transfer to mice. *N Engl J Med* 296:125-131.

17. Zhang, G. X., B. G. Xiao, X. F. Bai, P. H. van der Meide, A. Orn, and H. Link. 1999. Mice with IFN-gamma receptor deficiency are less susceptible to experimental autoimmune myasthenia gravis. *J Immunol* 162:3775-3781.

18. Tzartos, S. J., D. E. Rand, B. L. Einarson, and J. M. Lindstrom. 1981. Mapping of surface structures of electrophorus acetylcholine receptor using monoclonal antibodies. *J Biol Chem* 256:8635-8645.

19. Tamamizu, S., D. H. Butler, J. A. Lasalde, and M. G. McNamee. 1996. Effects of antibody binding on structural transitions of the nicotinic acetylcholine receptor. *Biochemistry* 35:11773-11781.

20. Tzartos, S., S. Hochschwender, P. Vasquez, and J. Lindstrom. 1987. Passive transfer of experimental autoimmune myasthenia gravis by monoclonal antibodies to the main immunogenic region of the acetylcholine receptor. *J Neuroimmunol* 15:185-194.

21. Asher, O., W. A. Kues, V. Witzemann, S. J. Tzartos, S. Fuchs, and M. C. Souroujon. 1993. Increased gene expression of acetylcholine receptor and myogenic factors in passively transferred experimental autoimmune myasthenia gravis. *J Immunol* 151:6442-6450.

22. Dedhia, V., E. Goluszko, B. Wu, C. Deng, and P. Christadoss. 1998. The effect of B cell deficiency on the immune response to acetylcholine receptor and the development of experimental autoimmune myasthenia gravis. *Clin Immunol Immunopathol* 87:266-275.

23. Yim, S. 2003. Role of IL-12 and Interferon-gamma in Active and Passive Experimental Autoimmune Myasthenia Gravis. *PhD Dissertation, University of Toledo*:1-107.

24. Whiting, P. J., A. Vincent, M. Schluep, and J. Newsom-Davis. 1986. Monoclonal antibodies that distinguish between normal and denervated human acetylcholine receptor. *J Neuroimmunol* 11:223-235.

25. Lindstrom, J., J. Luo, and A. Kuryatov. 2008. Myasthenia gravis and the tops and bottoms of AChRs - Antigenic structure of the MIR and specific immunosuppression of EAMG using AChR cytoplasmic domains. H. J. Kaminski, and R. J. Barohn, eds. Blackwell Publishing. 29-41.

26. Germann, T., and E. Rude. 1995. Interleukin-12. *Int Arch Allergy Immunol* 108:103-112.

27. Trinchieri, G. 1995. Interleukin-12: a proinflammatory cytokine with immunoregulatory functions that bridge innate resistance and antigen-specific adaptive immunity. *Annu Rev Immunol* 13:251-276.

28. Neurath, M. F., I. Fuss, B. Kelsall, K. H. Meyer zum Buschenfelde, and W. Strober. 1996. Effect of IL-12 and antibodies to IL-12 on established granulomatous colitis in mice. *Ann N Y Acad Sci* 795:368-370.

29. Trinchieri, G. 1994. Interleukin-12: a cytokine produced by antigen-presenting cells with immunoregulatory functions in the generation of T-helper cells type 1 and cytotoxic lymphocytes. *Blood* 84:4008-4027.

30. Adorini, L. 1999. Interleukin-12, a key cytokine in Th1-mediated autoimmune diseases. *Cell Mol Life Sci* 55:1610-1625.

31. Germann, T., J. Szeliga, H. Hess, S. Storkel, F. J. Podlaski, M. K. Gately, E. Schmitt, and E. Rude. 1995. Administration of interleukin 12 in combination with type II collagen induces severe arthritis in DBA/1 mice. *Proc Natl Acad Sci U S A* 92:4823-4827.

32. Leonard, J. P., K. E. Waldburger, and S. J. Goldman. 1995. Prevention of experimental autoimmune encephalomyelitis by antibodies against interleukin 12. *J Exp Med* 181:381-386.

33. Trembleau, S., G. Penna, E. Bosi, A. Mortara, M. K. Gately, and L. Adorini. 1995. Interleukin 12 administration induces T helper type 1 cells and accelerates autoimmune diabetes in NOD mice. *J Exp Med* 181:817-821.

34. Trembleau, S., T. Germann, M. K. Gately, and L. Adorini. 1995. The role of IL-12 in the induction of organ-specific autoimmune diseases. *Immunol Today* 16:383-386.

35. Karachunski, P. I., N. S. Ostlie, C. Monfardini, and B. M. Conti-Fine. 2000. Absence of IFN-gamma or IL-12 has different effects on experimental myasthenia gravis in C57BL/6 mice. *J Immunol* 164:5236-5244.

36. Germann, T., M. Bongartz, H. Dlugonska, H. Hess, E. Schmitt, L. Kolbe, E. Kolsch, F. J. Podlaski, M. K. Gately, and E. Rude. 1995. Interleukin-12 profoundly up-regulates the synthesis of antigen-specific complement-fixing IgG2a, IgG2b and IgG3 antibody subclasses in vivo. *Eur J Immunol* 25:823-829.

37. Morgutti, M., B. M. Conti-Tronconi, A. Sghirlanzoni, and F. Clementi. 1979. Cellular immune response to acetylcholine receptor in myasthenia gravis: II. Thymectomy and corticosteroids. *Neurology* 29:734-738.

38. Ahlberg, R., Q. Yi, R. Pirskanen, G. Matell, C. Swerup, E. P. Rieber, G. Riethmuller, G. Holm, and A. K. Lefvert. 1994. Treatment of myasthenia gravis with anti-CD4 antibody: improvement correlates to decreased T-cell autoreactivity. *Neurology* 44:1732-1737.

39. Mengle-Gaw, L., S. Conner, H. O. McDevitt, and C. G. Fathman. 1984. Gene conversion between murine class II major histocompatibility complex loci. Functional and molecular evidence from the bm 12 mutant. *J Exp Med* 160:1184-1194.

40. Bellone, M., N. Ostlie, S. J. Lei, X. D. Wu, and B. M. Conti-Tronconi. 1991. The I-Abm12 mutation, which confers resistance to experimental myasthenia gravis,

drastically affects the epitope repertoire of murine CD4+ cells sensitized to nicotinic acetylcholine receptor. *J Immunol* 147:1484-1491.

41. Christadoss, P., J. M. Lindstrom, R. W. Melvold, and N. Talal. 1985. Mutation at I-A beta chain prevents experimental autoimmune myasthenia gravis. *Immunogenetics* 21:33-38.

42. Infante, A. J., P. A. Thompson, K. A. Krolick, and K. A. Wall. 1991. Determinant selection in murine experimental autoimmune myasthenia gravis. Effect of the bm12 mutation on T cell recognition of acetylcholine receptor epitopes. *J Immunol* 146:2977-2982.

43. Karachunski, P. I., N. S. Ostlie, S. Lei, D. K. Okita, J. M. Lindstrom, and B. M. Conti-Fine. 1998. Immunization of bm12 mice with high doses of acetylcholine receptor overcomes their resistance to experimental autoimmune myasthenia gravis. *Ann N Y Acad Sci* 841:555-559.

44. Zhang, G. X., B. G. Xiao, X. F. Bai, A. Orn, P. H. van der Meide, and H. Link. 1998. IFN-gamma is required to induce experimental autoimmune myasthenia gravis. *Ann N Y Acad Sci* 841:576-579.

45. Balasa, B., C. Deng, J. Lee, L. M. Bradley, D. K. Dalton, P. Christadoss, and N. Sarvetnick. 1997. Interferon gamma (IFN-gamma) is necessary for the genesis of acetylcholine receptor-induced clinical experimental autoimmune myasthenia gravis in mice. *J Exp Med* 186:385-391.

46. Gu, D., L. Wogensen, N. A. Calcutt, C. Xia, S. Zhu, J. P. Merlie, H. S. Fox, J. Lindstrom, H. C. Powell, and N. Sarvetnick. 1995. Myasthenia gravis-like

syndrome induced by expression of interferon gamma in the neuromuscular junction. *J Exp Med* 181:547-557.

47. Jander, S., and G. Stoll. 2002. Increased serum levels of the interferon-gamma-inducing cytokine interleukin-18 in myasthenia gravis. *Neurology* 59:287-289.

48. Shi, F. D., H. B. Wang, H. Li, S. Hong, M. Taniguchi, H. Link, L. Van Kaer, and H. G. Ljunggren. 2000. Natural killer cells determine the outcome of B cell-mediated autoimmunity. *Nat Immunol* 1:245-251.

49. Im, S. H., D. Barchan, P. K. Maiti, L. Raveh, M. C. Souroujon, and S. Fuchs. 2001. Suppression of experimental myasthenia gravis, a B cell-mediated autoimmune disease, by blockade of IL-18. *FASEB J* 15:2140-2148.

50. Nakamura, K., H. Okamura, M. Wada, K. Nagata, and T. Tamura. 1989. Endotoxin-induced serum factor that stimulates gamma interferon production. *Infect Immun* 57:590-595.

51. Micallef, M. J., T. Ohtsuki, K. Kohno, F. Tanabe, S. Ushio, M. Namba, T. Tanimoto, K. Torigoe, M. Fujii, M. Ikeda, S. Fukuda, and M. Kurimoto. 1996. Interferon-gamma-inducing factor enhances T helper 1 cytokine production by stimulated human T cells: synergism with interleukin-12 for interferon-gamma production. *Eur J Immunol* 26:1647-1651.

52. Kohno, K., J. Kataoka, T. Ohtsuki, Y. Suemoto, I. Okamoto, M. Usui, M. Ikeda, and M. Kurimoto. 1997. IFN-gamma-inducing factor (IGIF) is a costimulatory factor on the activation of Th1 but not Th2 cells and exerts its effect independently of IL-12. *J Immunol* 158:1541-1550.

53. Yoshimoto, T., K. Takeda, T. Tanaka, K. Ohkusu, S. Kashiwamura, H. Okamura, S. Akira, and K. Nakanishi. 1998. IL-12 up-regulates IL-18 receptor expression on T cells, Th1 cells, and B cells: synergism with IL-18 for IFN-gamma production. *J Immunol* 161:3400-3407.

54. Dinarello, C. A., D. Novick, A. J. Puren, G. Fantuzzi, L. Shapiro, H. Muhl, D. Y. Yoon, L. L. Reznikov, S. H. Kim, and M. Rubinstein. 1998. Overview of interleukin-18: more than an interferon-gamma inducing factor. *J Leukoc Biol* 63:658-664.

55. Ahn, H. J., S. Maruo, M. Tomura, J. Mu, T. Hamaoka, K. Nakanishi, S. Clark, M. Kurimoto, H. Okamura, and H. Fujiwara. 1997. A mechanism underlying synergy between IL-12 and IFN-gamma-inducing factor in enhanced production of IFN-gamma. *J Immunol* 159:2125-2131.

56. Robinson, D., K. Shibuya, A. Mui, F. Zonin, E. Murphy, T. Sana, S. B. Hartley, S. Menon, R. Kastelein, F. Bazan, and A. O'Garra. 1997. IGIF does not drive Th1 development but synergizes with IL-12 for interferon-gamma production and activates IRAK and NFkappaB. *Immunity* 7:571-581.

57. Hunter, C. A., J. Timans, P. Pisacane, S. Menon, G. Cai, W. Walker, M. Aste-Amezaga, R. Chizzonite, J. F. Bazan, and R. A. Kastelein. 1997. Comparison of the effects of interleukin-1 alpha, interleukin-1 beta and interferon-gamma-inducing factor on the production of interferon-gamma by natural killer. *Eur J Immunol* 27:2787-2792.

58. Lauwerys, B. R., J. C. Renauld, and F. A. Houssiau. 1999. Synergistic proliferation and activation of natural killer cells by interleukin 12 and interleukin 18. *Cytokine* 11:822-830.

59. Wigginton, J. M., E. Gruys, L. Geiselhart, J. Subleski, K. L. Komschlies, J. W. Park, T. A. Wiltrout, K. Nagashima, T. C. Back, and R. H. Wiltrout. 2001. IFN-gamma and Fas/FasL are required for the antitumor and antiangiogenic effects of IL-12/pulse IL-2 therapy. *J Clin Invest* 108:51-62.

60. Voest, E. E., B. M. Kenyon, M. S. O'Reilly, G. Truitt, R. J. D'Amato, and J. Folkman. 1995. Inhibition of angiogenesis in vivo by interleukin 12. *J Natl Cancer Inst* 87:581-586.

61. Billiau, A. 1996. Interferon-gamma: biology and role in pathogenesis. *Adv Immunol* 62:61-130.

62. Nguyen, S., V. Morel, M. Le Garff-Tavernier, F. Bolgert, V. Leblond, P. Debre, and V. Vieillard. 2006. Persistence of CD16+/CD56-/2B4+ natural killer cells: a highly dysfunctional NK subset expanded in ocular myasthenia gravis. *J Neuroimmunol* 179:117-125.

63. Yamagiwa, S., J. D. Gray, S. Hashimoto, and D. A. Horwitz. 2001. A role for TGF-beta in the generation and expansion of CD4+CD25+ regulatory T cells from human peripheral blood. *J Immunol* 166:7282-7289.

64. Fantini, M. C., C. Becker, I. Tubbe, A. Nikolaev, H. A. Lehr, P. Galle, and M. F. Neurath. 2006. Transforming growth factor beta induced FoxP3+ regulatory T cells suppress Th1 mediated experimental colitis. *Gut* 55:671-680.

65. Zheng, S. G., J. Wang, P. Wang, J. D. Gray, and D. A. Horwitz. 2007. IL-2 is essential for TGF-beta to convert naive CD4+CD25- cells to CD25+Foxp3+ regulatory T cells and for expansion of these cells. *J Immunol* 178:2018-2027.

66. Mason, D., and F. Powrie. 1998. Control of immune pathology by regulatory T cells. *Curr Opin Immunol* 10:649-655.

67. Chen, W., W. Jin, and S. M. Wahl. 1998. Engagement of cytotoxic T lymphocyte-associated antigen 4 (CTLA-4) induces transforming growth factor beta (TGF-beta) production by murine CD4(+) T cells. *J Exp Med* 188:1849-1857.

68. Shi, F. D., H. Li, H. Wang, X. Bai, P. H. van der Meide, H. Link, and H. G. Ljunggren. 1999. Mechanisms of nasal tolerance induction in experimental autoimmune myasthenia gravis: identification of regulatory cells. *J Immunol* 162:5757-5763.

69. Asai, O., D. L. Longo, Z. G. Tian, R. L. Hornung, D. D. Taub, F. W. Ruscetti, and W. J. Murphy. 1998. Suppression of graft-versus-host disease and amplification of graft-versus-tumor effects by activated natural killer cells after allogeneic bone marrow transplantation. *J Clin Invest* 101:1835-1842.

70. Olson, J. A., R. Zeiser, A. Beilhack, J. J. Goldman, and R. S. Negrin. 2009. Tissue-specific homing and expansion of donor NK cells in allogeneic bone marrow transplantation. *J Immunol* 183:3219-3228.

71. Sun, J. C., A. Ma, and L. L. Lanier. 2009. Cutting edge: IL-15-independent NK cell response to mouse cytomegalovirus infection. *J Immunol* 183:2911-2914.

72. Feferman, T., P. K. Maiti, S. Berrih-Aknin, J. Bismuth, J. Bidault, S. Fuchs, and M. C. Souroujon. 2005. Overexpression of IFN-induced protein 10 and its receptor CXCR3 in myasthenia gravis. *J Immunol* 174:5324-5331.

73. Mantegazza, R., S. M. Hughes, D. Mitchell, M. Travis, H. M. Blau, and L. Steinman. 1991. Modulation of MHC class II antigen expression in human myoblasts after treatment with IFN-gamma. *Neurology* 41:1128-1132.

74. Michaelis, D., N. Goebels, and R. Hohlfeld. 1993. Constitutive and cytokine-induced expression of human leukocyte antigens and cell adhesion molecules by human myotubes. *Am J Pathol* 143:1142-1149.

75. Goebels, N., D. Michaelis, H. Wekerle, and R. Hohlfeld. 1992. Human myoblasts as antigen-presenting cells. *J Immunol* 149:661-667.

76. Stegall, T., and K. A. Krolick. 2000. Myocytes respond to both interleukin-4 and interferon-gamma: cytokine responsiveness with the potential to influence the severity and course of experimental myasthenia gravis. *Clin Immunol* 94:133-139.

77. Stegall, T., and K. A. Krolick. 2000. A monoclonal lewis rat myocyte line that responds to interferon-gamma: responsiveness with the potential to influence subsequent interactions with the immune system. *Clin Immunol* 94:125-132.

78. Reyes-Reyna, S. M., and K. A. Krolick. 2000. Chemokine production by rat myocytes exposed to interferon-gamma. *Clin Immunol* 94:105-113.

79. Reyes-Reyna, S., T. Stegall, and K. A. Krolick. 2002. Muscle responds to an antibody reactive with the acetylcholine receptor by up-regulating monocyte chemoattractant protein 1: a chemokine with the potential to influence the severity and course of experimental myasthenia gravis. *J Immunol* 169:1579-1586.

80. Scott, B. G., H. Yang, E. Tuzun, C. Dong, R. A. Flavell, and P. Christadoss. 2004. ICOS is essential for the development of experimental autoimmune myasthenia gravis. *J Neuroimmunol* 153:16-25.

81. Christadoss, P., E. Tuzun, J. Li, S. S. Saini, and H. Yang. 2008. Classical complement pathway in experimental autoimmune myasthenia gravis pathogenesis. *Ann N Y Acad Sci* 1132:210-219.

82. Piddlesden, S. J., S. Jiang, J. L. Levin, A. Vincent, and B. P. Morgan. 1996. Soluble complement receptor 1 (sCR1) protects against experimental autoimmune myasthenia gravis. *J Neuroimmunol* 71:173-177.

83. Tuzun, E., S. S. Saini, H. Yang, D. Alagappan, S. Higgs, and P. Christadoss. 2006. Genetic evidence for the involvement of Fcgamma receptor III in experimental autoimmune myasthenia gravis pathogenesis. *J Neuroimmunol* 174:157-167.

84. Tuzun, E., J. Li, S. S. Saini, H. Yang, and P. Christadoss. 2007. Pros and cons of treating murine myasthenia gravis with anti-C1q antibody. *J Neuroimmunol* 182:167-176.

85. Biesecker, G., and C. M. Gomez. 1989. Inhibition of acute passive transfer experimental autoimmune myasthenia gravis with Fab antibody to complement C6. *J Immunol* 142:2654-2659.

86. Lin, F., H. J. Kaminski, B. M. Conti-Fine, W. Wang, C. Richmonds, and M. E. Medof. 2002. Markedly enhanced susceptibility to experimental autoimmune myasthenia gravis in the absence of decay-accelerating factor protection. *J Clin Invest* 110:1269-1274.

87. Stapp, J. M., V. Sjoelund, H. A. Lassiter, R. C. Feldhoff, and P. W. Feldhoff. 2005. Recombinant rat IL-1beta and IL-6 synergistically enhance C3 mRNA levels and complement component C3 secretion by H-35 rat hepatoma cells. *Cytokine* 30:78-85.

88. Deng, C., E. Goluszko, E. Tuzun, H. Yang, and P. Christadoss. 2002. Resistance to experimental autoimmune myasthenia gravis in IL-6-deficient mice is associated with reduced germinal center formation and C3 production. *J Immunol* 169:1077-1083.

89. Koo, G. C., and J. R. Peppard. 1984. Establishment of monoclonal anti-Nk-1.1 antibody. *Hybridoma* 3:301-303.

90. Via, C. S., V. Rus, M. K. Gately, and F. D. Finkelman. 1994. IL-12 stimulates the development of acute graft-versus-host disease in mice that normally would develop chronic, autoimmune graft-versus-host disease. *J Immunol* 153:4040-4047.

91. Schoenhaut, D. S., A. O. Chua, A. G. Wolitzky, P. M. Quinn, C. M. Dwyer, W. McComas, P. C. Familletti, M. K. Gately, and U. Gubler. 1992. Cloning and expression of murine IL-12. *J Immunol* 148:3433-3440.

92. Karachunski, P. I., N. Ostlie, M. Bellone, A. J. Infante, and B. M. Conti-Fine. 1995. Mechanisms by which the I-ABM12 mutation influences susceptibility to experimental myasthenia gravis: a study in homozygous and heterozygous mice. *Scand J Immunol* 42:215-225.

93. Buchanan, J. M., L. A. Vogel, V. H. Van Cleave, and D. W. Metzger. 1995. Interleukin 12 alters the isotype-restricted antibody response of mice to hen eggwhite lysozyme. *Int Immunol* 7:1519-1528.

94. Lindstrom, J. M., A. G. Engel, M. E. Seybold, V. A. Lennon, and E. H. Lambert. 1976. Pathological mechanisms in experimental autoimmune myasthenia gravis II. Passive transfer of experimental autoimmune myasthenia gravis in rats with anti-acetylcholine receptor antibodies. *J. Exp. Med.* 144:739-753.

95. Dalton, D. K., S. Pitts-Meek, S. Keshav, I. S. Figari, A. Bradley, and T. A. Stewart. 1993. Multiple defects of immune cell function in mice with disrupted interferon-gamma genes. *Science* 259:1739-1742.

96. Turman, M. A., T. Yabe, C. McSherry, F. H. Bach, and J. P. Houchins. 1993. Characterization of a novel gene (NKG7) on human chromosome 19 that is expressed in natural killer cells and T cells. *Hum Immunol* 36:34-40.

97. Saifullah, M. K., D. A. Fox, S. Sarkar, S. M. Abidi, J. Endres, J. Piktel, T. M. Haqqi, and N. G. Singer. 2004. Expression and characterization of a novel CD6 ligand in cells derived from joint and epithelial tissues. *J Immunol* 173:6125-6133.

98. Car, B. D., V. M. Eng, B. Schnyder, M. LeHir, A. N. Shakhov, G. Woerly, S. Huang, M. Aguet, T. D. Anderson, and B. Ryffel. 1995. Role of interferon-gamma in interleukin 12-induced pathology in mice. *Am J Pathol* 147:1693-1707.

99. Wang, Z. Y., D. K. Okita, J. Howard, Jr., and B. M. Conti-Fine. 1997. Th1 epitope repertoire on the alpha subunit of human muscle acetylcholine receptor in myasthenia gravis. *Neurology* 48:1643-1653.

100. von Andrian, U. H., and T. R. Mempel. 2003. Homing and cellular traffic in lymph nodes. *Nat Rev Immunol* 3:867-878.

101. Forster, R., A. Schubel, D. Breitfeld, E. Kremmer, I. Renner-Muller, E. Wolf, and M. Lipp. 1999. CCR7 coordinates the primary immune response by establishing functional microenvironments in secondary lymphoid organs. *Cell* 99:23-33.

102. Gunn, M. D., S. Kyuwa, C. Tam, T. Kakiuchi, A. Matsuzawa, L. T. Williams, and H. Nakano. 1999. Mice lacking expression of secondary lymphoid organ chemokine have defects in lymphocyte homing and dendritic cell localization. *J Exp Med* 189:451-460.

103. Sallusto, F., J. Geginat, and A. Lanzavecchia. 2004. Central memory and effector memory T cell subsets: function, generation, and maintenance. *Annu Rev Immunol* 22:745-763.

104. Fehniger, T. A., M. A. Cooper, G. J. Nuovo, M. Cella, F. Facchetti, M. Colonna, and M. A. Caligiuri. 2003. CD56bright natural killer cells are present in human lymph nodes and are activated by T cell-derived IL-2: a potential new link between adaptive and innate immunity. *Blood* 101:3052-3057.

105. Ferlazzo, G., D. Thomas, S. L. Lin, K. Goodman, B. Morandi, W. A. Muller, A. Moretta, and C. Munz. 2004. The abundant NK cells in human secondary lymphoid tissues require activation to express killer cell Ig-like receptors and become cytolytic. *J Immunol* 172:1455-1462.

106. Martin-Fontecha, A., L. L. Thomsen, S. Brett, C. Gerard, M. Lipp, A. Lanzavecchia, and F. Sallusto. 2004. Induced recruitment of NK cells to lymph nodes provides IFN-gamma for T(H)1 priming. *Nat Immunol* 5:1260-1265.

107. Luster, A. D. 1998. Chemokines--chemotactic cytokines that mediate inflammation. *N Engl J Med* 338:436-445.

108. Bradding, P., A. F. Walls, and S. T. Holgate. 2006. The role of the mast cell in the pathophysiology of asthma. *J Allergy Clin Immunol* 117:1277-1284.

109. Flier, J., D. M. Boorsma, P. J. van Beek, C. Nieboer, T. J. Stoof, R. Willemze, and C. P. Tensen. 2001. Differential expression of CXCR3 targeting chemokines CXCL10, CXCL9, and CXCL11 in different types of skin inflammation. *J Pathol* 194:398-405.

110. Gottlieb, A. B., A. D. Luster, D. N. Posnett, and D. M. Carter. 1988. Detection of a gamma interferon-induced protein IP-10 in psoriatic plaques. *J Exp Med* 168:941-948.

111. Patel, D. D., J. P. Zachariah, and L. P. Whichard. 2001. CXCR3 and CCR5 ligands in rheumatoid arthritis synovium. *Clin Immunol* 98:39-45.

112. Balashov, K. E., J. B. Rottman, H. L. Weiner, and W. W. Hancock. 1999. CCR5(+) and CXCR3(+) T cells are increased in multiple sclerosis and their ligands MIP-1alpha and IP-10 are expressed in demyelinating brain lesions. *Proc Natl Acad Sci U S A* 96:6873-6878.

113. Sorensen, T. L., M. Tani, J. Jensen, V. Pierce, C. Lucchinetti, V. A. Folcik, S. Qin, J. Rottman, F. Sellebjerg, R. M. Strieter, J. L. Frederiksen, and R. M. Ransohoff. 1999. Expression of specific chemokines and chemokine receptors in the central nervous system of multiple sclerosis patients. *J Clin Invest* 103:807-815.

114. Raju, R., O. Vasconcelos, R. Granger, and M. C. Dalakas. 2003. Expression of IFN-gamma-inducible chemokines in inclusion body myositis. *J Neuroimmunol* 141:125-131.

115. Neville, L. F., G. Mathiak, and O. Bagasra. 1997. The immunobiology of interferon-gamma inducible protein 10 kD (IP-10): a novel, pleiotropic member of the C-X-C chemokine superfamily. *Cytokine Growth Factor Rev* 8:207-219.

116. Feferman, T., R. Aricha, K. Mizrachi, E. Geron, R. Alon, M. C. Souroujon, and S. Fuchs. 2009. Suppression of experimental autoimmune myasthenia gravis by inhibiting the signaling between IFN-gamma inducible protein 10 (IP-10) and its receptor CXCR3. *J Neuroimmunol* 209:87-95.

117. Aricha, R., T. Feferman, M. C. Souroujon, and S. Fuchs. 2006. Overexpression of phosphodiesterases in experimental autoimmune myasthenia gravis: suppression of disease by a phosphodiesterase inhibitor. *FASEB J* 20:374-376.

118. Menon, R. T., T. Feferman, R. Aricha, M. C. Souroujon, and S. Fuchs. 2008. Suppression of experimental autoimmune myasthenia gravis by combination therapy: pentoxifylline as a steroid-sparing agent. *J Neuroimmunol* 201-202:128-135.

119. Kikutani, H., and A. Kumanogoh. 2003. Semaphorins in interactions between T cells and antigen-presenting cells. *Nat Rev Immunol* 3:159-167.

120. Kumanogoh, A., S. Marukawa, K. Suzuki, N. Takegahara, C. Watanabe, E. Ch'ng, I. Ishida, H. Fujimura, S. Sakoda, K. Yoshida, and H. Kikutani. 2002. Class IV semaphorin Sema4A enhances T-cell activation and interacts with Tim-2. *Nature* 419:629-633.

121. Kumanogoh, A., and H. Kikutani. 2003. Immune semaphorins: a new area of semaphorin research. *J Cell Sci* 116:3463-3470.

122. Elhabazi, A., A. Marie-Cardine, I. Chabbert-de Ponnat, A. Bensussan, and L. Boumsell. 2003. Structure and function of the immune semaphorin CD100/SEMA4D. *Crit Rev Immunol* 23:65-81.